UiT
THE ARCTIC
UNIVERSITY
OF NORWAY

Faculty of Science & Technology

Department of Geology

# Interaction between ice streaming, glacitectonics and fluid flow in Håkjerringdjupet, SW Barents Sea.

—

**Frank Werner Jakobsen**

*Master thesis in Geology, GEO-3900*
*May 2016*

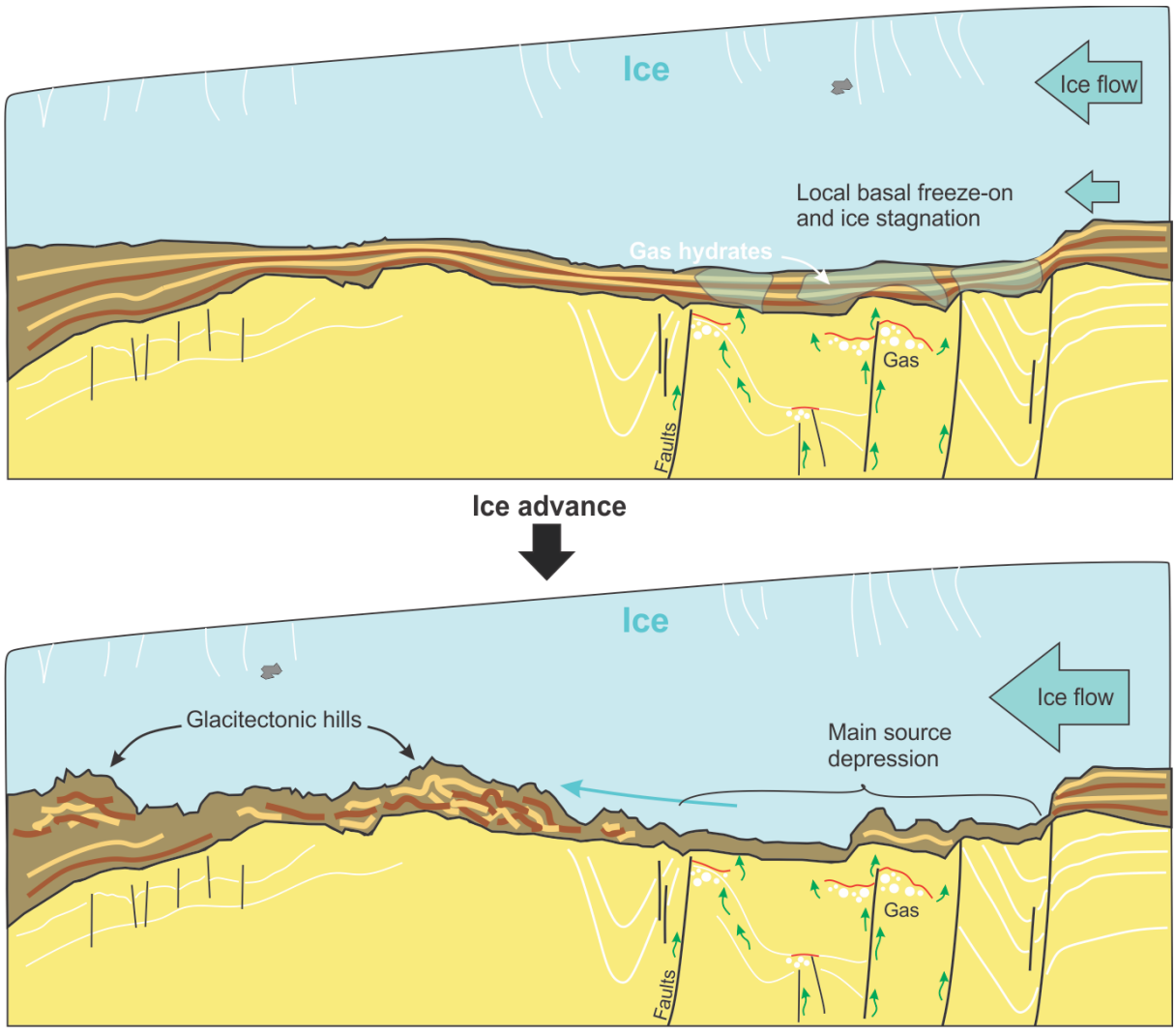

## Abstract

Håkjerringdjupet is a formerly glaciated over-deepened cross shelf trough, located in the SW Barents Sea, on the Norwegian Continental Shelf. This thesis uses high-resolution multibeam swath bathymetry and 2- and 3D seismic datasets to investigate in detail the interaction between ice streaming, glacitectonics and fluid flow in Håkjerringdjupet. In order to achieve our goals we have interpreted and mapped stratigraphy, faults, fluid flow features and glacial landforms within the trough. A ~200 $km^2$ over-deepening north in the trough, and irregular hills located directly downstream, are interpreted as a glacitectonic hill-hole pair with the over-deepening as its source area – indicating slow moving ice and possible a frozen bed. Mega-scale glacial lineations (MSGLs) and grounding zone wedges (GZWs) are documented in the trough's southern half, with no trace of any glacitectonic events – this is interpreted to indicate that the ice in the southern half of the trough were continuously fast flowing with stillstands or readvances of the ice margin during deglaciation. Hence, the landforms documented in the trough show evidence for both fast and slow ice movement.

Our study revealed that accumulation and seepage of shallow gas is spatially associated with a deep-seated fault complex located central in the trough. The fault complex and the shallow gas accumulations are located directly below the interpreted source area for the hill-hole pair. We suggest that shallow gas would form sub-glacial gas hydrates, due to low-temperature and high-pressure conditions induced by thick ice cover. The formation of gas hydrates within the subglacial sediments and bedrock would cause an increase in sediment shear strength and therefore basal drag, creating a sticky spot, preventing fast ice flow and possible stagnation. Hard sediments containing gas hydrates are implied to have frozen on to the ice-bed and subsequent advance of the ice margin is implied to have triggered detachment in the sub-strata - frozen sediments up to 50 – 100 m thick were transported sub-glacially, deformed and deposited as glacitectonic hills downstream.

Furthermore, we suggest that gas hydrate formation and ice stagnation in the northern half of Håkjerringdjupet caused a reorganization, or flow switching, of the ice stream. As a response to the stagnation in the north, we think the ice flow became concentrated in the trough's southern half. As implied by glacial landforms, this contributed to continuous ice streaming south in the trough, thus prevented a complete shutdown of Håkjerringdjupet Ice Stream.

# Acknowledgements

First, I would like to thank the Centre for Arctic Gas Hydrate, Environment and Climate (CAGE) for the cooperation and for giving me the opportunity to write this thesis, which have been both exciting and enlightening! A special thanks is in order to my supervisor, Monica Winsborrow, which have shown a great deal of interest in my project and always had an open door when it was needed! As they say (from now on at least): "Behind every great master student, there is an even greater supervisor!". I am very grateful!

*We are now reaching the end of something good. With these humble words, I will let the last drop of ink to dry. (PS: I don't want you to cry all over my thesis so I'm going to make it funny somehow…)*

*The past five years have been incredible for me; nothing to say about that – Years wells spent Frank! As a student, I have had the chance to travel to parts of the world I never thought I would go to, and participated in excursions that have been both enlightening and good old fun! These years have been a joy, and for that, I have my friends to thank! If life had a currency, it would be friendship! By "friendship", I am not referring to a boat or ship that belongs to your friend, but rather the people you would like to take with you if you went on a ship. …You still don't get it? Let me give you an example: If I were to sail across the Atlantic Ocean in a boat (it would be a sailboat with a pirate flag), I have no doubt whom I would have on my crew:*

*Andreas & Bendik – We have lived, drank and fought togethe(eer), and they have been my best friends for the last five years (Arr!). Our long talks on survival strats and how everything in life is easy would come in quite handy. Silje, Maren, Karianne & Sinthu – I got a pass into their girl's night out. For that, they have earned the pass to my heart. And my boat! They would also be pretty as figureheads (galleonsfigur) on the bow. Anders, André, Espen, Eivind & Vidar – They let me hang with them although they were older than me. That made me pretty cool! Now I returrn the favor. Through all these years of much appreciated guidance, they have shown to possess the perfect skills required to join the crew as deckhands and galley boys, much needed to maintain the ship and hoist up sails.*

*That is what friendship is - to me at least! What better company to conquer the world?*

# Table of Contents

# 1 Introduction

Håkjerringdjupet is a formerly glaciated over-deepened trough in the southwestern Barents Sea on the Norwegian continental shelf, located approximately 100 km north of Tromsø, Norway ( Figure 1.1). Previous marine-geological studies on Håkjerringdjupet have made three interesting observations from the study area:

1) The trough was occupied by an ice stream at Last Glacial Maximum (~20 - 25 ka), reaching all the way out to the shelf edge, indicating a fast flowing, warm-based ice flow (Ottesen *et al.*, 2005; Winsborrow *et al.*, 2010a; Winsborrow *et al.*, 2012).
2) A large over-deepened area and adjacent hummocky hills central in the trough were by Sættem (1994) suggested to be a glacitectonic hill-hole pair, indicating slow flowing and cold-based ice with high basal friction.
3) An abundance of pockmarks were observed widely within the trough. This indicates the presence of shallow migrating fluids located close to the seafloor (Rise *et al.*, 2014).

Two of these processes are indicators of quite opposite glacial dynamics, i.e. ice streaming and glacitectonics (fast and slow ice movement). As with the third one, how may the presence of shallow fluids interact on basal conditions and the dynamics of an ice stream?

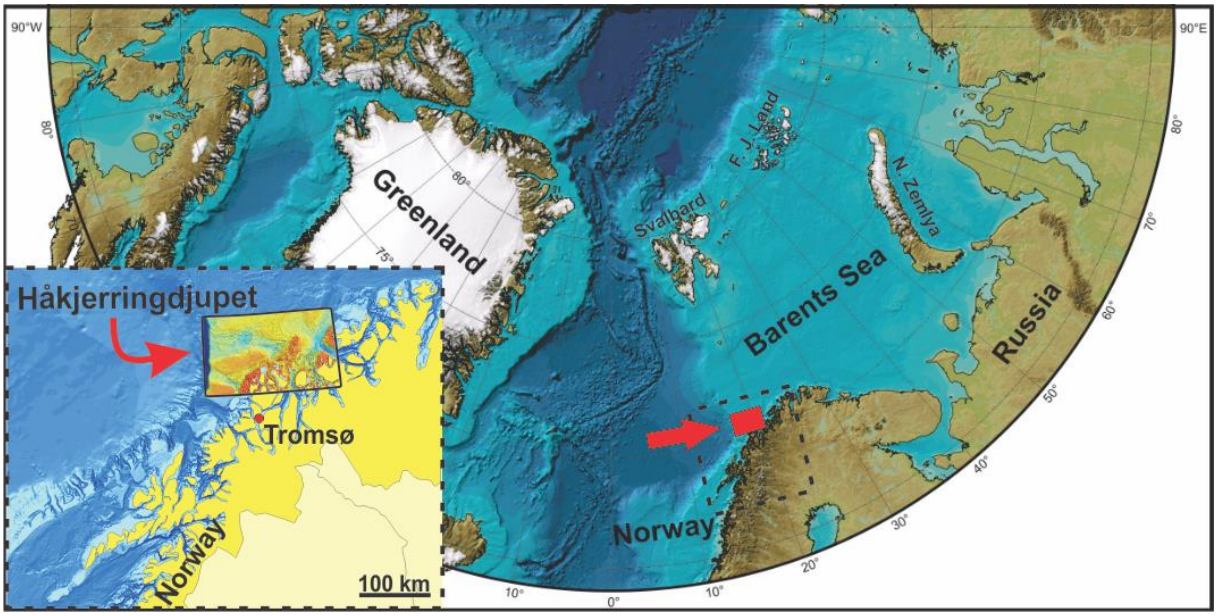


*Figure 1.1: The IBCAO, modified from Jakobsson et al. (2012), show parts of the northern hemisphere and the location of the study area is marked by a red square and a red arrow. Black dashed line show a zoom in on the continental shelf off northern Norway where the study area, Håkjerringdjupet, is located just north of Tromsø, Norway.*

With these studies in mind the main objectives of this thesis is, for the first time, to investigate the interactions between ice streaming, glacitectonics and fluid flow in Håkjerringdjupet. In order to do this we use a large dataset of high-resolution multibeam swath bathymetry (MBB), together with 2- and 3D seismic data to interpret and reconstruct Late Weichselian glacimarine landforms, ice dynamics and map the distribution of faults and shallow gas indicators at the seafloor and subsurface. We then discuss the possible interactions between shallow fluids and basal conditions of an ice stream, and if there are any connection to the glacitectonic landforms present.

First of all we will give you a brief introduction on the basics of the three different processes observed by previous work: ice-streaming, glacitectonics and fluid flow.

## 1.1 Ice streaming

Ice sheets are vast domes of ice covering large areas or even continents, such as today's Antarctic and Greenland Ice Sheets. Most of the ice within an ice sheet is moving slowly, however, veins of fast flowing and warm based ice, so called ice streams, drain the ice much faster than its surroundings and are very efficient distributors of sediments from the inner ice sheet to its margins (Vorren *et al.*, 1991; Laberg & Vorren, 1996; Ó Cofaigh *et al.*, 2003). They are therefore very important for the mass balance and stability of an ice sheet (Benn & Evans, 2010). The location and velocities of the ice streams are found to be strongly affected by basal conditions, such as topography (often located in troughs, fjords and valleys), hard or soft bed and subglacial meltwater, where soft beds saturated with meltwater enhance ice flow (Alley, 1993; Ottesen *et al.*, 2005; Stokes *et al.*, 2007; Benn & Evans, 2010; Winsborrow *et al.*, 2010b).

Ice streams are found in contemporary ice sheets and implied from reconstructions of paleo-ice sheets. They are recognized by their distinct glacial landforms, indicating grounded, fast flowing ice: Mega-scale glacial lineations (MSGLs), grounding zone wedges (GZW), trough mouth fans, topographic relief (a trough for instance), convergent flow pattern on the onset of an ice stream, and abrupt lateral margins (Stokes & Clark, 1999; C. D. Clark *et al.*, 2003a; Ó Cofaigh *et al.*, 2003; Ó Cofaigh *et al.*, 2005; Ottesen *et al.*, 2005; Ottesen *et al.*, 2008; E. C. King *et al.*, 2009; Benn & Evans, 2010; Winsborrow *et al.*, 2010a; Winsborrow *et al.*, 2010b; Rydningen *et al.*, 2013).

As we are facing global warming and sea level rise, more research have been done on ice streams and what controls them, and basal conditions are regarded as a key issue. Research on contemporary and paleo-ice streams have shown that they are not always consistent with areas of continuously fast flowing ice as we fist may have thought. In fact, they seem to have highly varying velocities and may even completely shut down or change ice flow direction on relative short time scales - events which are often associated with sticky spots, local areas of high basal friction at the ice-bed interface known to slow the ice down (see Figure 1.2) (Alley, 1993; Anandakrishnan & Alley, 1997; Conway *et al.*, 2002; Christoffersen & Tulaczyk, 2003a, 2003b; Stokes *et al.*, 2006; Hulbe & Fahnestock, 2007; Stokes *et al.*, 2007; Winsborrow *et al.*, 2012).

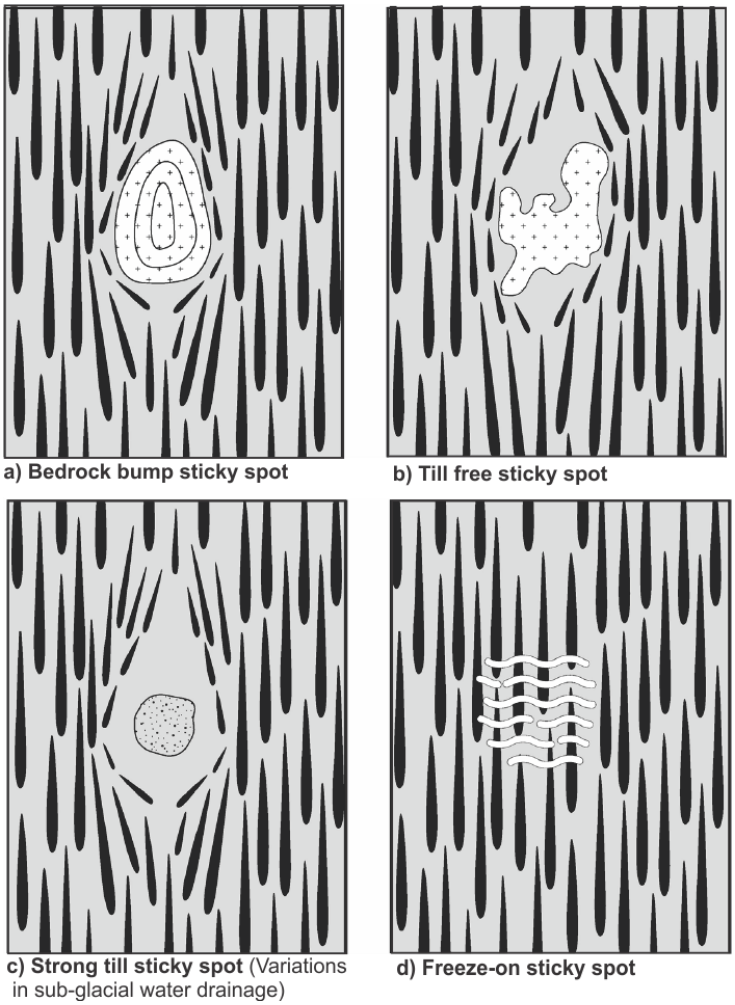


*Figure 1.2: A conceptual sketch on four different types of sticky spots, local areas of high basal friction. Black lines indicate fast ice flow. Modified from Stokes et al. (2007).*

## 1.2 Glacitectonics

Glacitectonic landforms were first studied in 1926, but did not get much attention as they were thought to be rare and many scientists doubted that glaciations could form large structural deformations (Slater, 1927; Aber & Ber, 2007). Today the importance of understanding the cause of glacitectonic deformation have grown as they occur more frequently than we first thought, especially in marine environments, and it is implied to give us important information on subglacial conditions (Sættem, 1990, 1994; Aber & Ber, 2007; Andreassen & Winsborrow, 2009; Benn & Evans, 2010; Lee & Phillips, 2013).

Aber and Ber (2007) defines glacitectonic processes as *"glacially induced structural deformation of bedrock or sediment masses as a direct result of glacier-ice movement or loading"*. Glacitectonics are signs ice flowing over hard ground of high basal friction, preventing fast ice flow, often associated with a frozen bed. Advancing of the ice cause detachment and deformation of underlying sediments or rocks when the shear stress exceeds the shear strength of the underlying material (Moran *et al.*, 1980; Bluemle & Clayton, 1984; Sættem, 1990; Ottesen *et al.*, 2005; Andreassen & Winsborrow, 2009).

Aber *et al.* (1989) classified the most common and relevant glacitectonic landforms, where characteristics as structural relief, lateral extent, primary material and morphology have been used to separate the landforms (Table 1.1) and Figure 1.3 gives a nice illustration on their morphology. However, these are ideal characteristics of glacitectonic landforms. Thus, it must be taken into account that intermediate, transitional or mixed landforms between these can exist.

| **Landform** | **Height (m)** | **Area (km$^2$)** | **Primary material** | **Primary morphology** |
|---|---|---|---|---|
| *Large composite ridges* | 100 - 200 | 20 - >100 | Bedrock | Subparallel ridge and valley system, arcuate in plan |
| *Hill-hole pair* | 20 – 200 | <1 - >100 | Variable | Ridged hill associated with source depression |
| *Small composite ridges* | 20 - <100 | 1 - >100 | Quaternary strata/drift | Subparallel ridge and valley system, arcuate in plan |

| | | | | |
|---|---|---|---|---|
| *Cupola hills* | 20 - >100 | 1 – 100 | Variable | Smoothed dome to elongated drumlin with till cover |
| *Mega-blocks/rafts* | 0 - <30 | <1 – 1000 | Bedrock | Often concealed, flat buttes or irregular hills |

*Table 1.1: Characteristics of common glacitectonic landforms based on Aber et al. (1989).*

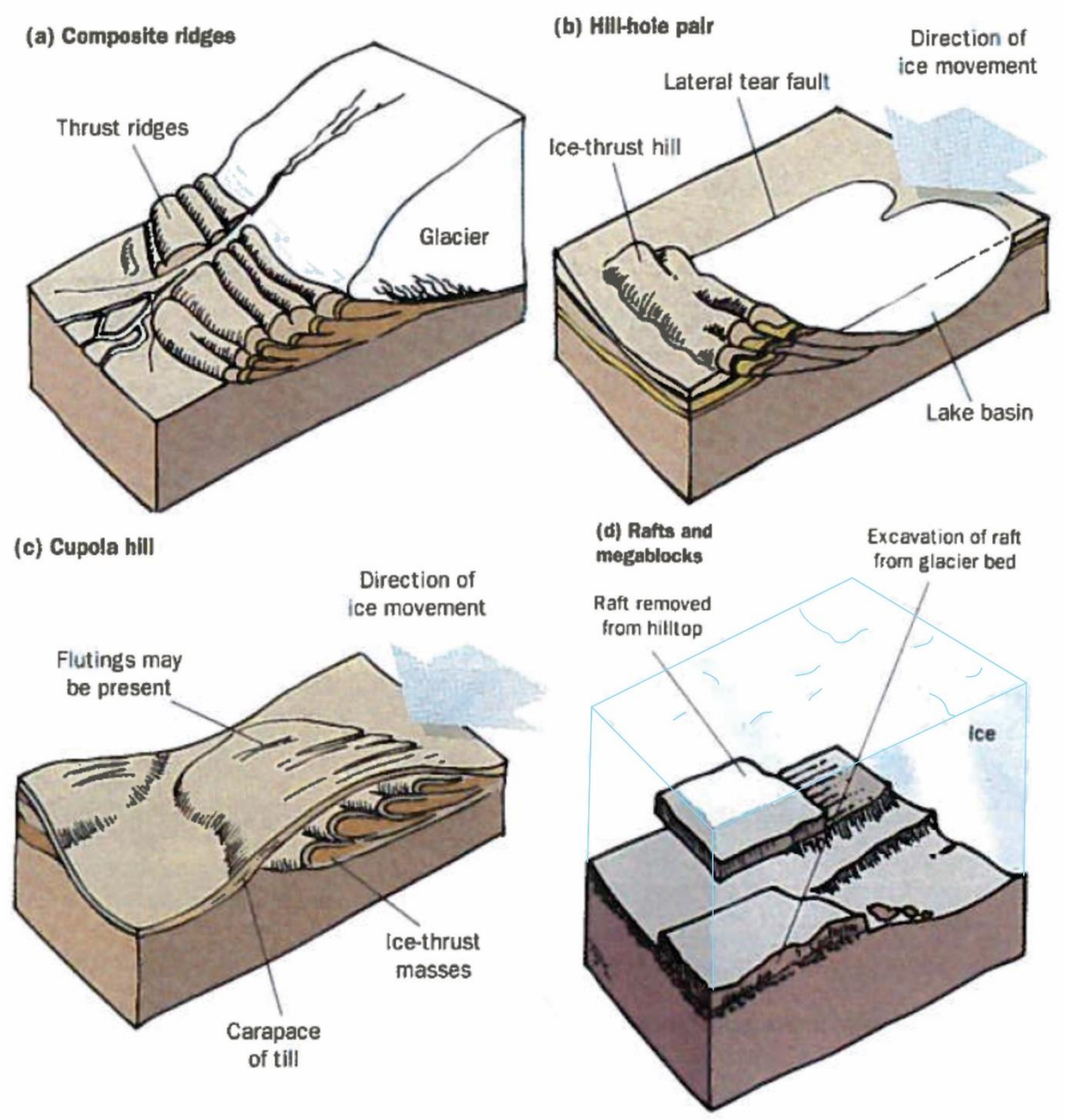


*Figure 1.3: A sketch of the main glacitectonic landforms and their characteristics. Modified from Benn and Evans (2010).*

*Composite ridges* (called transverse-ridges by Bluemle and Clayton (1984)) are composed of multiple slices of up-thrusted and folded proglacial bedrock and/or sediments often with inter- and overlain glacigenic sediments (Figure 1.3a). Composite ridges is normally composed of several smaller ridges that can build up to a couple of kilometres wide and become up to 50 km long and often arcuate of shape in map view (Bluemle & Clayton, 1984; Aber & Ber, 2007; Benn & Evans, 2010).

Bluemle and Clayton (1984) describes a *hill-hole pair* as "a discrete hill of ice-thrust material, often slightly crumpled, situated a short distance downstream from a depression of a similar size and shape" (Figure 1.3b). The hills may be found up to several kilometres downstream from its associated source depression (hole), or not even found at all. Thus, it can be imagined that a lack of a hill may be because a positive structure is vulnerable for continuing subglacial erosion. The same goes for the source depression. The depression can be filled in with younger sediments after the glacitectonic event, making it hard to recognize as a surface feature (Bluemle & Clayton, 1984; Aber & Ber, 2007; Benn & Evans, 2010).

*Cupola hills* have a smoothed, elongated and dome-like surface with a basal till layer deposited on top by over-riding ice. The shape of the hill is varying from near circular to elongated with a length of 1-15 km (Figure 1.3c) (Aber & Ber, 2007; Benn & Evans, 2010). Benn and Evans (2010) points out that cupola hills have the characteristics indicating that cupola hills are glacially overridden composite ridges or hill-hole pairs (Figure 1.3).

*Megablocks* and rafts are large pieces of detached slabs of pre-Quaternary bedrock and unconsolidated Quaternary strata, transported from their original position by glacial movement (Figure 1.3d). Its inner structure is often slightly deformed by shear zones, faults, folds, breccia and more. The megablocks are usually horizontal and often buried by thick glacigenic sediments, making it very hard to recognize them on the surface. Data from the subsurface is often needed, either by drilling or seismic data (Andreassen *et al.*, 2004; Aber & Ber, 2007; Benn & Evans, 2010).

## 1.3 Fluid flow

Vertical to sub-vertical migration of fluids are associated with pressure differences and density driven flows, were lighter fluids are *pushed* up by heavier ones (gas lighter than water and so on). In the SW Barents Sea, fluid flow features are mainly related to major faults, and there are several fault complexes where fluid migration have been observed (Dore & Jensen, 1996; Chand *et al.*, 2012; Vadakkepuliyambatta *et al.*, 2013; Edvardsen, 2015), one of them is Troms-Finnmark Fault Complex, which is oriented NE-SW through Håkjerringdjupet. Loading and unloading by several glaciations and following extensive erosion and isostatic uplift during Cenozoic is a possible reason for the majority of the fluid leakage from deeper reservoirs observed through the SW Barents Sea (Vorren *et al.*, 1991; Reemst *et al.*, 1994; Dore & Jensen, 1996; Faleide *et al.*, 1996; Vadakkepuliyambatta *et al.*, 2013).

There are many ways of recognizing indicators of fluid flow both on the seabed and in the subsurface. On the seabed, pockmarks, circular to sub-circular craters formed in soft sediments, are the most common seafloor feature related to escaping fluids, where gas flares have sporadically been observed in the water column above by echo sounders, interpreted as migrating gas bubbles (L. H. King & Maclean, 1970; Hovland *et al.*, 2002; Berndt, 2005; Chand *et al.*, 2012; Rise *et al.*, 2014). Hydrothermal vents, mud-volcanoes, submarine pingoes and methane-derived authigenic carbonates (MDAC) are other surface features often related to past or ongoing fluid flow (Aloisi *et al.*, 2002; Hovland & Svensen, 2006; Judd & Hovland, 2007; Serie *et al.*, 2012).

In the sub-surface, fluid migration and accumulations are recognized by using seismic data (Figure 1.4), or by taking samples while drilling. A seismic trace of Anomalously high amplitudes and reversed phase, compared to the seafloor reflection, are known as *bright spots* (see Figure 1.4), and is a typical indicator for the presence of fluids in the sub-surface

(Andreassen *et al.*, 2007a; Chand *et al.*, 2012; Vadakkepuliyambatta *et al.*, 2013). Other indicators of fluid migration or accumulation are acoustic *masking* – areas or vertical zones of low seismic reflectivity (Andreassen *et al.*, 2007a). *Flat spot* – indicating base of gas zone by a positive acoustic impedance contrast (Andreassen *et al.*, 2007a). Pull-down – a drop in seismic velocity causes the seismic signal to arrive later and causes a pull-down on the seismic trace (Figure 1.4).

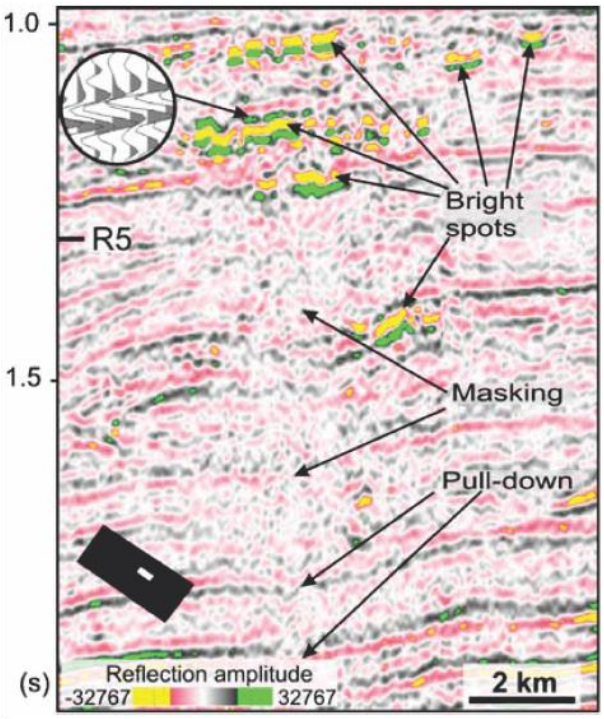


*Figure 1.4: A seismic profile which indicate bright spots and associated acoustic masking and pull-down. Modified from Andreassen et al. (2007a)*

Another indicator for fluids is a Bottom Simulating Reflector (BSR). The BSR indicate the transition between overlying high velocity gas hydrates and the underlying low velocity free gas bearing unit. Thus a BSR indicates the base of the Gas Hydrate Stability Zone (GHSZ) (see section 1.3.1) (Andreassen *et al.*, 1997; Selley, 1998; Kvenvolden & Lorenson, 2001; Berndt, 2005; Hovland, 2005; Chand *et al.*, 2012).

### 1.3.1 Gas hydrates

Gas hydrates are a solid substance composed of frozen water molecules which are physically trapping guest molecules within a cage-like structure (Figure 1.5). The guest molecules are normally methane (called methane hydrates or structure I hydrates), but may also be heavier hydrocarbons, such as butane or propane (structure II), or even $CO_2$ and $H_2S$ (Hovland, 2005; Maslin *et al.*, 2010). This is an efficient way of storing natural gas. At standard atmospheric

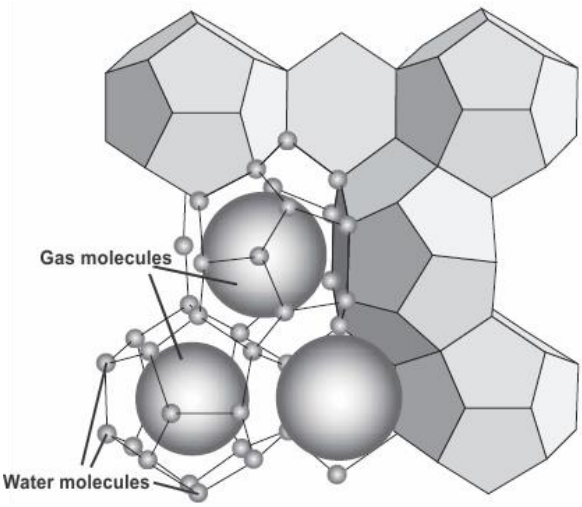


*Figure 1.5: Water molecules form a cage-like structure trapping gas mulecules within them. Modified from Maslin et al. (2010).*

temperature (20°C) and pressure (1atm), 1m$^3$ of solid methane hydrate is equivalent to 160 m$^3$ of free gas (Kvenvolden & Lorenson, 2001; Maslin *et al.*, 2010; Amundsen & Landrø, 2012). Gas hydrates are found worldwide and form in sediments below deep oceans or in polar regions, both marine and terrestrial, under supporting conditions of high pressure and low temperature (Kvenvolden & Lorenson, 2001). Their formation rely on four factors. (1) Sufficient gas flux and saturation in the sediments. (2) Sufficient water to supply the cage-structure. (3) Low temperature. (4) High pressure. Other factors which may affect the formation of gas hydrates are pore and grain sizes – hydrates are favoured in coarse sediments, rather than fine grains sediments. Chemical compositions within the sediments/fluids are important – saline water may destabilize hydrates.

The GHSZ indicate the theoretical window where the temperature – pressure conditions could sustain stable gas hydrates, and is therefore greatly affected by these factors (Figure 1.6) (Ben Clennell *et al.*, 1999; Hovland, 2005; Judd & Hovland, 2007; Chand *et al.*, 2008). Today most of the SW Barents Sea is outside the pressure-temperature conditions needed to support stable gas hydrates. However, during glaciations, a deepening in the GHSZ could occur as a result of increased pressure and lowered temperatures, induced by thick ice cover (Figure 1.6) (Chand *et al.*, 2008).

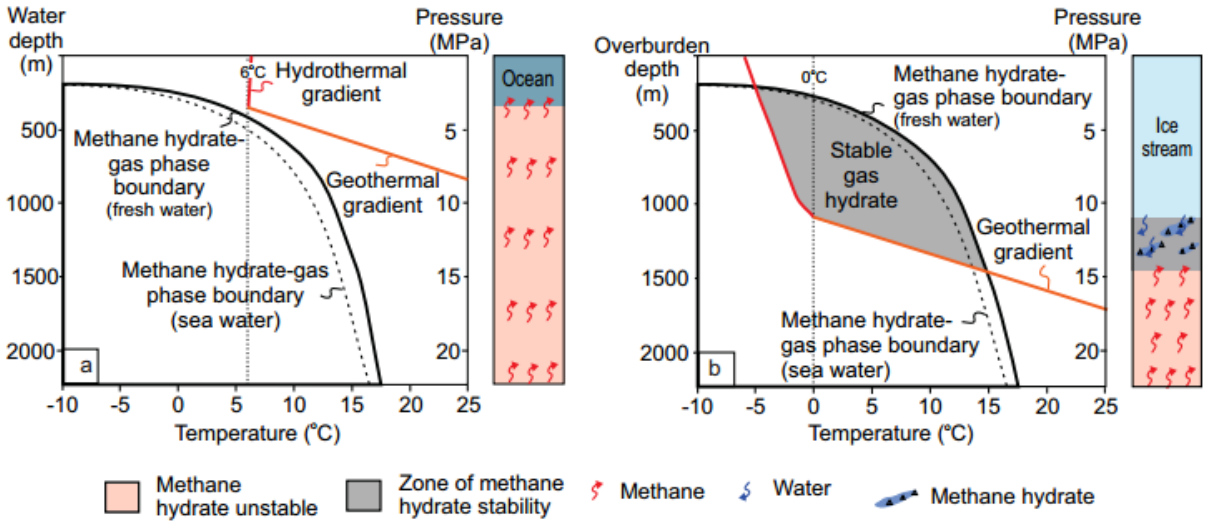


*Figure 1.6: A theoretical stability diagram for methane hydrates in a marine and subglacial environment.* ***a)*** *Today, most of the SW Barents Sea is outside of the methane hydrate stability zone.* ***b)*** *Under past glacial ice cover, high pressure – low temperature conditions could potentially create a 400 m thick gas hydrate stability zone in the SW Barents Sea. Figure from Winsborrow et al. (2016).*

# 2 Geological background

Håkjerringdjupet is located on the Norwegian Continental shelf, in the southwestern-most Barents Sea. The Barents Sea is an epi-continental shelf north of the Norwegian and Russian coast (Ramberg *et al.*, 2007). It is the largest continental shelf on Earth with an average depth of 300 m and cover an area of about 1.3 million km$^2$, limited by the deep Norwegian-Greenland sea in the west and Svalbard, Franz Josef Land and Nova Zemlya in the north and east ( Figure 1.1).

## 2.1 SW Barents Sea

The geomorphology of the SW Barents Sea is a complex seascape of shallow platforms and deeper basins, often cut by E-W to N-S trending troughs (Dore, 1995). As a part of the collapse of the Caledonides through Paleozoic to Cenozoic, the SW Barents Sea have been heavily faulted by multiple fault complexes, thereby the NE-SW oriented Troms-Finnmark Fault Complex (TFFC), crossing through Håkjerringdjupet (Figure 2.1) (Faleide *et al.*, 1984; Gabrielsen, 1984; Faleide *et al.*, 1993; Reemst *et al.*, 1994; Dore, 1995; Gudlaugsson *et al.*, 1998; Faleide *et al.*, 2008; Nøttvedt *et al.*, 2008; Indrevær *et al.*, 2013). Today these fault complexes are often associated with ongoing or past upwards fluid migration, caused by erosion and uplift before, during and after glaciations (Reemst *et al.*, 1994; Dore, 1995; Dore & Jensen, 1996; Andreassen *et al.*, 2007a; Chand *et al.*, 2012; Ostanin *et al.*, 2012, 2013; Vadakkepuliyambatta *et al.*, 2013).

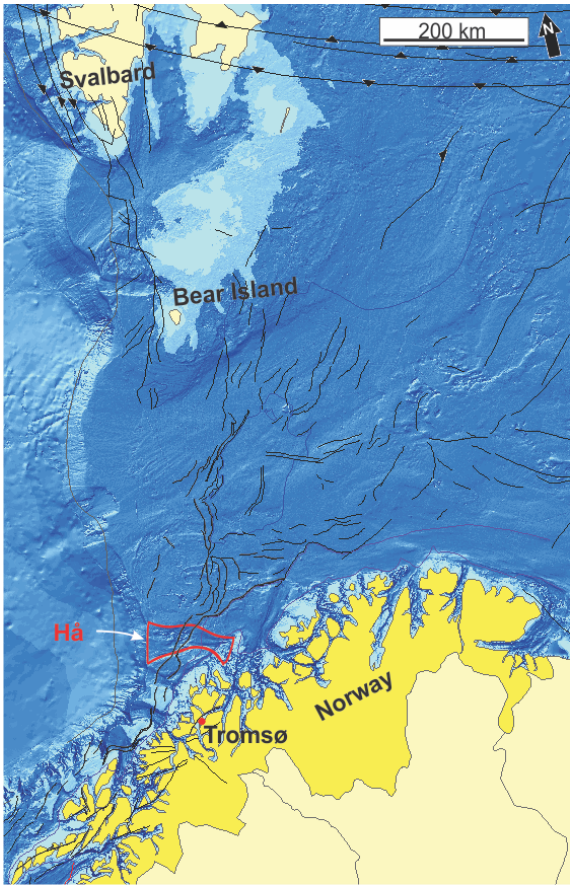


*Figure 2.1: A bathymetrical map showing the SW Barents Sea and the location of our study area (Hå = Håkjerringdjupet). Black lines indicates mapped faults and fault complexes done by NPD . Modified from Jakobsson et al. (2012).*

## 2.2 Quaternary

Through the last ~2.6 Ma (million years), a period referred to as Quaternary, the Barents Sea and Scandinavia have been covered with thick ice by several major glaciations, many extending out to the shelf edge. Through Quaternary, glaciations have eroded the mainland and the shelf, depositing thick sedimentary sequences at the slopes, off the continental margin (Vorren *et al.*, 1991; Sættem *et al.*, 1992a; Reemst *et al.*, 1994; Faleide *et al.*, 1996; Laberg & Vorren, 1996; Svendsen *et al.*, 2004; Knies *et al.*, 2009; Laberg *et al.*, 2010). Ice streams, areas of fast flowing ice, have contributed to most eroding and sediment transportation, forming troughs and through mouth fans at the shelf and shelf edge (Laberg & Vorren, 1996).

The latest glaciation of northern Europe, called the Late Weichselian, had its western maximum between 20 - 25 ka (thousand years), referred to as the Last Glacial Maximum (LGM) (Laberg & Vorren, 1996; Boulton *et al.*, 2001; P. U. Clark *et al.*, 2009; Hughes *et al.*, 2015; Patton *et al.*, 2015). Two major ice sheets dominated the SW Barents Sea, the Fennoscandian Ice Sheet (FIS) - located over the terrestrial and marine part of today's Scandinavia, and the marine-based Barents Sea Ice Sheet (BSIS) – covering most of the Barents Sea, including Svalbard. These were probably merging into one another and drained large amount of ice through ice streams towards the western margin of the Barents Sea, reaching the shelf edge, one of them Håkjerringdjupet (Sættem *et al.*, 1992a; Svendsen *et al.*, 2004; Ottesen *et al.*, 2005; Andreassen *et al.*, 2008; Ottesen *et al.*, 2008; Winsborrow *et al.*, 2010a; Nesje, 2012; Hughes *et al.*, 2015; Patton *et al.*, 2015).

The deglaciation phase in the SW Barents Sea was rapid, but halted by several episodes of ice margin stability and rapid readvance. During these periods ice streams formed grounding zone wedges, which often were overprinted by MSGLs, indicating continuously fast flowing ice (Ottesen *et al.*, 2005; Andreassen *et al.*, 2008; Ottesen *et al.*, 2008; Winsborrow *et al.*, 2010a; Winsborrow *et al.*, 2012; Andreassen *et al.*, 2014). The BSIS probably retreated more rapidly than the FIS, as it was fully marine based and ice loss contributed by calving. The last deglaciation of the Fennoscandian Ice Sheet was going slowly as it was terminating at crystalline bedrock and shallow marine banks, decreasing the loss of ice by calving and preventing an efficient discharge (Ottesen *et al.*, 2008; Winsborrow *et al.*, 2010a; Winsborrow *et al.*, 2012).

## 2.3 Study area

Håkjerringdjupet is a glacially over-deepened cross-shelf trough located in the southwestern-most Barents Sea on the Norwegian continental shelf (Figure 2.1). As seen in Figure 2.2, the trough extends 100 km in an E-W orientation, from the rough crystalline bedrock at the inner shelf and westwards across the sedimentary bedrock of the mid and outer shelf to the shelf break (Ottesen *et al.*, 2008; Indrevær *et al.*, 2013). It is 20 km wide in the east, widening towards west where it is up to 40 km wide at the shelf break. Water depths in the trough range from about 200 - 400 m, and the Quaternary sediment thickness is no more than 100 m (Vorren *et al.*, 1992). A seafloor escarpment central in the trough is related to a fault zone associated to the Troms-Finnmark Fault Complex oriented NE-SW through Håkjerringdjupet (Figure 2.2) (Gabrielsen, 1984; Gabrielsen *et al.*, 1990; Sættem, 1994; Indrevær *et al.*, 2013).

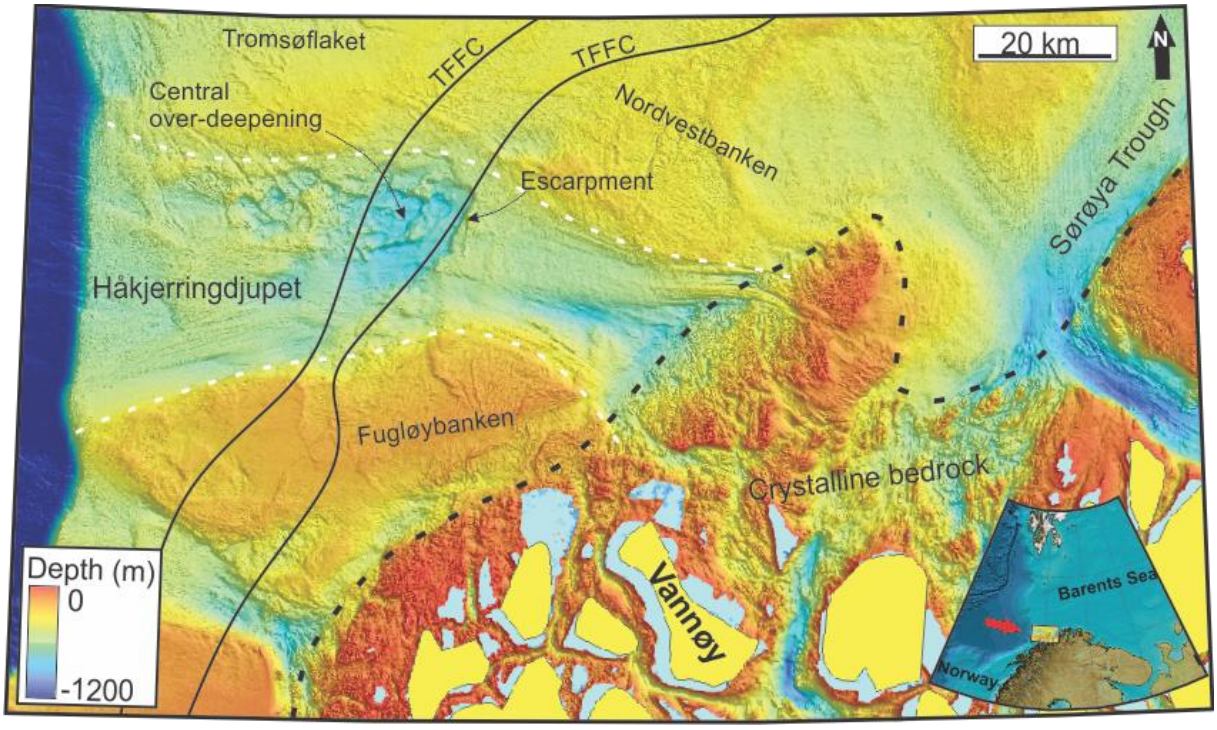


*Figure 2.2: A 50 m resolution bathymetric map of Håkjerringdjupet (within the white stippled area) and the surrounding areas. The black stippled line show the approximate location of the transition between crystalline bedrock in the east, and sedimentary rocks west of It (Ottesen et al., 2008). An escarpment is seen at the onset of the Troms-Finnmark Fault Complex (TFFC), marked with black lines. Data: Mareano/Kartverket and IBCAO.*

## 2.4 Previous work on Håkjerringdjupet

Three interesting processes have previously been documented from studies in Håkjerringdjupet: (1) ice streaming – sings of grounded, fast flowing ice with a well lubricated bed. (2) Glacitectonics – glacially displaced sediments indicates slow ice flow and

perhaps frozen ice-bed i.e. high basal drag. (3) Fluid flow – pockmarks indicates upward migration of fluids and their presence in the sub-surface. We will go a little further into the studies and their findings.

### 2.4.1 Ice streaming

Recent marine-geological studies used high-resolution multibeam bathymetry, 2D and 3D seismic to map the mega-scale glacial geomorphology of the southern Barents Sea, including Håkjerringdjupet. This study documented several flow-sets of mega-scale glacial lineations, interpreted as evidence for a paleo warm based and fast flowing ice stream (Ottesen *et al.*, 2005; Winsborrow *et al.*, 2010a; Winsborrow *et al.*, 2012). Grounding zone wedges and recessional moraines were also observed, suggesting an episodic deglaciation of the ice sheet with intermediate stagnation or readvances of the ice margin (Ottesen *et al.*, 2005; Winsborrow *et al.*, 2010a; Winsborrow *et al.*, 2012). An arcuate moraine located on the northern bank described by Winsborrow *et al.* (2012) were suggested to be deposited during deglaciation as a result of stagnation of the ice stream over rough bedrock which triggered a reorganization or flow switching of the ice flow onto the bank in the north, depositing what she called Fugløybanken lobe (Figure 2.3).

Following five-stage reconstruction of the Late Weichselian maximum and deglaciation of the southern BSIS and the northern FIS were proposed by Winsborrow *et al.* (2010a) and Winsborrow *et al.* (2012) (Figure 2.3). We will focus on the results which consider our study area. *Stage 1:* Last Glacial Maximum. Håkjerringdjupet Ice Stream extended to the shelf edge, fed by ice from the northern FIS. *Stage 2:* At the onset of deglaciation, the Håkjerringdjupet Ice Stream retreated rapid, but episodic from the shelf edge, with at least two stillstands or readvances, forming grounding zone wedges within the trough. *Stage 3:* Håkjerringdjupet ice stream continued retreating east until reaching shallower crystalline bedrock north of Vannøy, hypothetically preventing an efficient discharge. A change from rapid to slow retreat are indicated by De Geer moraines superimposed on mega-scale glacial lineations. Stagnation of the ice stream may have occurred, with a possibility of development of a frozen bed, resulting in flow switching and a short lived readvance onto the northern bank (Fugløybanken lobe in Figure 2.3). *Stage 4:* Slow retreat of the BSIS and FIS continues. All active ice drainage to Håkjerringdjupet have stopped, and Håkjerringdjupet

is ice free. *Stage 5:* Approximately 14.5 ka. The western ice margin continue to slowly retreat into the fjords of northern Norway.

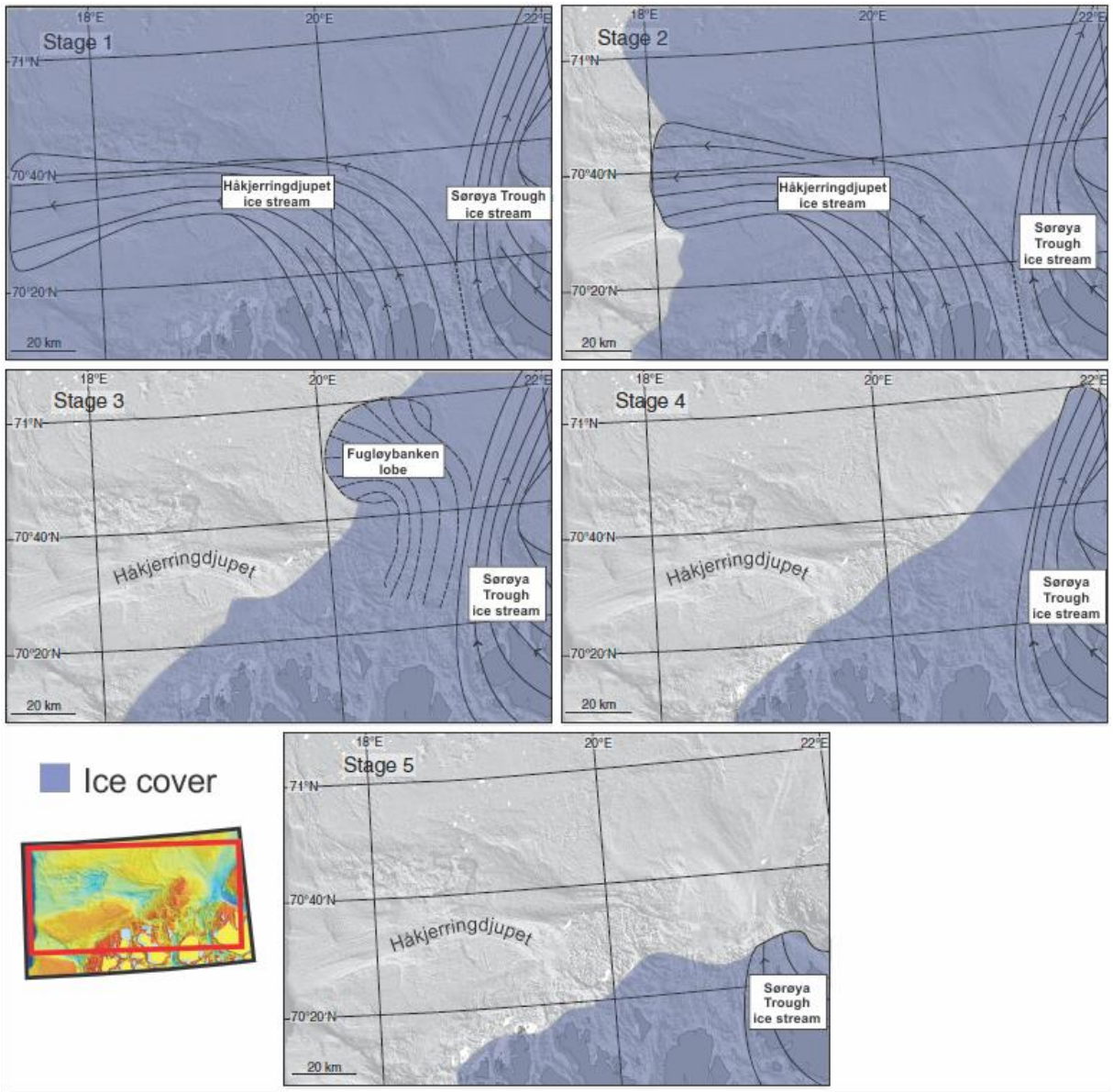


*Figure 2.3: The proposed 5 stage reconstruction of the Late Weichselian maximum and following deglaciation of Håkjerringdjupet, SW Barents Sea by Winsborrow et al. (2012). The figure show how Håkjerringdjupet was close to ice free at stage 3 and the ice stream flow switching towards what she calls Fugløybanken lobe (preferably Nordvestbanken lobe). Figure modified from Winsborrow et al. (2012).*

### 2.4.2 Glacitectonics

Previous work by Sættem (1994), observed an over-deepened area in central Håkjerringdjupet, at both sea bed and URU (Upper Regional Unconformity) level, with the use of 2D seismic. The central over-deepening were interpreted as an erosional feature, proposed to originate from one or more glacitectonic events that occurred during the last glacial period. Sættem (1994) suggested that this event squeezed old sediments of what he

called unit E and T, interpreted to be of glacigenic origin, from the over-deepened source area, depositing them as irregular hummocky hills observed further west (Figure 2.4). He also observed a resemblance to cupola-hills of similar morphology and acoustic signature described in outer Bjørnøyrenna, suggesting a similar origin. Such a glacitectonic event is believed to indicate cold-based and slow moving ice, with possibilities of basal freezing. He further observed that some of the hills had a drumlinoid shape and interpreted the glacitectonic hills to have undergone subsequently erosion and deposition of a superimposed glacigenic unit, referred to as Nordvestnaget Drift of Late Weichselian age in Rokoengen *et al.* (1979) and Sættem (1994) (see Figure 2.4). The same irregular and hummocky deposits were briefly described by Rokoengen *et al.* (1979). He suggested it may be dead ice terrain.

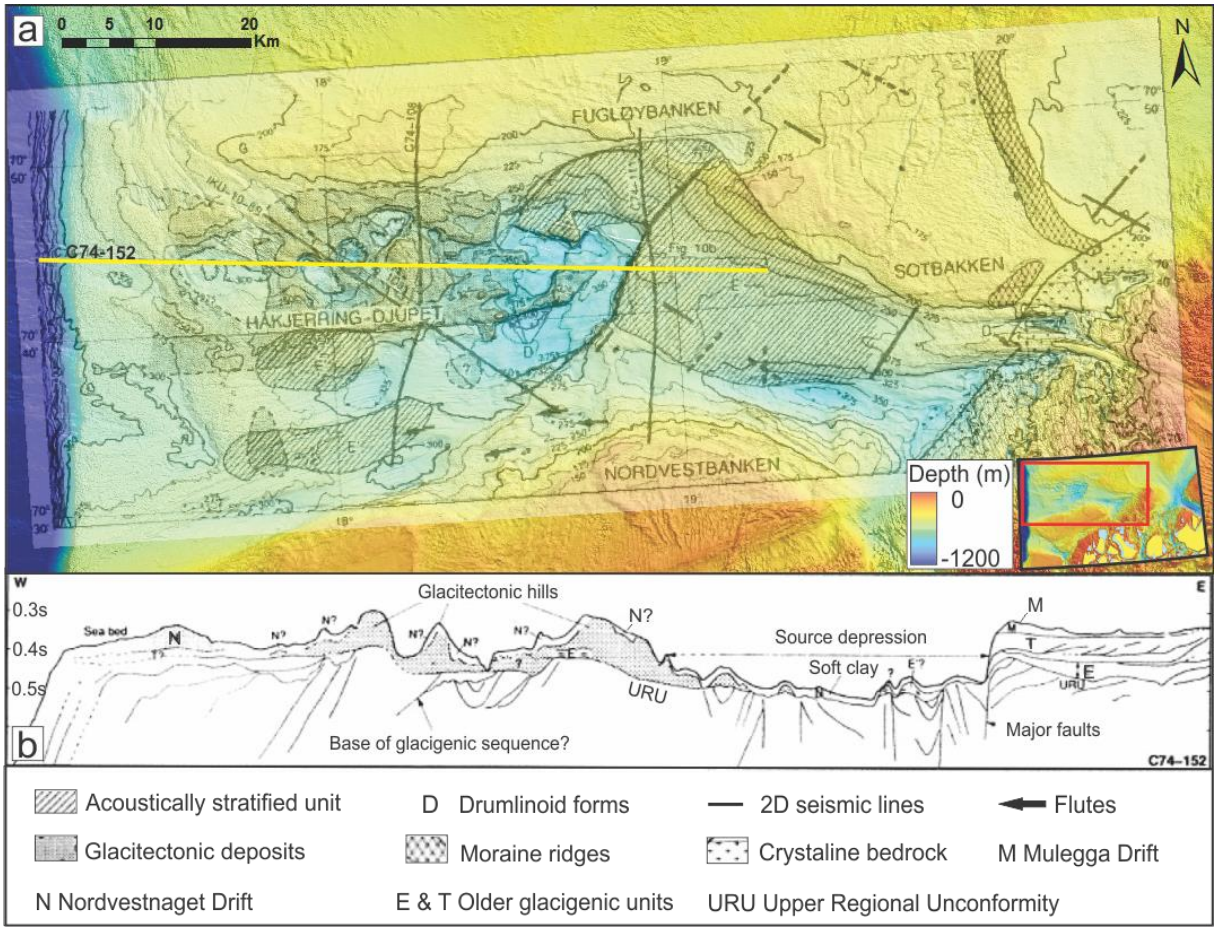


*Figure 2.4: A modified figure of the interpretation done by Sættem (1994) in Håkjerringdjupet.* ***a)*** *His interpretations is placed transparent upon bathymetry data from Mareano. Yellow line show the location of one of the seismic lines (C74-152) Sættem (1994) used to interpret glacitectonic deposits in Håkjerringdjupet.* ***b)*** *A seismostratigraphic interpretation by Sættem (1994) done along the E-W oriented seismic line C74-152 (yellow line in 'a'). Below is a legend of his interpretation. Figures are modified from Sættem (1994).*

### 2.4.3 Fluid flow

In a study on pockmarks in the southwestern Barents Sea, Rise *et al.* (2014) also included Håkjerringdjupet. The study used multibeam bathymetry (MBB), side-scan sonar (SSS) and Topas lines with limited penetration to investigate the seafloor (Figure 2.5). During this study, a Topas line from within the central over-deepening in Håkjerringdjupet revealed the uppermost unit interpreted to be postglacial glacimarine and marine sediments to be 10 – 20 m thick, some places located directly above pre-glacial sedimentary bedrock (Figure 2.5). Densities of up to 150 – 200 pockmarks per square kilometres were observed on the seabed within Håkjerringdjupet. Fewer on the lower slopes of the glacitectonic hills described by Sættem (1994) (Figure 2.5).

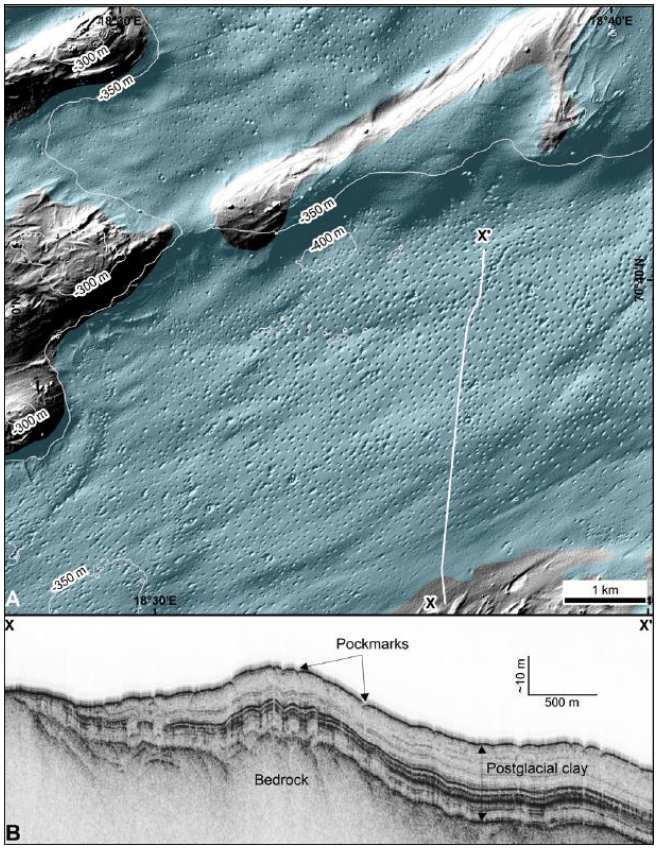


*Figure 2.5: **A)** Pockmarks in Håkjerringdjupet (blue shaded area). White line show the location of Topas line in B. **B)** Topas line of postglacial glacimarine and marine sediments with the occurrence of pockmarks on the seafloor, and no evidence of buried pockmarks. Figure from Rise et al. (2014).*

Pockmarks are indicators of presence of fluids within the sediments and escape of these fluids through the seafloor and into the water column (Berndt *et al.*, 2003; Chand *et al.*, 2009; Chand *et al.*, 2012; Ostanin *et al.*, 2013). Various data interpreted by Rise *et al.* (2014) suggested that formation of pockmarks might be due to melting of gas hydrates releasing free gas after deglaciation of the ice sheets and inflow of warmer water masses. However, this was not specified for Håkjerringdjupet. Further the paper concludes that: The occurrence of pockmarks seem to be in areas of soft postglacial glacimarine and marine sediments, and small pockmarks (20-50 m wide and 2-4 m deep) are very common in the southern Barents Sea. There were no evidence that the formation of pockmarks were caused by catastrophic outbursts, and they occur with and without shallow gas identified on seismic data. However, the source of the gas causing the pockmarks are suggested to origin from

deeper sedimentary bedrock, rather than biogenic gas from Quaternary deposits (Rise *et al.*, 2014).

### 2.4.4 Summary

Previous work from Håkjerringdjupet have done interesting documentations of landforms related to past glacial dynamics and fluid flow. However, no study have investigated the potential relationship between these processes until now. This study aim to investigate, in detail, the interaction between ice streaming, glacitectonics and fluid flow in Håkjerringdjupet, using high resolution multibeam swath bathymetry and 2- and 3D seismic datasets.

# 3 Data & methods

This study uses high resolution multibeam swath bathymetry and 2- and 3D seismic data to investigate glacial landforms on the seabed and in the subsurface, and their possible interaction between fluid flows. This chapter will present our data, starting with the seismic.

## 3.1 Seismic data

A total of 80 regional two-dimensional (2D) seismic lines divided on six surveys are used in this project, acquired by various companies and projects now publically available. The location of the 2D regional lines is shown in Figure 3.1 (black lines). These generally have a lower resolution than the 3D seismic (Table 3.2), but cover a larger area, and are here used to gain an understanding of the regional seismic stratigraphy of the study area.

We used one 3D seismic cube, survey FP12_PRCMIG acquired by TGS. This survey is located in central Håkjerringdjupet (red polygon Figure 3.1). Our 3D seismic dataset cover a smaller area of a closely spaced data volume and give us increased resolution to help the interpretation of the subsurface (Table 3.2) (Brown, 1999). The 3D survey will be the most important resource of subsurface seismic data in this thesis as it covers our core area.

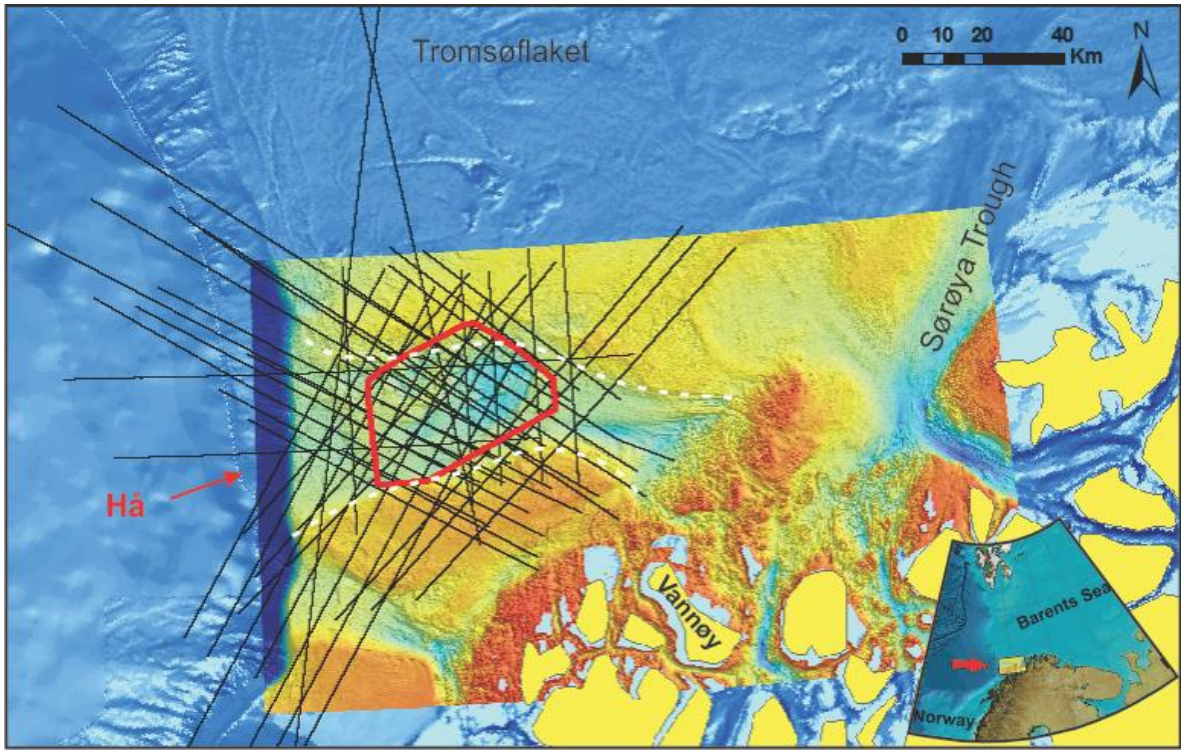


*Figure 3.1: 2D seismic data (black lines) available for this study cover a large regional area, both within the trough and the adjacent banks. The 3D seismic survey FP12_PRCMIG is located within the red polygon and covers our core area. White dotted lines indicate the margins of the trough. Hå = Håkjerringdjupet.*

### 3.1.1 Acoustic contrasts & seismic reflectors

In this thesis we will use the terms acoustic impedance and reflection coefficient to describe the acoustic contrast between seismic units. In the light of that, we will briefly describe these terms.

Sediments and rocks in the subsurface all have a specific acoustic properties as a result of density and sonic velocity, referred to as *acoustic impedance (AI)* (density x velocity). Every seismic reflection or reflector is a result of density-velocity contrasts between two layers and is referred to as *reflection coefficient (RC)* (Figure 3.2). The reflection coefficient can be calculated as follows: $RC = AI_2 – AI_1/AI_2 + AI_1$, where $AI_1$ is the acoustic impedance for the upper layer and $AI_2$ for the lower. The reflection coefficient can be positive or negative depending on whether softer rock overly harder rocks (positive) or vice versa (see Figure 3.2) (Anstey, 1977; Brown, 1999; Simm & Bacon, 2014).

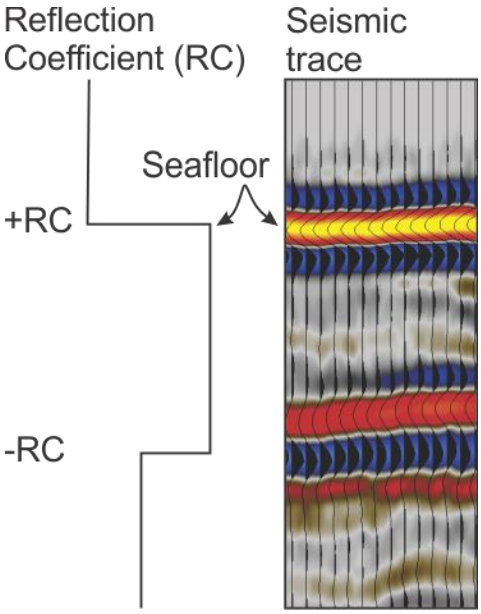


*Figure 3.2: Contrasts in acoustic impedance between low density/velocity saline water and relative high density/velocity sediments at the seafloor cause a positive RC, while a deeper layer have a negative RC – indicating harder rocks above softer ones.*

### 3.1.2 Polarity standards

Our seismic datasets have been processed in various ways. We therefore have datasets in zero and minimum-phase, in both normal and reversed polarities. As this could affect our interpretation if we are not aware of the differences, we want to briefly introduce the polarity standards of our datasets.

The SEG (Society of Exploration Geophysicist) polarity standard of Sheriff (2006) is used to define polarity and phase of seismic reflections. SEG defines a wavelet with a positive central amplitude (a black peak) that corresponds to an increase in acoustic impedance, or positive reflection coefficient, as a zero-phase wavelet with normal polarity (Figure 3.3). If the opposite was true – a negative central amplitude (a white trough) corresponding with a positive reflection coefficient, it is defined as a zero-phase wavelet with reversed polarity, as is the case in the 3D survey FP12_PRCMIG (Table 3.1 & Figure 3.3).

For a minimum-phase wavelet with normal polarity (Figure 3.3), a reflection caused by a positive reflection coefficient will start with a negative amplitude (white trough) at the intersection, followed by a positive greater amplitude (black peak). A reversed minimum-phase wavelet will show the opposite – starting with a positive amplitude (black peak) followed by a greater negative amplitude (white trough). A list of the surveys and their respective polarity and phase is shown in Table 3.1.

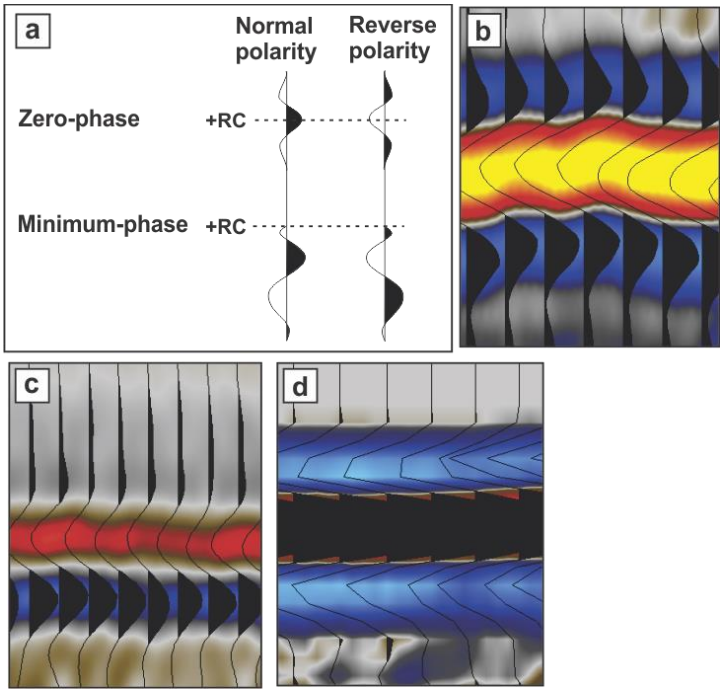


*Figure 3.3: **a)** Polarity conventions used for plotting of seismic signals. Figure modified from Sheriff (2006). **b)** An example from the 3D seismic survey FP12_PRCMIG at the seafloor of zero-phase, reverse polarity. **c)** The seafloor of a 2D seismic line show an example of minimum-phase wavelets with reverse polarity. **d)** Zero-phase wavelets with normal polarity at the seafloor (+RC). The colouring of the seismic wavelets is chosen so a blue – red/yellow – blue reflection signal (b & d) corresponds to a positive reflection coefficient for any zero-phase wavelet, regardless of polarity.*

| Acquisition method (survey) | Survey name | Polarity | Phase | Streamline orientation |
|---|---|---|---|---|
| 3D | FP12_PRCMIG | Reverse | Zero-phase | E-W |
| 2D | IKU-TR-89 | Normal | Zero-phase | NW-SE |
| 2D | NH-9703 | Normal | Zero-phase | N-S, NW-SE, NE-SW & NNE-SSW |
| 2D | TGS-90 | Normal | Zero-phase | NNE-SSW, NE-SW & NW-SE |
| 2D | NPD-TR-85 | Normal | Zero-phase | N-S, E-W, NE-SW & NW-SE |
| 2D | MN-87-6 | Reverse | Minimum-phase | NE-SW & NW-SE |
| 2D | T-89 | Reverse | Minimum-phase | NE-SW & NW-SE |

*Table 3.1: A summary of the surveys available for this thesis and their polarity, phase and inline orientation.*

### 3.1.3 Seismic resolution

Seismic resolution is defined as the ability to distinguish between two individual reflectors, and has both vertical and horizontal aspects to it (Anstey, 1977; Brown, 1999). The

resolution of seismic data is dependent on the seismic wavelength, which is a quotient of velocity over frequency of a seismic pulse, as seen in Equation 3.1.

*Equation 3.1*

$$\lambda = \frac{v}{f}$$

*λ = Wavelength (m)*

*v = Velocity (m/s)*

*f = Frequency (Hz)*

As the seismic pulse travels deeper, the velocity is expected to increase with depth as the rocks become more compacted, while the frequency will decrease as the higher frequencies are attenuated. As a result the wavelength will increase and therefore the resolution will decrease proportional with depth as shown in Figure 3.4 (Anstey, 1977; Brown, 1999; Rafaelsen, Unpublished).

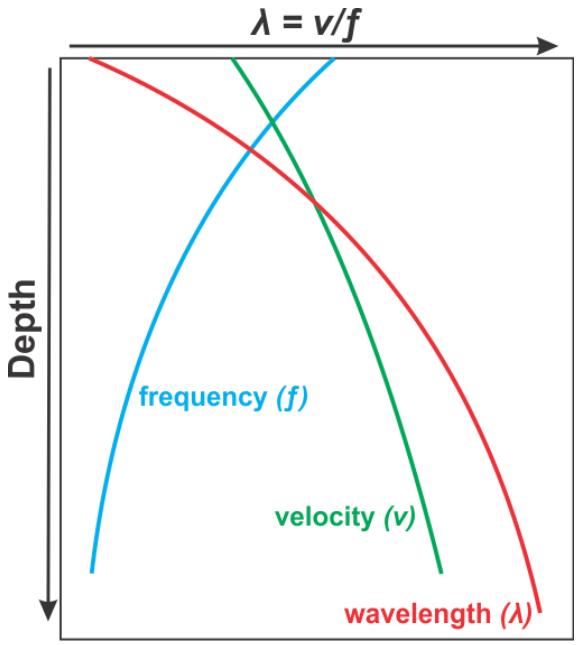


*Figure 3.4: Frequency and velocity changes with depth, increases the wavelength, resulting in decreased seismic resolution. Figure modified from Brown (1999).*

*Vertical resolution*

The vertical resolution is a measure of the size an object or a thinning bed need to be in order to be detected by seismic data, and is given by the Equation 3.2 (Brown, 1999; Rafaelsen, Unpublished).

*Equation 3.2*

$$Rv = \frac{\lambda}{4}$$

*Rv = Vertical resolution (m), λ = Wavelength (m)*

Two reflectors can be recognized and separated from each other if they are separated by, or more than, one quarter of the wavelength, which is the limit of separability. If the reflectors are separated by less than one quarter of a wavelength the wavelets will interfere destructively (i.e. attenuate) until the reflecting signal reach the limit of visibility and is obscured by the background noise normally at 1/32 wavelength (Brown, 1999).

*Horizontal resolution*

When speaking of horizontal resolution, the concept of the Fresnel zone is commonly used, and is a measure of the lateral distance two adjacent reflectors must have to be detected as two separate objects on the seismic. The Fresnel zone is defined by Chaouch and Mari (2006) as "the subsurface area that reflects energy that arrives the receivers (geo/hydrophones) within a time delay of a half-cycle of the dominant period (T/2)". The radius of the Fresnel Zone increases with depth, increased velocity and lower frequency (Equation 3.3), i.e. increasing depth, velocity and lower frequency will therefore decrease the horizontal resolution (Sheriff, 1985; Brown, 1999). For un-migrated seismic data, the radius of the Fresnel zone is given in Equation 3.3:

*Equation 3.3*

$$rf = \frac{v}{2}\sqrt{\frac{t}{f}}$$

*rf = Fresnel zone radius (m)*

*v = Velocity (m/s)*

*t = two-way travel time (s)*

*f = Dominant frequency (Hz)*

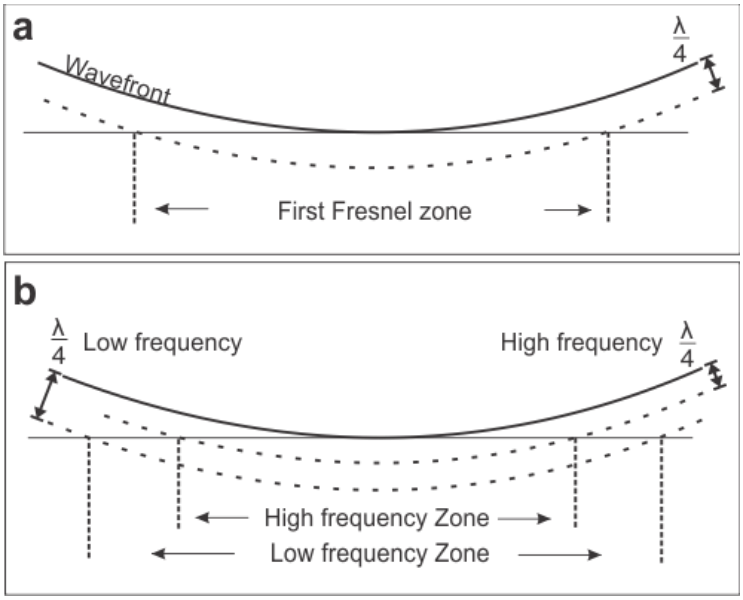


*Figure 3.5: **a)** The Fresnel Zone is defined as the area from the point of first reflection interface of the wavefront, limited to the area covered by the wavefront quarter of a wavelength later at the same reflector. **b)** A sketch that show how frequency (i.e. therefore also wavelength) affects the radius of the Fresnel Zone. High frequency increase horizontal resolution by decreasing the radius. Figures modified from Sheriff (1985).*

Migration of seismic data improve the horizontal resolution by shrinking the Fresnel zone. In 2D-seismic data the Fresnel zone can only be collapsed in the inline direction, resulting in a highly elliptic Fresnel zone (Figure 3.6). 3D- seismic surveys can reach a much higher resolution by collapsing the Fresnel zone in all directions until focused at a small circular area (Figure 3.6) (Brown, 1999). The horizontal resolution for migrated seismic data is given by Equation 3.4.

*Equation 3.4*

$$Rh = \frac{\lambda}{4} = \frac{v}{4f}$$

*Rh = Horizontal resolution (m)*

*λ = Wavelength (m)*

*v = Velocity (m/s)*

*f = Frequency (Hz)*

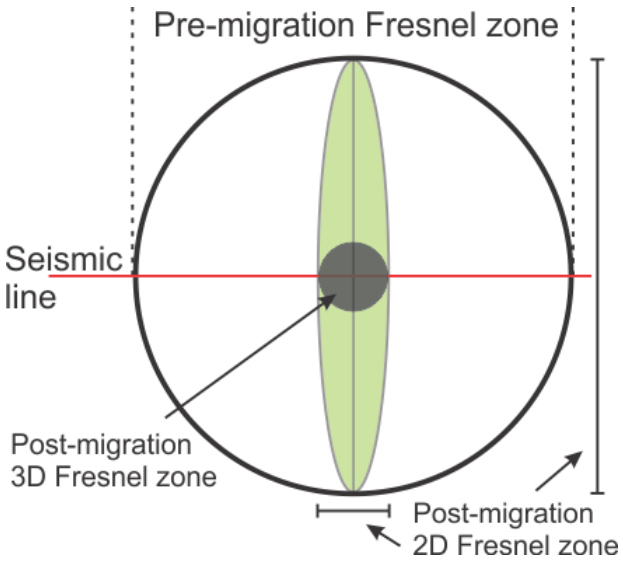


*Figure 3.6: An illustration of the Fresnel zone before and after migration of the seismic. The green shaded area show how the 2D seismic data only can be collapsed in an inline direction (red line), while the 3D seismic (grey shaded area) is collapsed in all directions and reduces the Fresnel zone to a small circle, increasing horizontal resolution. Figure modified from Brown (1999).*

In order to calculate our respective resolutions the software SeiSee were used to extract the dominant frequency from 2D seismic lines and 2D converted seismic lines from the 3D survey. One seismic line were used from each survey, and the frequency is for the whole section. Smaller sampling of frequencies within one line caused large variabilities in measured dominant frequency. These frequencies are plotted in Table 3.2 below and were used to calculate the resolution for each seismic survey with an estimated velocity of 1500 m/s for saline water and shallow sediments, at an average depth of 400 ms TWT, equivalent to approximately at or close to the seafloor. The 3D survey FP12_PRCMIG, our most important seismic dataset, seem to have a vertical and horizontal resolution of 14 m post migration (Table 3.2). We have not calculated the resolution at any deeper strata but we assume the resolution, both vertical and horizontal, will decrease drastically when the velocity increase by depth and the frequencies are attenuated.

| Survey | Dominant Frequency (*f*) (Hz) | Wavelength (*λ*) (m) | **Vertical resolution (Rv) (m)** | Horizontal resolution pre-migration (rf) (m) | **Horizontal resolution post-migration (Rh) (m)** |
|---|---|---|---|---|---|
| FP12_PRCMIG | 27 | 55 | **14** | 91 | **14** |
| IKU-TR-89 | 40 | 37 | 9,5 | 75 | 9,5 |
| NH-9703 | 18 | 83 | 21 | 111 | 21 |
| TGS-90 | 15 | 100 | 25 | 122 | 25 |
| NPD-TR-85 | 22 | 68 | 17 | 101 | 17 |
| MN-87-6 | 17 | 88 | 22 | 115 | 22 |
| T-89 | 7,5 | 200 | 50 | 173 | 50 |

*Table 3.2: This table shows the dominant frequency measured using SeiSee and the calculated relevant resolution for each survey available for this project, using 1500 m/s as an estimated velocity for saline water and shallow sediments at an average depth of 400 ms TWT. The resolution of the 3D survey FP12_PRCMIG is highlighted with bold font.*

### 3.1.4 Seismic interpretation

All seismic datasets were visualized and interpreted using Petrel 2014 software by Schlumberger. The Petrel software comprise several tools used to extract information from 2D and 3D seismic, e.g. interpreting of horizons, creating attributes of horizons and volumes and time-slices. On a seismic profile, the Y-axis shows the depth, measured in time. The time a seismic wave uses traveling from the source, down to a reflector and up to the hydrophones is referred to as two way travel time (TWT). The depth on seismic profiles are therefore normally given in milliseconds as TWT and with a negative sign (e.g. -450 ms TWT). The X-axis in a seismic profile show the lateral extension of a seismic line and is given in, preferably, km.

We convert the sonic two-way travel time of shallow seismic units into approximate real thickness by using half the measured two-way travel time converted into seconds, then multiplied by an average velocity of 1,500 m/s. we have used an assumed average sonic velocity of 1,500 m/s for saline water and shallow sediments. This means, if a unit is 100 ms TWT thick, this is approximately equal to a 75 m thick unit (0,05s x 1,500 m/s). 100ms = 0,1s. Because it is two-way travel time we divide the time depth by two, as we only want to measure the thickness “one way” (0,1s/2 = 0,05s). This method will only work on shallow buried seismic units as the velocity is assumed to increase with depth, thus the margin of error will increase (Figure 3.4).

## 3.2 Multibeam Swath Bathymetry

This study uses high resolution multibeam swath bathymetry (MBB) to investigate the seafloor in great detail (Figure 3.7). The data were collected and distributed by Mareano, a cooperation program between the Institute of Marine Research (Havforskningsinstituttet), Geological survey of Norway (NGU) and the Norwegian Hydrographic Service (Kartverket sjødivisjon). The data is provided in three resolutions of 50 m, 25 m and 5 m (Figure 3.7). The 50 m resolution bathymetry extends over the whole of Håkjerringdjupet, including the surrounding banks and nearby troughs and islands, and covers in total an area of approximately 20.000 $km^2$ (Figure 3.7). The extent of the other two datasets of 25 m and 5 m is smaller (~4.000 $km^2$), and cover only the most central part in Håkjerringdjupet, and portions of the shallower banks located north and south (Figure 3.7).

Different resolutions and colour tables are used depending on what we want to show. 50 and 25 m resolution can be used to show larger seafloor features. While the 5 m resolution is needed to show smaller features in detail. Figure 3.8 show an example on how important the resolution are when interpreting smaller features on the seafloor.

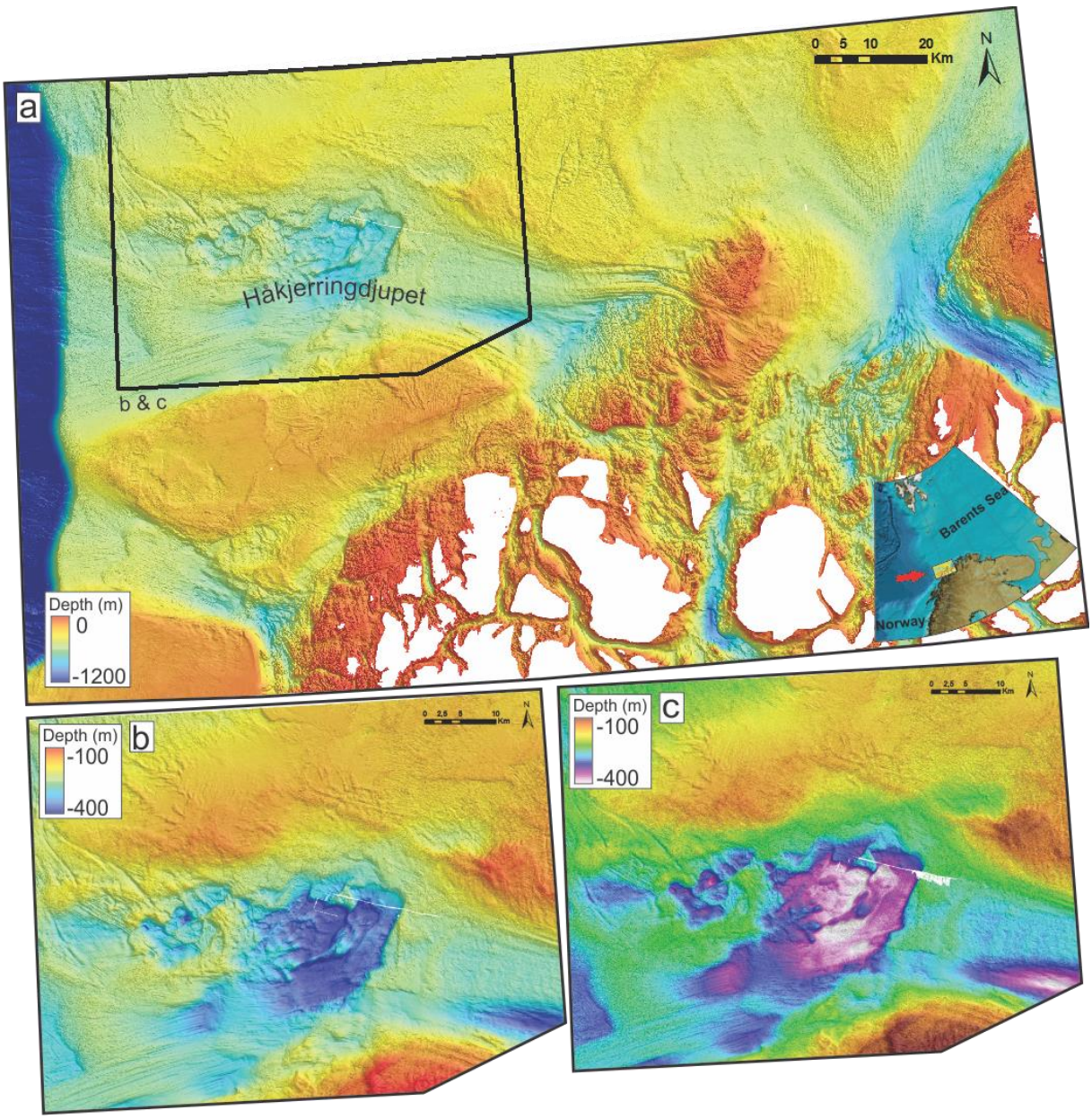


*Figure 3.7: The multibeam swath bathymetry data have been provided by Mareano in three different resolutions of 50, 25 and 5m.* ***a)*** *50 m resolution. Covers a large area of ~20.000 km², including the shelf edge in the west, troughs and shallower banks. The black box indicate the location and extent of the 25 and 5 m resolution datasets in 'b' and 'c'.* ***b)*** *25 m resolution. Cover the most central part of Håkjerringdjupet and parts of the shallower banks in the north and south. Cover an area of ~4.000km².* ***c)*** *5 m resolution. Cover the same area as the 25 m resolution in 'b'. The Colour scale were changed to show the various colours used in this thesis. Bathymetry data: Mareano/Kartverket.*

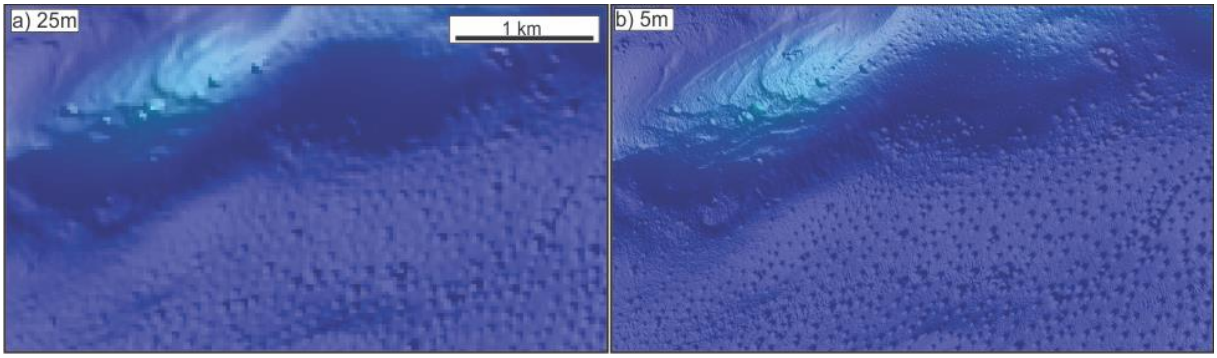


*Figure 3.8: An example on how the same seafloor appear on the different resolution while zooming in.* ***a)*** *25 m resolution look very blurry, only the larger seafloor features can be distinguished.* ***b)*** *This image show a clear picture of the seafloor in 5 m resolution. Seafloor depressions can easily be distinguished and recognized.*

### 3.2.1 Interpretation tools

Esri, ArcMap 10.3 have been used to map, interpret and document most of the features located at the seafloor in Håkjerringdjupet. The software is complex but extremely useful and allow you to do measurements and modify your data to get the best interpretation and documentation needed. In this study we have used it a great deal to map glacial landforms and evidence for fluid flow on the seafloor. We have also done correlations between our seismic data and our MBB data, helped by tools like georeferencing, which allow us to insert new datasets (e.g. maps) into ArcMap, pinpointed to its correct location.

We have used Fledermaus 7.4.1d as a tool to visualize our MBB data in 3D-view, providing us with a better understanding of our study area. It also allow us to make depth profiles, which have been very useful to measure depths of small features like pockmarks, or make longer depth profiles along the trough.

# 4 Results

This chapter will focus on documenting our observations from the study area. Observations and interpretation will be done using multibeam swath bathymetry and 2- and 3D seismic datasets, starting with the stratigraphy of Håkjerringdjupet.

## 4.1 Stratigraphy of Håkjerringdjupet

Håkjerringdjupet is an over-deepened trough, pointing to an origin of glacial erosion. The stratigraphy is here divided into one horizon and two units considered important. Standards for reflection geometry determination by Veeken (2007) and Veeken and Moerkerken (2013) are used when interpreting seismic sections. The 3D survey FP12_PRCMIG will provide most of the seismic profiles used in this chapter. However, to provide an extended understanding of the study area, 2D seismic datasets will be used wherever it seems suitable.

Most units are buried at relatively shallow depths, and many of them probably terminating at, or close to the seafloor at one or several locations. However, a thin layer of postglacial sediments, mainly glacimarine stratified clay (Rise *et al.*, 2014) is probably covering the surface of the whole area, according to Rokoengen *et al.* (1979) and Sættem (1994).

Figure 4.1 show the locations of seismic profiles used to describe and interpret the stratigraphy of Håkjerringdjupet.

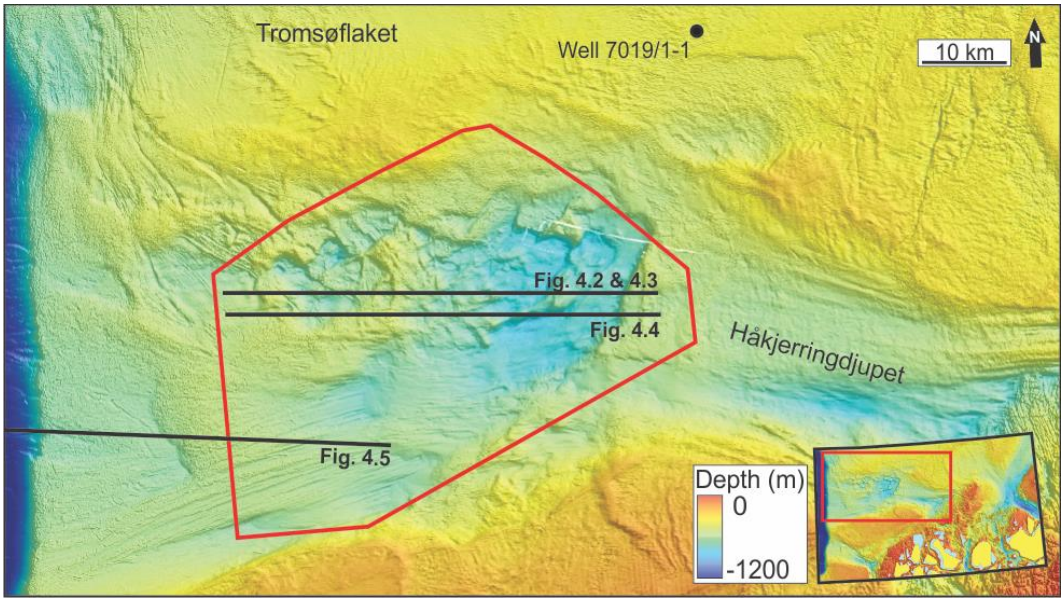


*Figure 4.1: A bathymetric map with an overview of the locations of the seismic profiles used to describe the stratigraphy of Håkjerringdjupet. Red polygon show the extent of the 3D-survey (xlines and inlines).*

### 4.1.1 Lower unit & erosional horizon: Pre-glacial sedimentary rock & URU

*Description*

The lowermost unit that can be recognized in the subsurface within the trough is a unit of highly variable seismic reflectivity. Deep within the unit, the reflectors tend to be weak, discontinuous and chaotic (circle 1. Figure 4.2), with a few exceptions of continuous relatively high amplitude reflectors (circle 2. Figure 4.2). At shallower depths, the reflectors tend to have higher amplitudes and are more continuous and sub-parallel to each other (circle 3. Figure 4.2). At shallow depths very east in the trough and 3D survey, this unit seem to be slightly dipping towards west, except where reflectors are tilted between vertical offsets (i.e. faults, see section 4.2.1 & Figure 4.2).

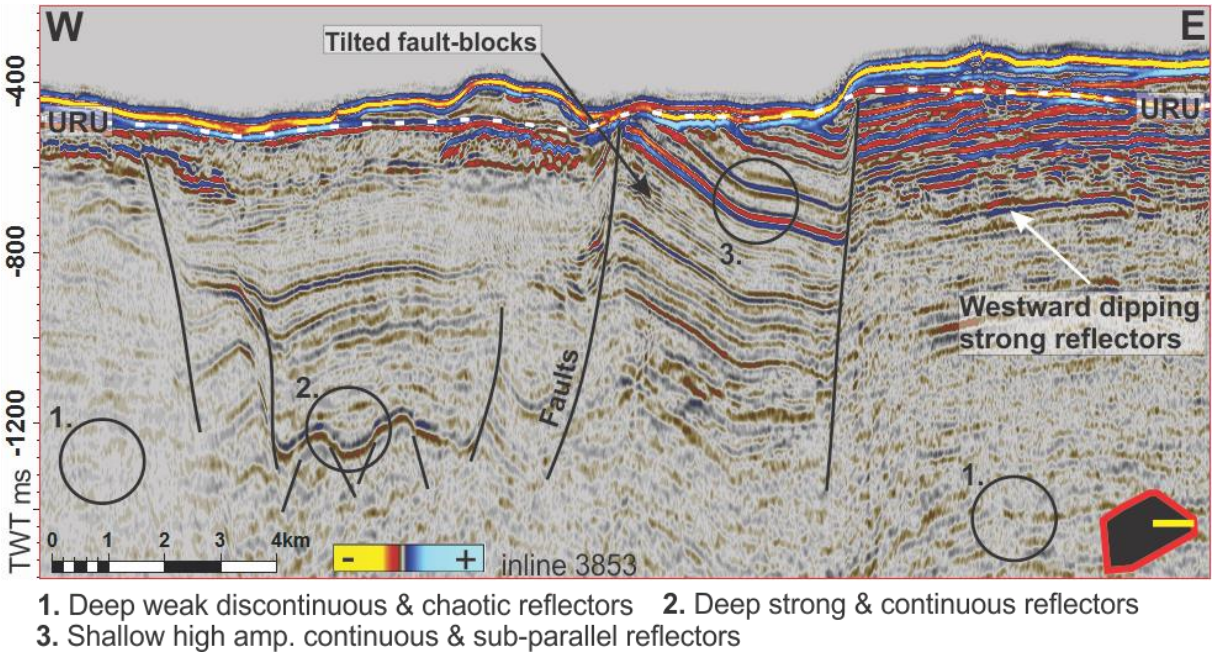


*Figure 4.2: Dipping and tilted reflectors of the lower unit shown in a seismic profile from within the 3D survey. Their seismic trace is changing with depth as seen in circle 1, 2 & 3, where the seismic amplitude is strongly attenuated with depth. URU is located along the white stippled line. Location and extent of the seismic line is shown in the black polygon (bottom right) and Figure 4.1.*

The whole unit seem to cover a regional area as it can be traced for large distances within the study area. At several locations within the trough, dipping reflectors are abruptly terminating at its upper reflector (white dashed line Figure 4.2).This unit's upper boundary/reflector is a relatively shallow buried reflector, mostly between 50 – 150 ms below the seafloor (~40 - 110m), and very uneven (white dashed line in Figure 4.2).

The upper reflector of this buried unit has a mostly strong acoustic impedance. However, the reflection coefficient (RC) experiences phase shifting centrally in the trough, and therefore, has both positive and negative reflection coefficient (Figure 4.3). At the western half of survey FP12_PRCMIG, this buried horizon have a strong negative reflection coefficient compared to the seafloor, indicating a contrast in acoustic impedance, were the overlying unit have a higher density/velocity than the unit below (Figure 4.3). A phase reversal to a positive reflection coefficient occurs within the central seafloor depression in the trough, where the reflector have a positive RC east of here (Figure 4.3). This indicates that the overlying unit have a lower density/velocity than the underlying unit, e.g. reversed from the latter.

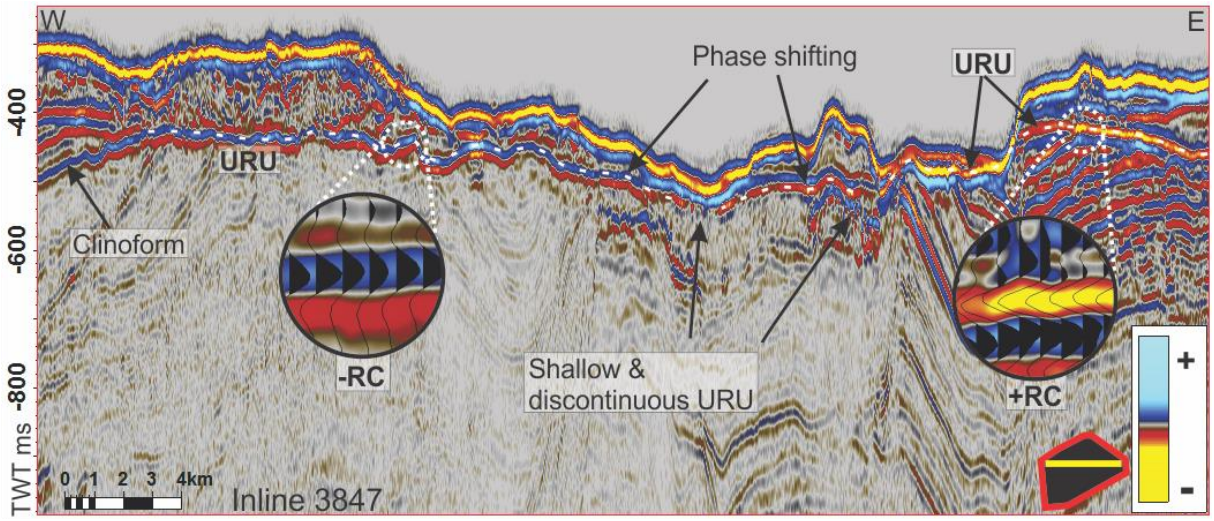


*Figure 4.3: A vertical exaggerated seismic profile from the 3D survey FP12_PRCMIG. This line goes through the whole survey, showing how the phase of the seismic wavelets are shifting from east to west in the trough. Location of the seismic line shown in Figure 4.1.*

*Interpretation*

Based on the unit's stratigraphic location and internal sub-parallel reflection pattern, the interpretation of this unit is that it is probably a unit of buried sedimentary rock of pre-Quaternary age. The weak reflections observed deep within this unit is implied to be caused by attenuation of the seismic signal with depth (see section 3.1.3). The same interpretation was done by Sættem (1994) in a study from the same area, and a similar unit have been interpreted likewise in several studies at different locations in the SW Barents Sea (Rokoengen *et al.*, 1979; Vorren *et al.*, 1991; Andreassen *et al.*, 2007a).

This unit have a regional prevalence and its inner dipping reflectors are abruptly terminating at its upper boundary. This unit's upper boundary or reflector have therefore been interpreted to be an erosional upper regional unconformity (URU), separating the lower pre-glacial sedimentary rocks from overlying glacial sediments, indicating the maximum erosion during the past glaciations in the area. This interpretation coincides with Sættem (1994) and is a regionally extensive unconformity correlatable across much of the Barents Sea (Solheim *et al.*, 1996).

Inside the major central depression URU appear discontinuously and is located very shallow, making the interpretation of the horizon difficult at this location (Figure 4.3). Lack of any strong reflectors from a buried horizon below the seafloor and comparison with earlier work by Sættem (1994), led to the interpretation that URU is located just below the seafloor at this location. This indicates a shallow termination of the pre-glacial sedimentary rock probably just covered by a thin layer of soft sediments, as mentioned by Rise *et al.* (2014), and further supports that this is an erosional boundary.

In western Håkjerringdjupet, as you approach the shelf edge, URU is more difficult to interpret as several reflectors are dipping towards west (left in Figure 4.3, see section 4.1.2).

### 4.1.2 Upper unit: Glacimarine deposits

*Description*

The upper unit is deposited sub-parallel upon URU, and its top is terminating at the seafloor, showing a positive reflection coefficient. Its vertical extent is highly variable within the trough, alternating between absent to almost 150 ms TWT thick (equivalent to ~110m), often with a rough surface (Figure 4.4). In comparison to the adjacent banks, the depths of these deposits are found to be 250 ms TWT on Tromsøflaket in the north, and 200 ms TWT on Fugløybanken in the south (respectively ~190 – 150 m), with very little surface variations.

Its internal reflection signals are highly variable and rapidly changing. Depending on location within the study area, they alternate between acoustically horizontal and continuous (acoustically stratified) to discontinuous and chaotic with both strong and weak amplitudes, even seismically transparent (Figure 4.4).

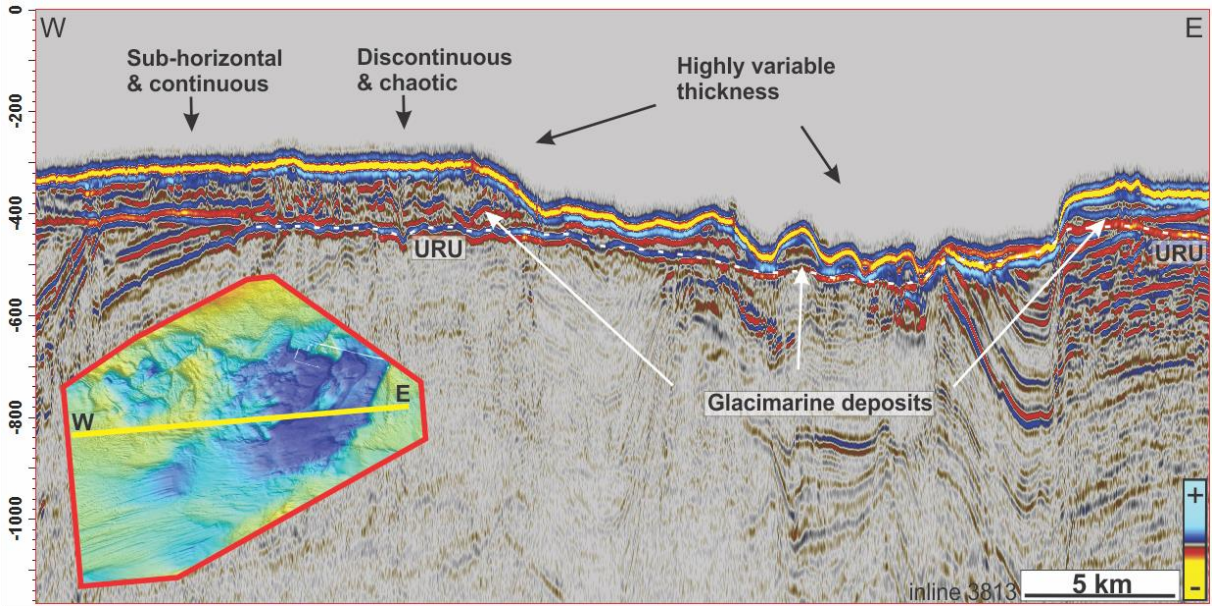


*Figure 4.4: Mini-map in bottom left corner show the area covered by the 3D survey (Figure 4.1) and the location of the 3D seismic line. The seismic profile show glacimarine sediments of various thickness and inner reflection pattern, superimposed on pre-glacial sedimentary rock and URU (white stippled line).*

The unit is thickest west of the study area, at the shelf edge and slope (measuring 1000 – 1500 ms TWT at the shelf edge) and quickly thinning towards east as it enters the trough (Figure 4.5). Well-developed sequences of west-ward dipping clinoform reflection configurations, indicating a west-ward prograding depositional front (Figure 4.5 & Figure 4.4).

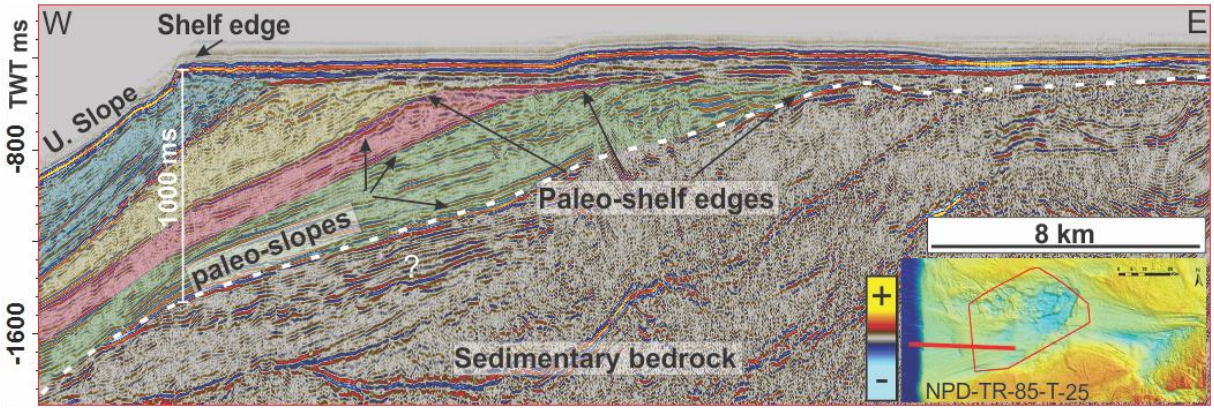


*Figure 4.5: A 2D seismic line of the upper slope, shelf edge and outer trough. The coloured shaded areas on the profile indicate paleo-slopes and -shelf edges and the shelf edge and upper slope today. The thickness of the glacimarine units (above white dotted line) decrease rapidly towards east in the trough. Location of the seismic line is shown in the mini-map (bottom right) and Figure 4.1.*

*Interpretation*

Superimposed on an erosional surface of pre-glacial sedimentary rock, this unit is interpreted to be glacimarine deposits, deposited under varying conditions during several

glaciations. A negative reflection coefficient at URU is suggested to imply that the glacigenic sediments are of high density relative to the underlying unit, possibly subglacial till. High density, clayey till may possibly be impermeable. Publicly available data from NPD show that well 7019/1-1, drilled on the bank of Tromsøflaket just 20 km north of Håkjerringdjupet, proved that the uppermost sediments were very hard with imbedded boulders, causing a slow drilling process, the same results were found by Sættem *et al.* (1992b). We suggest that this infer the presence of sub-glacially produced till on the banks, and that glacigenic till also will be a natural content of the glacigenic deposits in the trough. The highly variable seismic amplitudes shown within these deposits are implied to indicate rapid change in this unit's acoustic characteristics, heavily affected by density/velocity contrasts. This indicates a heterogeneous and unsorted unit, supporting that it might be of glacigenic origin

The west-ward dipping reflectors close to the shelf edge are interpreted to be paleo-slopes and paleo-shelf edges (Figure 4.5), made up by prograding and rapid deposition of glacimarine sediments during glaciations (Solheim *et al.*, 1996; Ó Cofaigh *et al.*, 2003).

Rokoengen *et al.* (1979) and Sættem (1994) also interpreted this unit to be glacimarine deposits. However, Rokoengen *et al.* (1979) are describing three glacigenic units (drifts), the Older Drift, Nordvestnaget Drift and Mulegga Drift. The Older Drift is partly eroded and rest on Cenozoic and Mesozoic sediments and were suggested to be older than 18,000 years B.P. Nordvestnaget and Mulegga Drift represent the Late Weichselian deposits respectively on the outer and inner shelf and is estimated to be deposited latest at 13,300± 110 years B.P (Nordvestnaget) and 11,000 – 13,000 years B.P (Mulegga). The dates from Nordvestnaget Drift is commented to be surprisingly low compared to assumptions from terrestrial work. Sættem (1994) uses Nordvestnaget and Mulegga Drifts in his paper but adds two more units (E and T) to describe older glacigenic deposits, which he suggest the acoustically chaotic unit consists of, overlain by Nordvestnaget Drift.

## 4.2 Non-sedimentary seismic anomalies

Not all seismic reflectors are of sedimentary or lithologic origin. Some are caused by other processes, such as structural or fluids. These anomalies are important to interpret to gain an understanding of the geological processes that may occur in the area.

### 4.2.1 Acoustic vertical offsets: Fault complex

*Description*

The centre of the trough is an area which its stratigraphy have been greatly affected by vertical offsets and discontinuities of seismic reflectors (Figure 4.6). This is seen within all seismic datasets that goes through this area. On a seismic profile, they are recognized by a varying vertical offset between the reflectors and sometimes a narrow zone of acoustic wipe-out in the centre of the offset (i.e. the reflectors are not continuous through the offset) (Figure 4.6). Approaching the discontinuities, the reflectors tend to abruptly bend in either an up- or downward direction on one or both sides of the offset (Figure 4.6b). Some of these offsets are observed continuing very deep within the pre-glacial sedimentary rock, as seen in Figure 4.6 below.

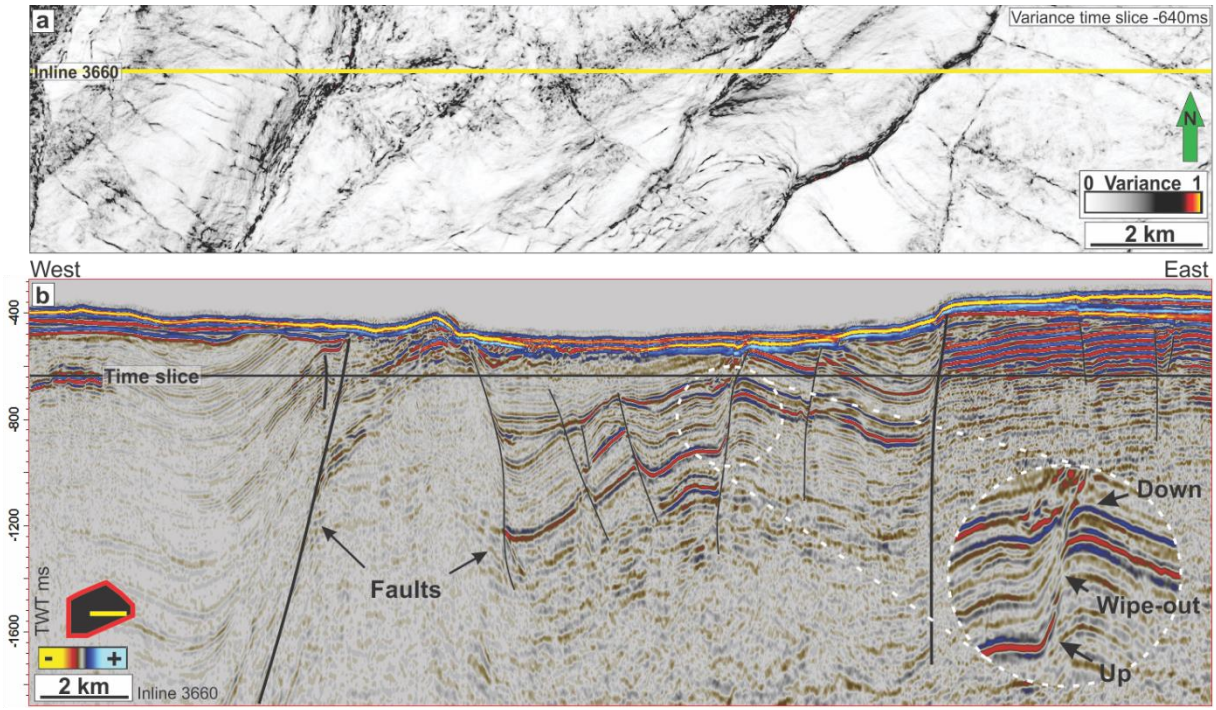


*Figure 4.6: **a)** A Variance attribute time slice at -640ms show the faults as black NE-SW oriented uneven lines.Yellow line indicate the location of the seismic line (b). **b)** Seismic reflectors with vertical offsets are common within the centre of the trough. A zoom in on the one of the vertical offsets show how the intersecting reflectors are bend up (left) and down (right), and a narrow zone of acoustic wipe-out in the offset. Black horizontal line (time slice) show the location of the time slice in 'a' and Figure 4.8. Location of this 3D line is shown in the black polygon (bottom left) and in Figure 4.9.*

Similar, but smaller vertical offsets were observed SW in the trough. Small scale shallow vertical offsets are observed occurring closely spaced in a limited area beneath URU at -450ms to -1000ms TWT (Figure 4.7). Their vertical offset range approximately from 25ms to 100ms TWT, and seem to occur along the same dipping reflector. These offsets do not seem

to have any connection with the larger offsets described above, as they are quite far apart and do not have the same vertical extent.

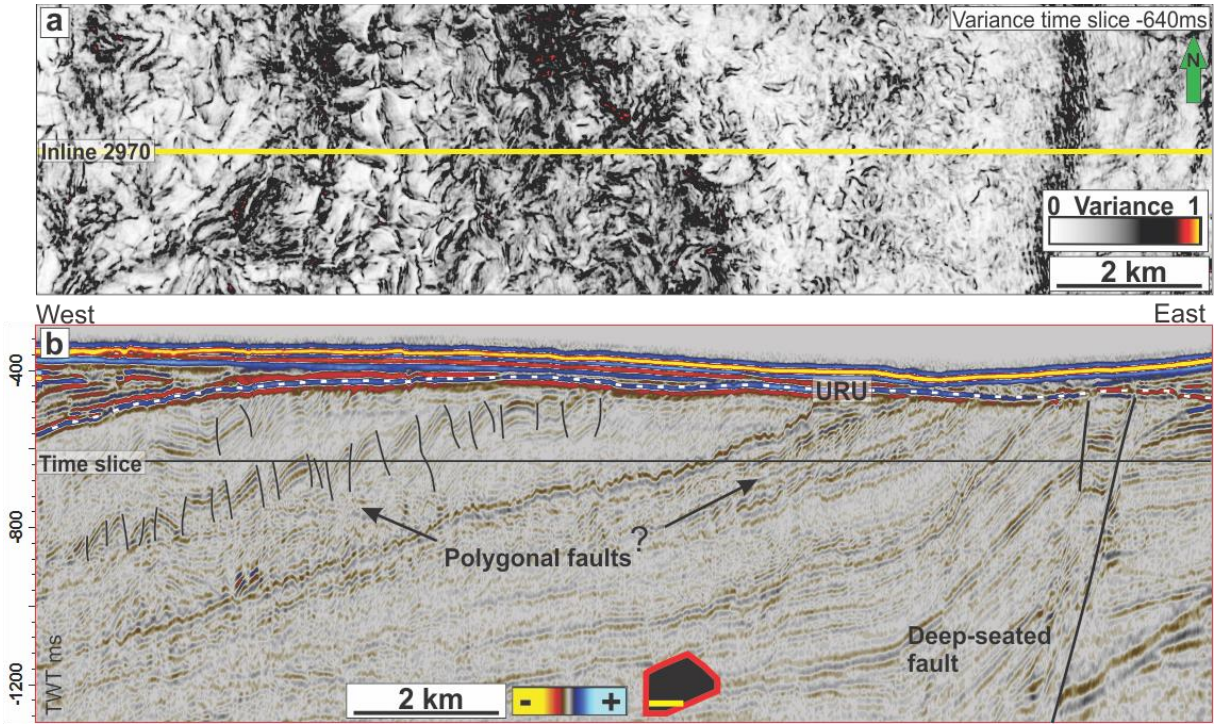


*Figure 4.7: **a)** Variance attribute time slice at -640ms of polygonal faults southwest in the 3D survey FP12_PRCMIG. Yellow line show the location of seismic line in b. **b)** Polygonal faults are seen in the 3D seismic dataset southwest within the trough. This seismic profile show how they are restricted to a small area in the upper pre-glacial sedimentary rock unit. The location of this 3D seismic line is shown in Figure 4.9.*

The lateral distribution of these discontinuities are well visualized in a variance time slices from the 3D survey, which show the degree of trace-to-trace variability of a specific sample interval (Figure 4.6, Figure 4.7 & Figure 4.8). Major deep-seated coherent offsets can be traced through the whole survey, oriented NE - SW. The offset tend to migrate horizontally with depth, mostly towards west, northwest. Smaller offsets seen contiguous to these are oriented in a perpendicular to oblique direction on the deep-seated faults (NW - SE) (Figure 4.8).

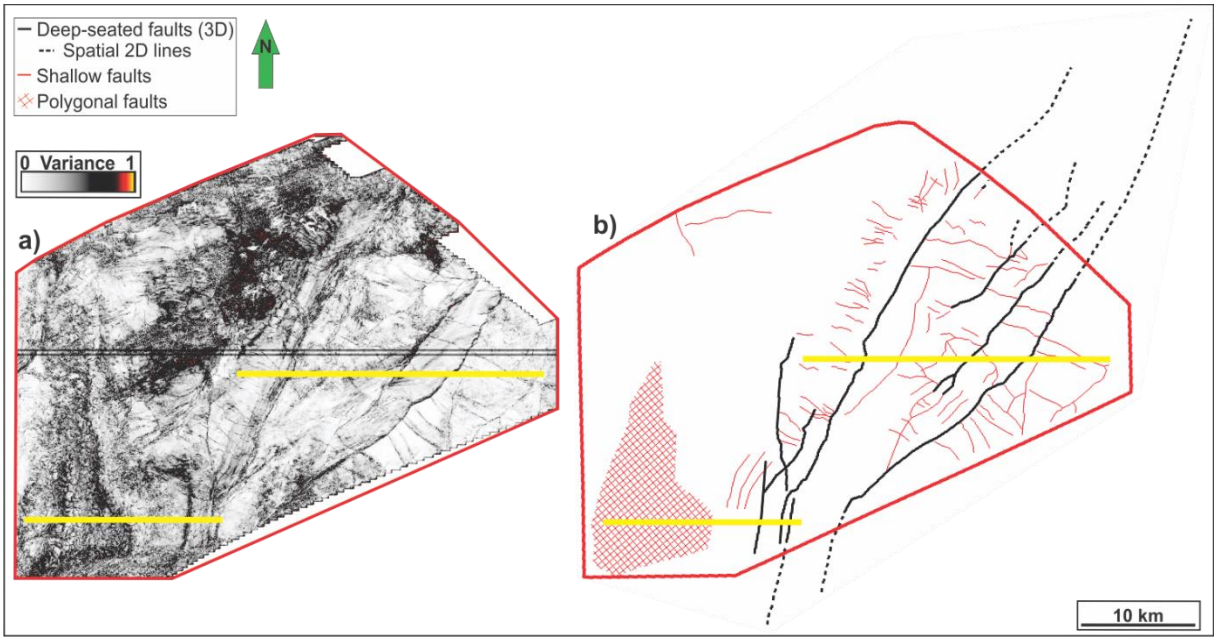


*Figure 4.8: **a)** time slice at –640ms TWT from a variance attribute cube (depth shown in Figure 4.6b & Figure 4.7b). Faults are easily distinguished by their sharp appearance as black lines and southwest in the survey polygonal faults were recognised. **b)** An interpretation of the lateral extension of the faults by the use of variance cube time slices, as well as 2- and 3D seismic lines. 2D seismic line were used to interpret the faults outside the 3D survey (black dotted lines).*

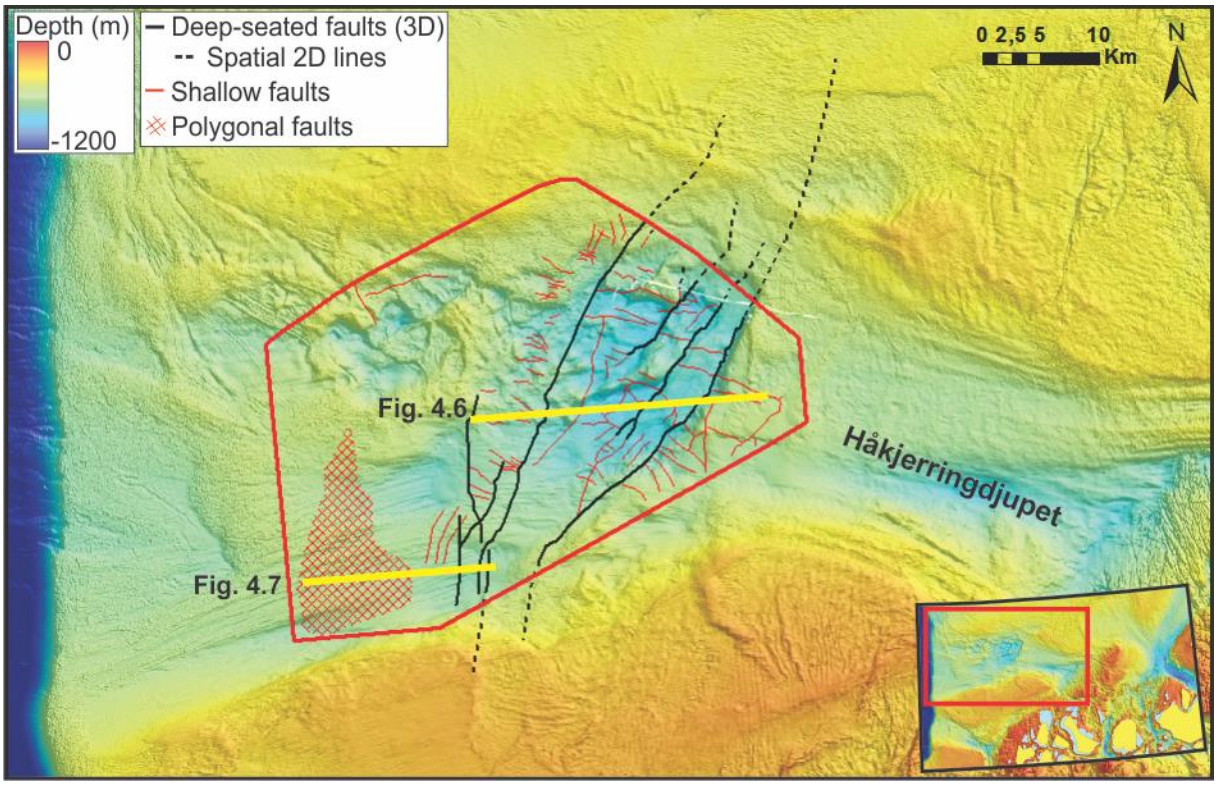


*Figure 4.9: Vertical offsets in the sub-seabed mapped on a bathymetric map of Håkjerringdjupet. Most of the mapping is done within the 3D survey FP12_PRCMIG (red polygon). However, available 2D seismic lines have been used to gain an expanded knowledge on the orientation and prevalence of the fault complex (stippled lines). Smaller faults associated with the major ones have also been mapped (red lines) as well as an area of shallow polygonal faults (red squares).*

*Interpretation*

These vertical discontinuities are interpreted to be offsets along a fault complex that move through the whole study area. The location and orientation of the faults fits with the Troms-Finnmark Fault Complex that stretch from the south along the continental shelf, through the study area and continue into the SW Barents Sea in a NE-wards direction (Faleide *et al.*, 1984; Faleide *et al.*, 1993; Indrevær *et al.*, 2013). The faults do not affect the glacimarine deposits, but do extent up to URU which is an erosional surface. This fault complex is therefore interpreted to last have been active before the last glaciation and probably a lot older than that. Some of the faults are deep seated – reaching deep into the pre-glacial sedimentary rock.

The smaller faults southwest in the trough are interpreted as polygonal faults within the upper part of the pre-glacial sedimentary rock unit. Similar features have been documented in a study by Ostanin *et al.* (2012) in the SW Barents Sea. The formation of polygonal faults are inferred to be non-tectonic and implied mechanisms are density inversion, dewatering contraction and fluid transport to overlying units, gravitational loading and dissolution-induced shear failure (Berndt *et al.*, 2003; Cartwright *et al.*, 2004; Ding *et al.*, 2013).

### 4.2.2 Acoustic high reverse amplitude anomalies: Fluid contacts

*Description*

Within the pre-glacial sedimentary rock, reflectors of high amplitude anomalies are observed below URU at several depths within the 3D survey FP12_PRCMIG. These anomalies have a negative reflection coefficient compared to the seafloor, indicating a decrease in velocity/density below these reflectors, and are often referred to as bright spots (Figure 4.10). The lateral extent and shape of these anomalies vary greatly. However, laterally they appear to have a slightly rounded to highly elongated shape, and migrate laterally with depth.

The bright spots are observed at and along lithological reflectors at varying depths and in areas of faults and along fault planes (Figure 4.11). When switching through 3D seismic profiles the bright spots are seen occurring at different vertically and laterally positions along lithological boundaries and through fault planes.

Vertical zones of discontinuous low amplitudes sporadically occur below bright spots with an equal lateral extent (acoustic masking), abruptly cutting the adjacent sub-horizontal sedimentary reflectors (Figure 4.10). The vertical extent of these zones of acoustic masking vary, and reflectors within or beneath these zones often show signs being pulled down.

Figure 4.11 show a seismic section where bright spots are observed along sedimentary boundaries and faults, with associated masking and pull-down, terminating at or below URU.

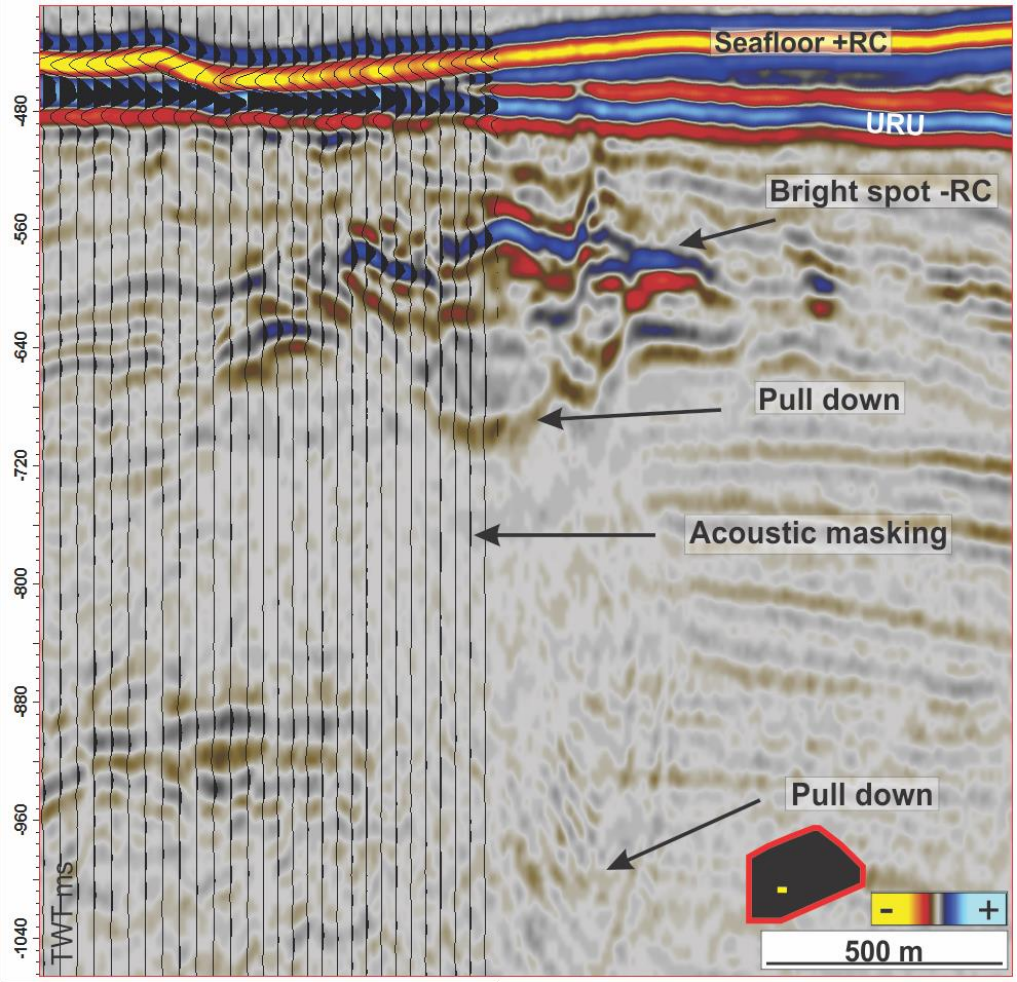


*Figure 4.10: This small 3D seismic profile show a bright spot and associated acoustic masking and pull down effects, located southwest in the trough just below URU. The same bright spot and its migration pathway can be seen in Figure 4.11 (white dotted square) together with other bright spots.*

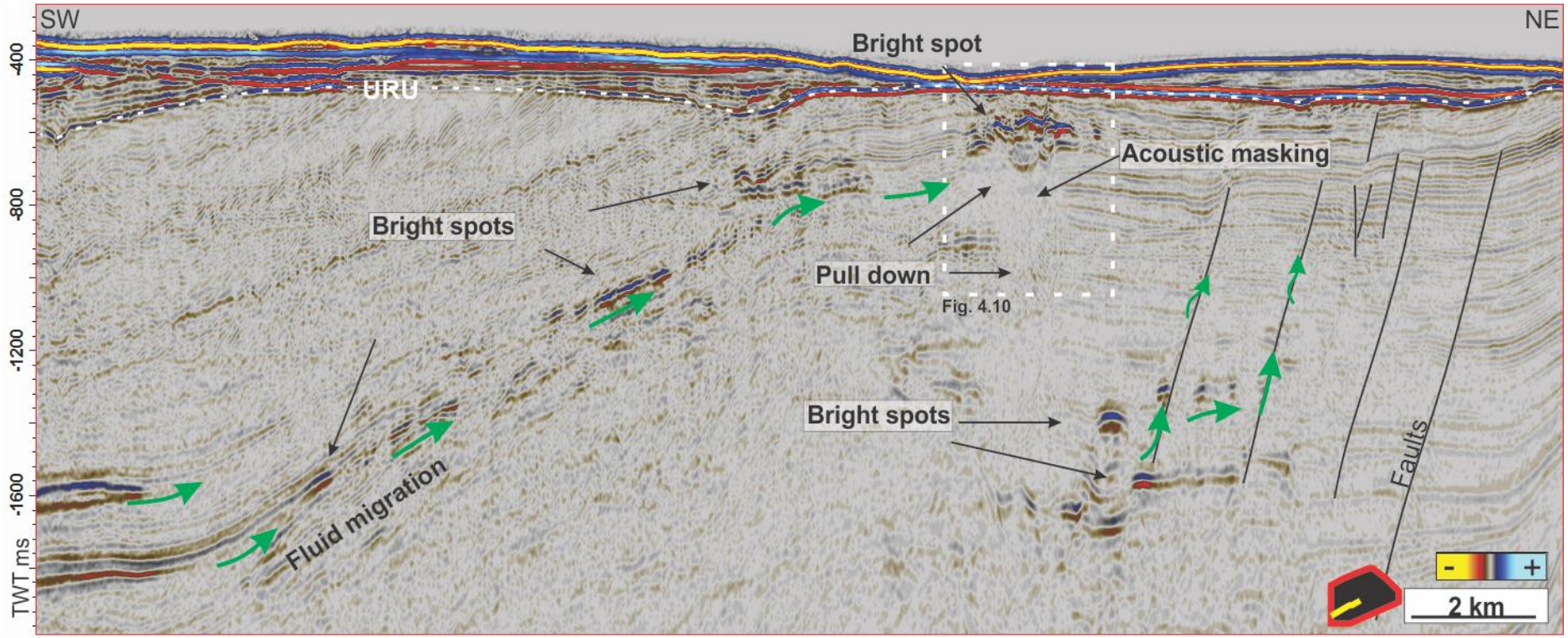


*Figure 4.11: A created NE-SW oriented arbitrary seismic line within the 3D survey FP12_PRCMIG. The profile show a bright spot located southwest in the trough and interpreted fluid migration pathways (green arrows) along lithological boundaries in sedimentary bedrock. It also show fluid migration pathways along fault planes NE in the profile. The location of Figure 4.10 is shown within the white dotted square.*

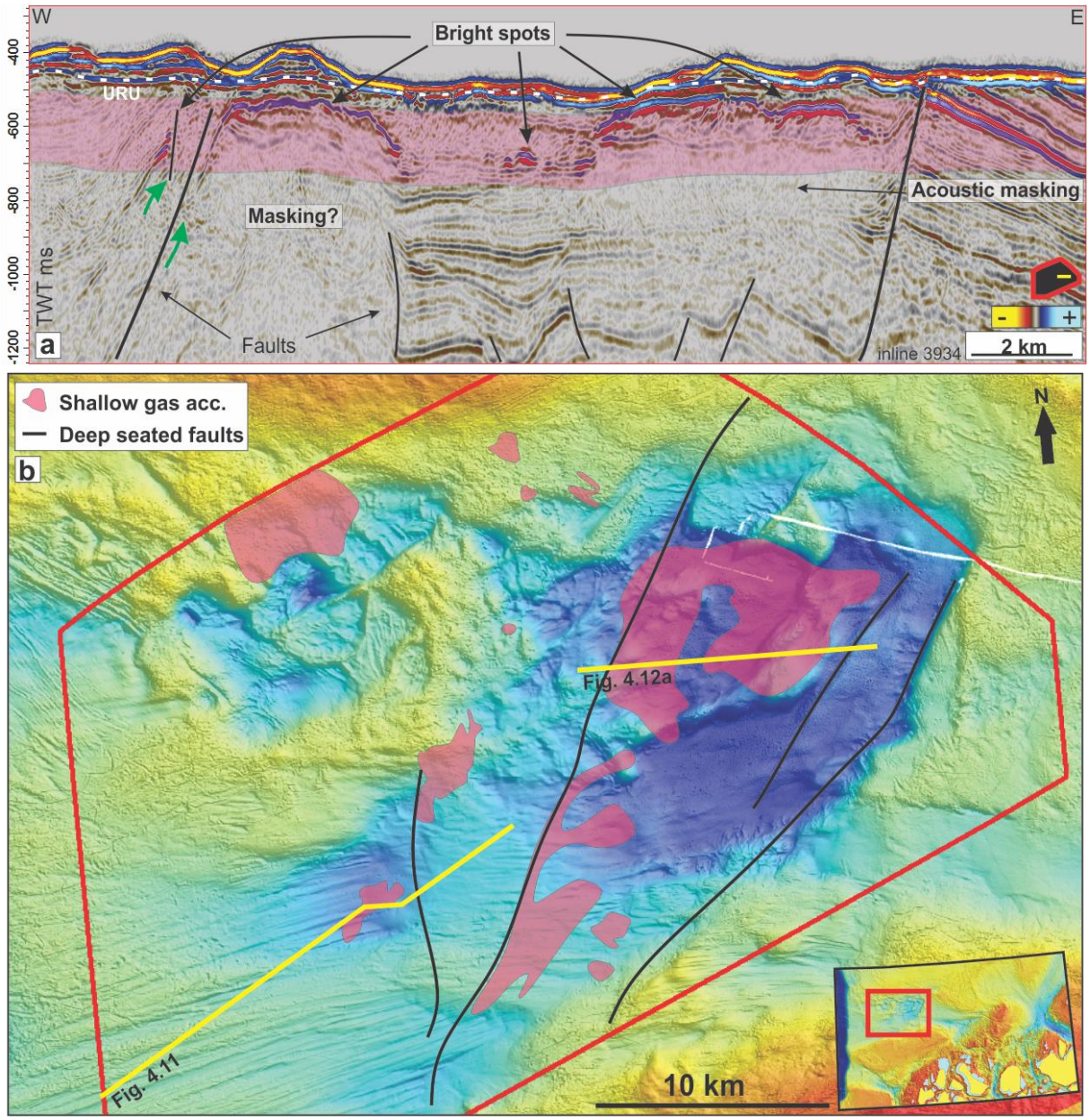


*Figure 4.12:* ***a)*** *Several bright spots with associated acoustic masking are observed within the centre of the trough. Also bright spots along fault planes were observed here. The pink shaded area show the time interval used when creating a RMS amplitude map.* ***b)*** *An RMS amplitude map were made at -50ms below URU to -250ms below URU (pink shaded area in 'a') to map the distribution of shallow gas anomalies close to the seafloor. Anomalies interpreted as shallow gas accumulations are visualized on the bathymetry as pink shaded areas. The location of seismic line in Figure 4.11 & Figure 4.12a are indicated on the map.*

*Interpretation*

Based on these high negative RC seismic anomalies, their distribution and their connection to deeper sedimentary rock, these are interpreted as indicators of low velocity, probably gas-filled, fluids in the subsurface. These anomalies are observed along lithological boundaries and close to faults (Figure 4.12). These anomalies seem to be migrating through lithological boundaries when it is exposed to faulting. A lithological origin is therefore not

enough to describe the high amplitude anomalies alone. The interpretation is therefore that most of these negative RC high amplitude anomalies are due to accumulation and migration of gas-filled fluids within the pre-glacial sedimentary bedrock. The fluids are believed to migrate along tilted permeable units and faults. Figure 4.12b show an interpretation of the occurrence of shallow gas accumulations, most of them associated with faults. This indicate that these faults act as migration pathways and suggest an origin of the fluids from the deeper source/reservoir in the sedimentary bedrock (Cartwright *et al.*, 2007).

The acoustic masking (Figure 4.10 - Figure 4.12) that occurs beneath the gas-filled fluids is probably due a gas-bearing intervals ability to absorb the seismic energy better than a water-bearing interval, attenuating the seismic signal. The concentration of gas does not need to be high for the acoustic wave to be attenuated, according to Andreassen *et al.* (2007a) the most dramatic loss in compressional wave velocity potentially happens below a free gas concentration of 4%. This rapid decrease in wave velocity is suggested to cause the pull-down within the gas-bearing interval, increasing the time of arrival of a seismic signal. This interpretation correspond to well-known techniques for recognizing accumulation of gas-filled fluids on seismic data (Andreassen *et al.*, 2007a; Cartwright *et al.*, 2007).

## 4.3 Seafloor geomorphology

The seafloor geomorphology can tell us much about geological processes that have occurred if the landforms are preserved. In the following section we will describe and interpret landforms observed on the seafloor and shallow subsurface that are relevant to the thesis.

### 4.3.1 Circular to sub-circular depressions: Pockmarks

*Description*

In certain areas in the trough, relatively small circular depressions appear in groups on the seafloor, only seen on the high-resolution bathymetric data of 25 and 5 m, and some seismic lines (Figure 4.13). Their shape is circular to sub-circular. Their sizes range from 20 m to 150 m in diameter, and between 0.5 m to rarely more than 10 m deep. Some of the largest ones, however, seem made up by several smaller ones merging into a bigger depression. Some of these largest circular depressions also occur with a, somehow, positive relief cone-shaped feature (up to 7 m high and 30 – 70 m wide) in the middle of the crater, that sometimes

exceed the surrounding bathymetry as shown in the profile by the red arrow in Figure 4.13b & d. Some are more asymmetrically shaped than others.

The distribution of the circular depressions seem to be concentrated in the centre of the trough and to the east. The eastern extension of these depressions is unclear as the high-resolution bathymetric data stops here (black polygon Figure 4.13a). With a density of over 100 circular depressions per square kilometre, the concentration seem to be highest in the centre of the trough, limited to the deeper areas, and absent on the hills inside this depression (Figure 4.13).

A correlation between backscatter-data from Mareano/NGU and the distribution of these sub-circular features show us that the majority of them are found within areas of low backscatter, e.g. soft sediments (Figure 4.14). However, some of the largest features have higher backscatter within the depression, including the positive relief features in Figure 4.13b & d.

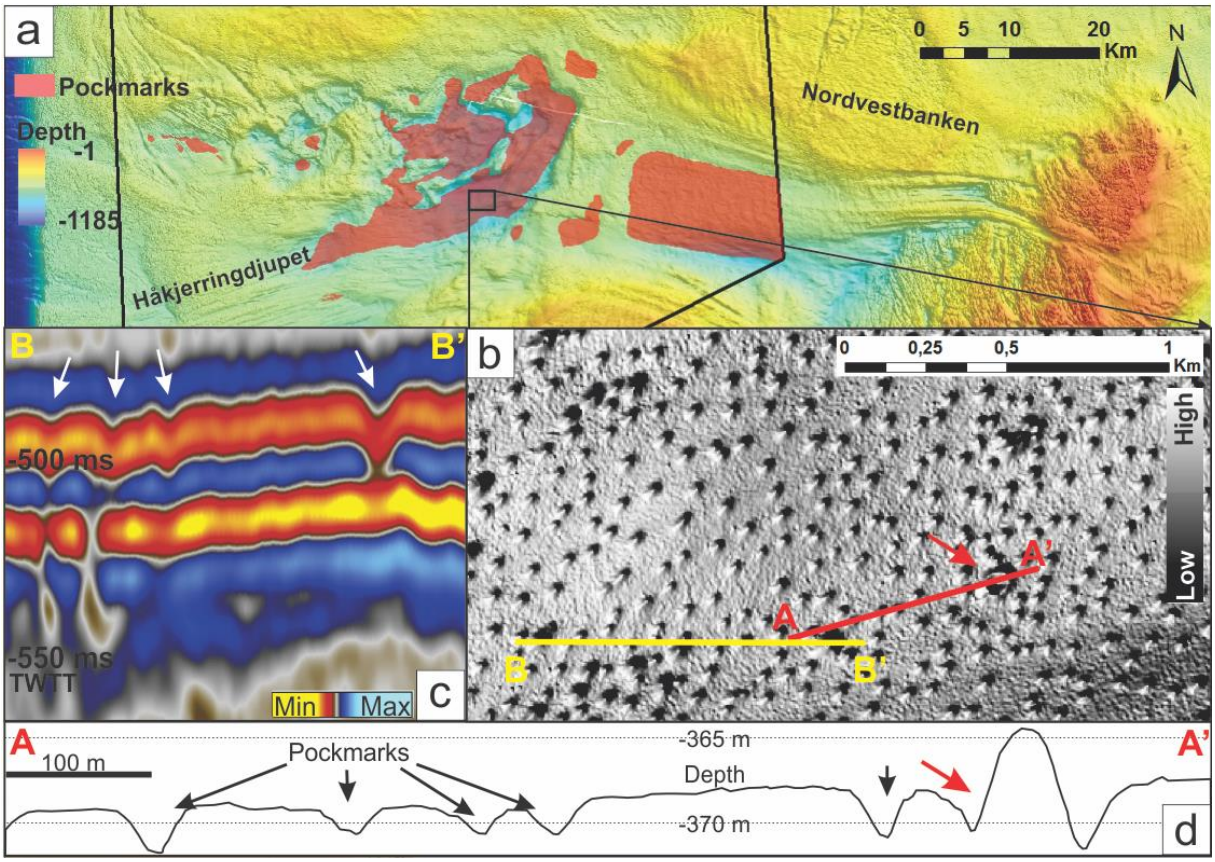


*Figure 4.13* ***a)*** *An overview of the distribution of mapped pockmarks inside the trough, where high resolution bathymetric data is available. Location of b shown as a black box.* ***b)*** *A close up in the centre of Håkjerringdjupet where the pockmarks are dominating the seabed. The red line A – A' indicate the location of the profile d, and the line B – B' show the location of the seismic line in c. Red arrow indicate a large depression with a positive relief feature, compared to the surroundings,*

*inside it.* ***c)*** *Seismic profile (Inline 3636) from the 3D survey. The seismic profile show depressions at the seabed pointed at by white arrows.* ***d)*** *Profile A – A' clearly show the depressions at the seabed and a positive feature pointed at by a red arrow.*

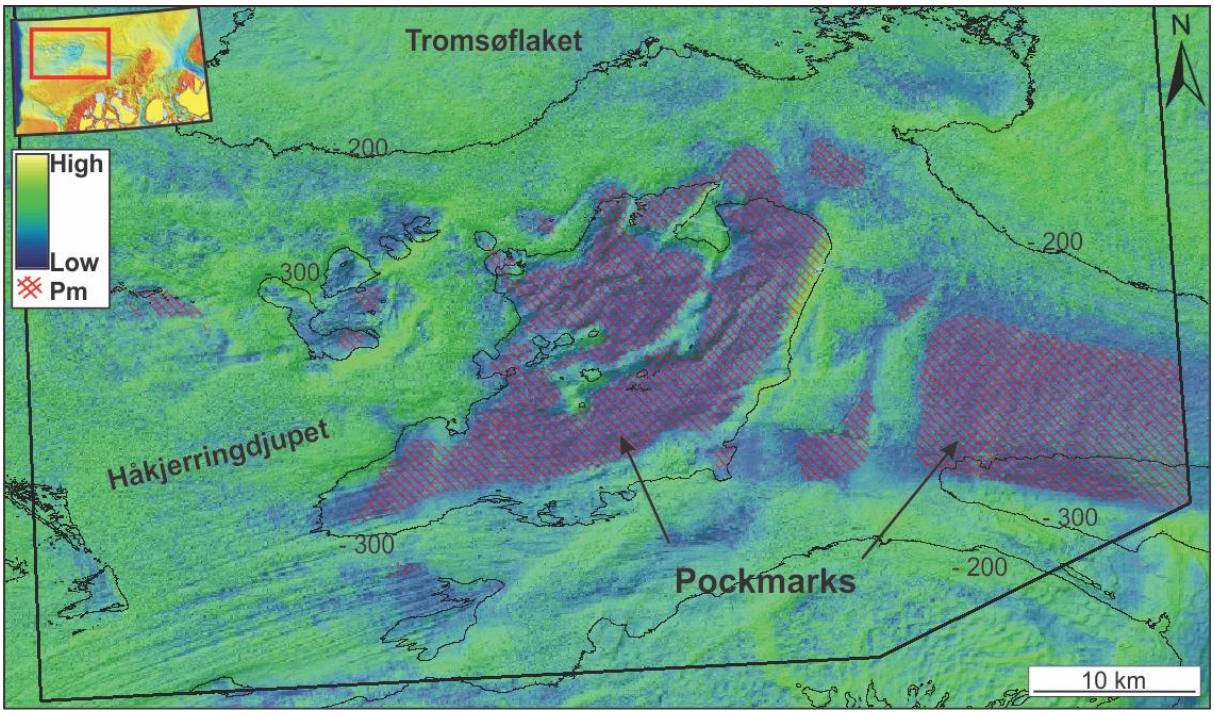


*Figure 4.14: Acoustic backscatter from multibeam echosounder data acquired by Mareano/NGU in Håkjerringdjupet. Green colour indicate high backscatter, e.g.harder sediments, while blue colours indicate low backscatter and softer sediments. The pockmarks (red hatched area) are mostly observed within areas dominated by soft sediments. Black outline show the extent of the 5 m resolution bathymetry data used to map the distribution of pockmarks.*

*Interpretation*

We interpret these circular sub-circular depressions to be pockmarks located at the seafloor. Similar depressions in the Barents Sea and elsewhere have previously been interpreted as pockmarks (L. H. King & Maclean, 1970; Hovland *et al.*, 2002; Judd & Hovland, 2007; Chand *et al.*, 2009; Chand *et al.*, 2012; Rise *et al.*, 2014). Pockmarks are believed to be indicators of active or past fluid migration and leakage from deeper reservoirs, often related to faults (Judd & Hovland, 2007; Chand *et al.*, 2009; Chand *et al.*, 2012). They are formed as gas and fluids migrates up through rocks and sediments, released as periodic flares at the seabed, blowing away the surrounding fine grained sediments leaving a circular-sub-circular depression (Chand *et al.*, 2012). The size of the pockmark seem to be affected by both grain size and sediment thickness, whereas thick and soft fine-grained (clays and silt) sediments are more likely to form larger pockmarks, while coarse and shallow sediments form smaller pockmarks (Chand *et al.*, 2012; Rise *et al.*, 2014). The pockmarks occur inside mega-scale glacial lineations, but there is not observed any signs of these pockmarks being overprinted

by anything. This indicate that they are likely to be relatively young (post-glacial) and may still be active today.

This description and interpretation of the pockmarks and their distribution coincides well with the study by Rise *et al.* (2014). However, they do not mention that some of the larger pockmarks occur with a positive relief cone-shaped feature with high backscatter located in their centre. It is impossible to make any certain interpretation of these without any more information, but three suggestions to what may form these are: (1) Large submarine pingoes/gas hydrate mounds due to local build-up of gas hydrates (preferably structure II) (Hovland & Svensen, 2006; Serie *et al.*, 2012). (2) Growth of coral reefs feeding on nutrient fluids escaping from the pockmarks (Hovland *et al.*, 2012). (3) Formation of methane-derived authigenic carbonate rock due to biochemical processes in the proximity of pockmarks and presence of, assuming, methane-rich fluids (Aloisi *et al.*, 2002; Hovland *et al.*, 2005).

### 4.3.2 Large trough-parallel lineations: Mega-Scale Glacial Lineations

*Description*

Large trough-parallel lineated ridge-groove features have been observed on the seafloor in the study area (Figure 4.15). Especially well developed in the bathymetric datasets, but also in the 3D survey on interpreted horizons of the seafloor and URU in the subsurface. Their large size and highly elongated appearance make them easily noticeable on the bathymetric map, measuring over 20 km long, with troughs up to 600 m wide and up to 10 m deep. This means they have a high elongated ratio (length to width ratio) well over 20:1. An exception is in the east of Håkjerringdjupet nearby the crystalline bedrock, where the depth of these may exceed over 40 m.

These features occur exclusively inside the trough. They are observed from the transition between crystalline bedrock and sedimentary rocks in the east (white dotted line Figure 4.15a) to the shelf edge in the west. Their orientation is respectively WNW-ESE and SW-NE to WSW-ENE (Figure 4.15). The occurrence seem to be best developed along the troughs southern side and in the east, and are absent in the central over-deepening and adjacent hills (Figure 4.15). Southwest in the trough, lineations are seen developed superimposed on trough-transverse ridges where they terminate (section 4.3.3). An exception is on the largest

ridge closest to the shelf edge, where they overprint its southern part creating a positive relief tongue continuing all the way to the shelf edge.

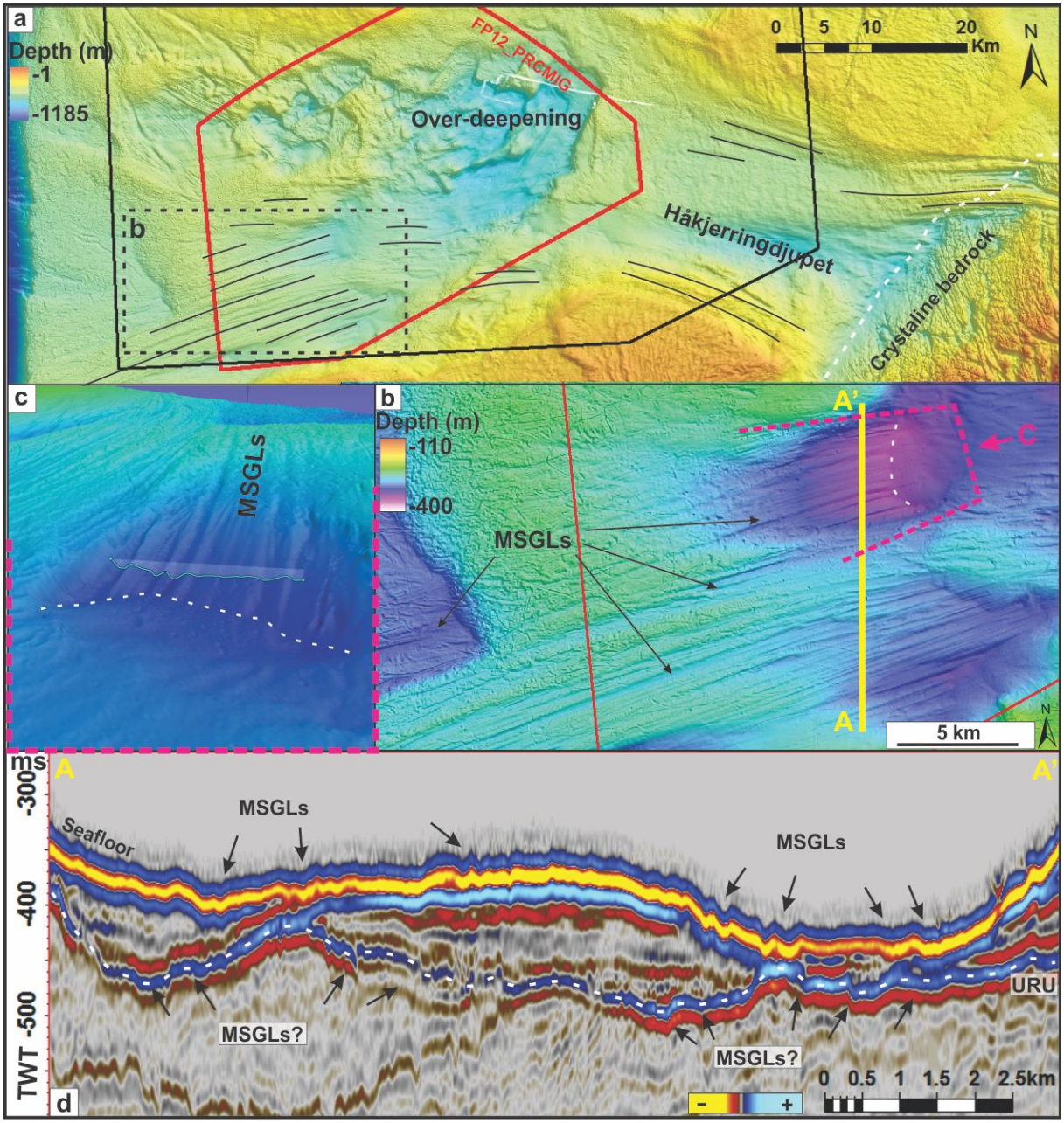


*Figure 4.15:* ***a)*** *An overview of the MSGLs (black lines) mapped within the trough. Stippled square b show the location of the zoom in in 'b'. White stippled line show the location of the transition between Caledonian bedrock (east of) and sedimentary bedrock (west of). Black box show location of high resolution bathymetry data and red box show location of 3D seismic survey FP12_PRCMIG.* ***b)*** *High resolution bathymetry of an area of MSGLs in the mid-trough. The MSGLs clearly overprint the western most ridge in a tongue shape (bottom) and are overprinted by another ridge in the east. Stippled purple line 'c' show the location and direction of which 'c' is looking. Yellow line show the location of the seismic line A – A' in 'd'.* ***c)*** *A 3D-visualization of the MSGLs looking towards the shelf edge (west). The MSGLs is abruptly terminating as a trough transverse ridge that overprints them (white stippled line). A small profile of the surface is located central within the figure.* ***d)*** *Seismic line A – A' from the 3D survey show the MSGLs on the surface, and possible buried MSGLs at URU level (white dotted line). Location of A – A' shown in 'b'.*

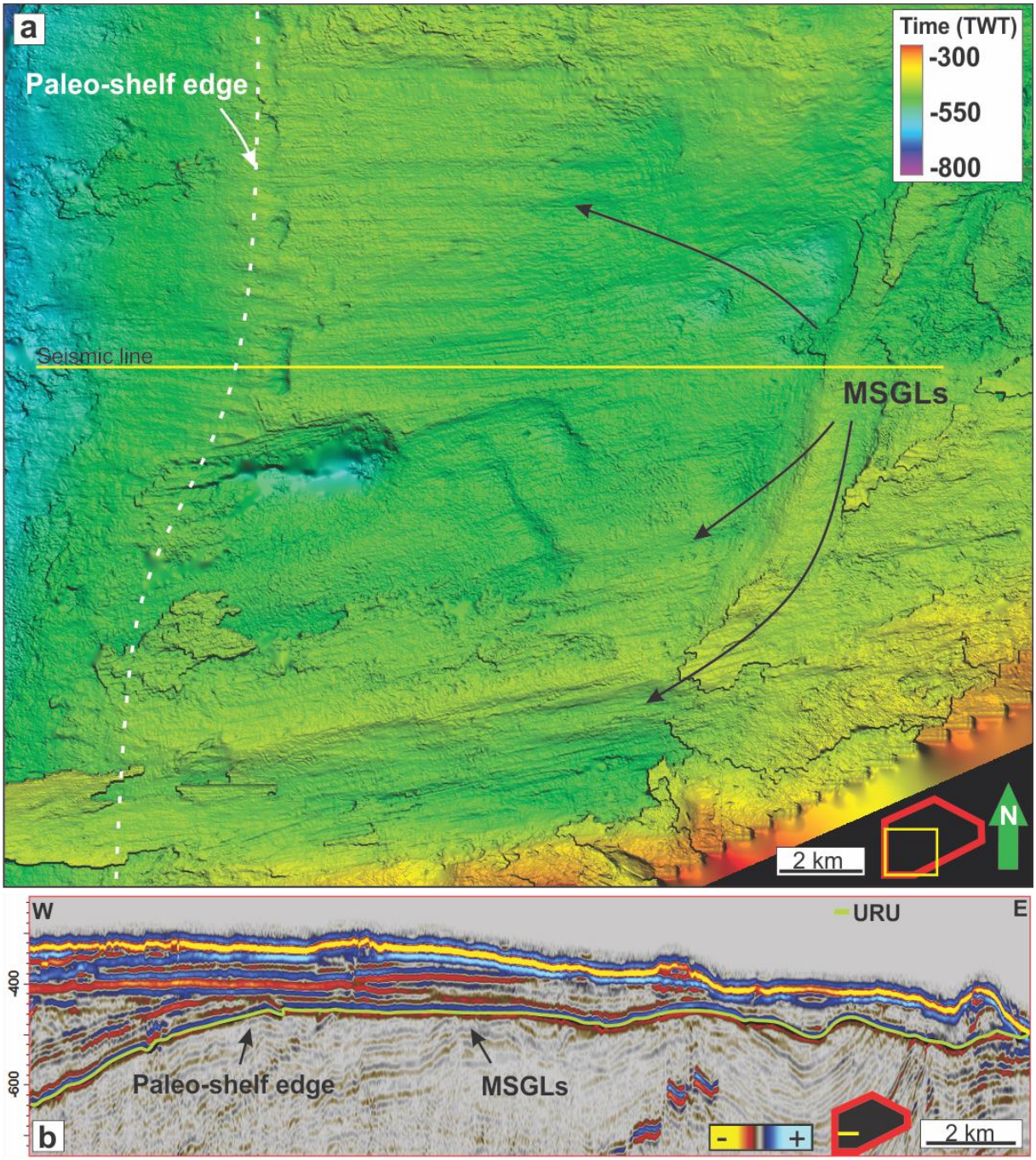


*Figure 4.16:* ***a)*** *Mega-scale glacial lineations are also visible on a buried surface (URU) but only preserved southwest in the trough. Here they are terminating at the paleo-shelf edge.* ***b)*** *A 3D seismic line to show the location of the buried horizon URU and that the MSGLs are located on the sub-horizontal part on the profile below an acoustically stratified unit.*

Similar depressions are seen on the buried surface URU on seismic profiles (Figure 4.15d), but better visualized on the interpreted surface of URU. Here streamlined lineations are seen at the southwestern end of the 3D survey (Figure 4.16). They are not as well-developed/preserved at the buried horizon as at the seafloor, however, the resolution of the data may affect the interpretation.

*Interpretation*

Similar features are common in areas which have been glaciated, like the Norwegian continental shelf. Previous terrestrial and marine studies have described and interpreted such features as Mega Scale Glacial Lineations (MSGLs), we do likewise (C. D. Clark *et al.*, 2003b; Andreassen *et al.*, 2004; Ottesen *et al.*, 2005; Andreassen *et al.*, 2007b; Andreassen *et al.*, 2008; Ottesen *et al.*, 2008; E. C. King *et al.*, 2009; Hogan *et al.*, 2010; Winsborrow *et al.*, 2010a). Winsborrow *et al.* (2012) describes the same lineations in her previous work from the same area. These streamlined lineations are features indicating grounded and fast flowing ice, commonly associated with ice-streams and surges, where sediments are deformed sub-glacially by moving ice, a theory confirmed by E. C. King *et al.* (2009). We therefore interpret the lineations to origin from a previously grounded ice stream located in Håkjerringdjupet.

The inferred direction of the ice flow is from east to west, where ice drained from the Fennoscandian Ice Sheet towards the shelf edge (Ottesen *et al.*, 2008; Winsborrow *et al.*, 2010a; Winsborrow *et al.*, 2012). The presence of MSGLs on the URU surface are interpreted to indicate that this boundary was indeed caused by erosion of fast flowing ice that extended out to the paleo-shelf edge and demonstrates the possibilities for multiple generations of active ice streams within this trough, probably through several glaciations (Figure 4.16). Several sets of MSGLs overprinting- and being overprinted by trough-transverse ridges located on the seafloor are pointing towards episodes of change in ice flow activity on a far shorter time-scale (Figure 4.15).

### 4.3.3 Trough-transverse ridges: Grounding zone wedge

*Description*

Two noticeable large ridges are located west, south-west in the trough, approximately 12 and 32 km from the shelf edge. They both have an elongated shape stretching in a NNW-SSE

direction, transverse to the troughs' E-W axis, but does not extend across the whole trough (Figure 4.17). In an E-W profile, both are wedge-shaped, with the steeper side towards the shelf edge and a gentle slope in the east (Figure 4.17b).

The western-most of the ridges (GZW 1) are by far the biggest one, 10-15 kilometres wide (E-W direction) and about 20 km long (N-S), and have a positive relief between 40 - 50 m. Its surface is heavily covered by ploughmarks and MSGLs (see section on ploughmarks 4.3.5). The MSGLs are visible from the GZW 1 maximum height and prograding east of here. Exceptions are in its southern part where these MSGLs overprint the ridge, creating a positive relief tongue stretching to the shelf-edge (Figure 4.17a).

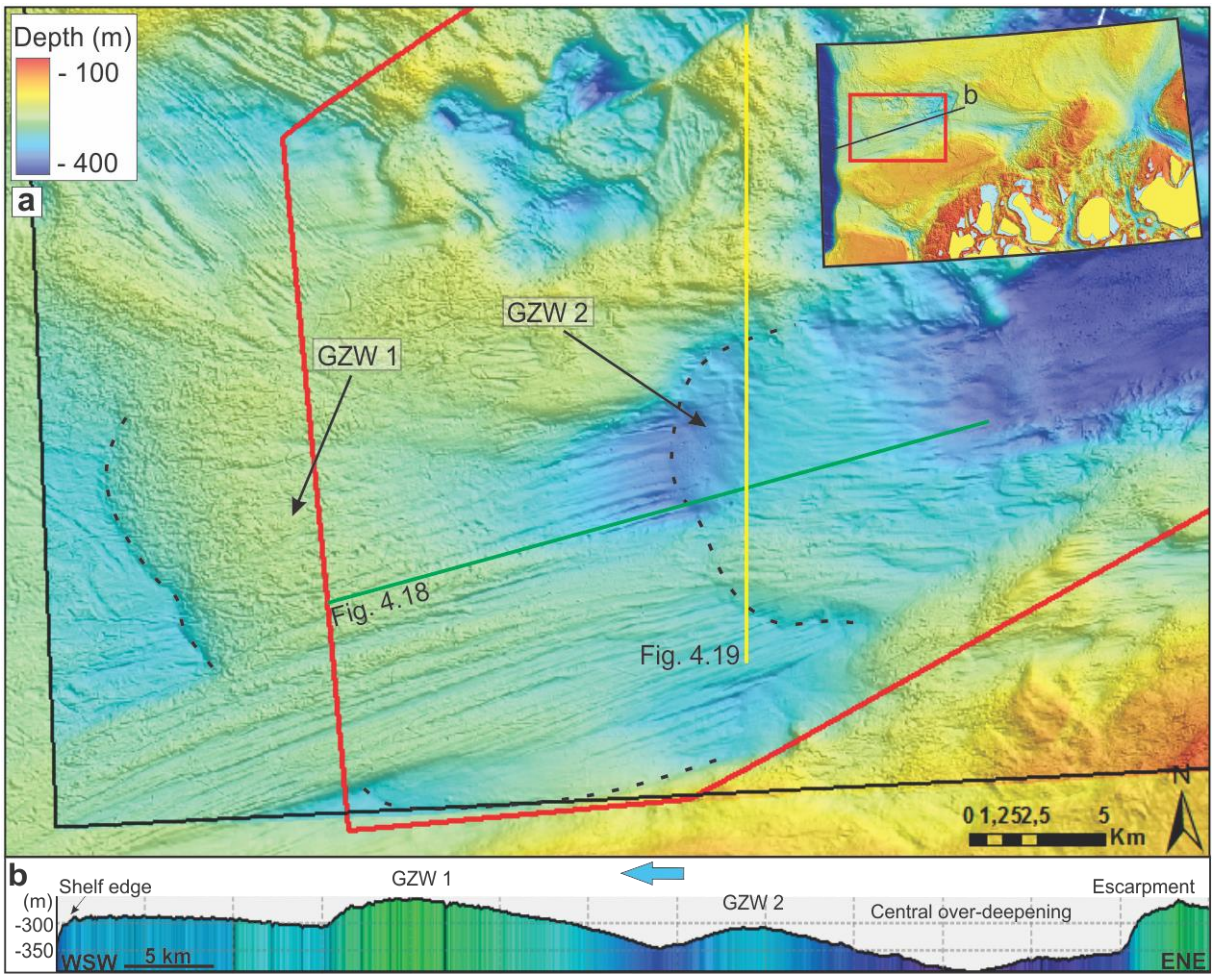


*Figure 4.17: **a)** Two grounding zone wedges (GZW) were observed within the trough. The front of each GZW is marked by black stippled lines. The westernmost GZW have a coarse surface, covered by ploughmarks and large MSGLs. The smaller GZW to the east has a much smoother surface, covered by some MSGLs. The coloured lines indicate the location of the seismic profiles in Figure 4.18 & Figure 4.19. Mini-map in upper right corner show the location of this figure (red box) and the depth profile in b (black line). **b)** An ENE-WSW oriented depth profile from the shelf edge to the mid-trough escarpment (black line in mini-map in Figure 4.17a). This exaggerated depth profile show how prominent these features are on the seafloor. Blue arrow indicate the direction of the ice flow.*

A smaller ridge, from now on called GZW 2, is located just east of the GZW1, almost overlapping each other (Figure 4.17). It measures approximately 10 x 12 km and c. 30 - 35 m high. The northern part of GZW 2 ends in an area of an irregular seafloor. Its surface is smoother with less ploughmarks, only present on its southern end. MSGLs are also present on the ridge, but in a less extent than in GZW 1. South on GZW 2 the MSGLs seem to be prograding far west on the ridge, looking like it maybe an eastern continuation of the tongue over-riding GZW 1 in the west. GZW 2 itself overprints several glacial lineations at its western boundary (Figure 4.17, see section 4.3.2). Some of the MSGLs that prograde east-west on GZW 1 seem to be connected to these.

On seismic data GZW 1 seem to be seismically stratified where it is thinnest (Figure 4.18). However, further towards the shelf edge where it is thicker, 2D seismic lines indicate that is has parts where it is acoustic transparent, as GZW 2 show in Figure 4.18. Two lens shaped seismic units in an N-S cross profile through GZW 2 are relative acoustically transparent, with very little reflectors within it. GZW 2 also seem to slightly overprint the chaotic and discontinuous reflections north of it (Figure 4.19).

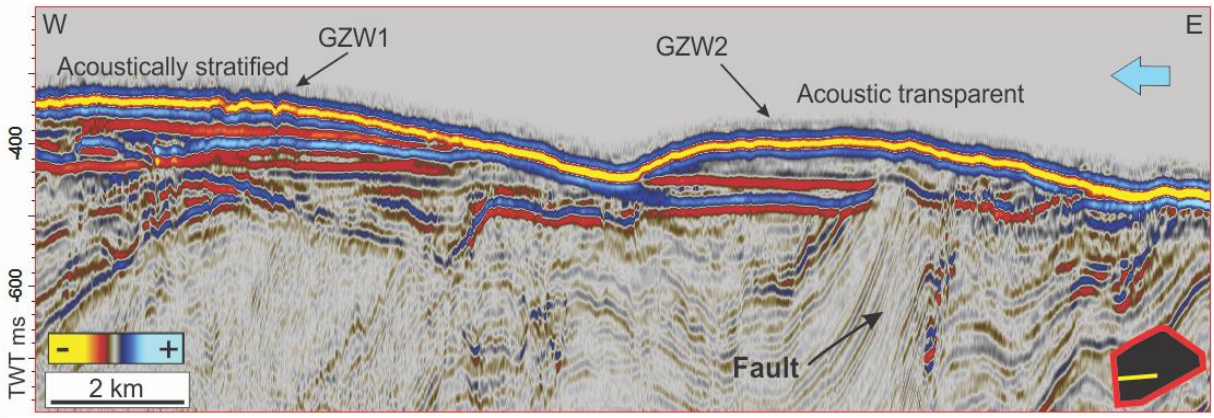


*Figure 4.18: An ENE-WSW oriented arbitrary 3D seismic line through the grounding zone wedges in the trough (line A-A' in Figure 4.17). Blue arrow indicate the direction of the ice flow.*

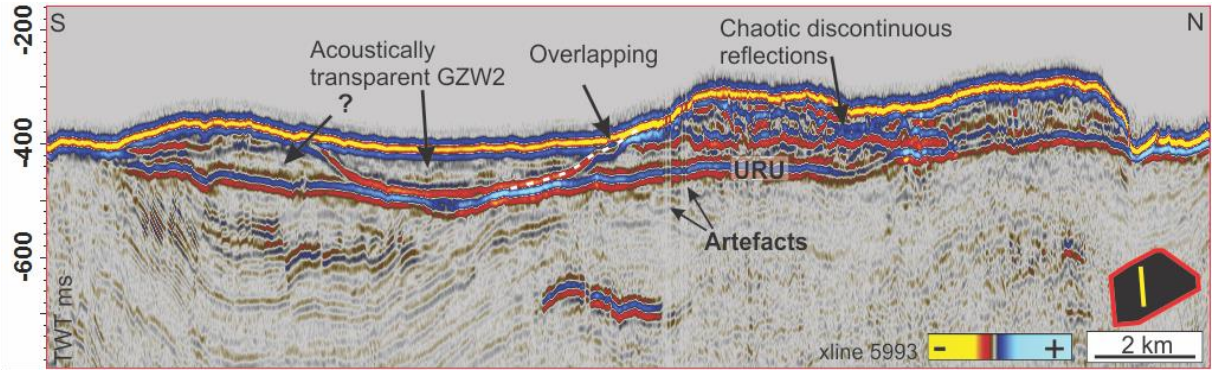


*Figure 4.19: An N-S oriented 3D seismic profile through GZW 2, showing an almost completely acoustic transparent lens shaped unit, compared to surrounding units above URU. The inferred ice flow in this figure would be away from us.*

*Interpretation*

Based on the observations from both bathymetry and seismic data of their morphology and location, these trough-transverse wedge-shaped features are interpreted to be grounding zone wedges (GZW). Grounding zone wedges are accumulations of sediments due to a longer period of stillstand or readvancing of a grounded marine terminating ice margin (Ó Cofaigh *et al.*, 2005; Ottesen *et al.*, 2008; Hogan *et al.*, 2010; Winsborrow *et al.*, 2010a; Winsborrow *et al.*, 2012; Batchelor & Dowdeswell, 2015). This is indicating a zone of where the transition between grounded ice (ice sheet) and floating ice (ice shelf) occurs (Benn & Evans, 2010). This suggests that at least two events of stillstand/readvance occurred during the last glacial period, and confirms the inferred direction of the ice flow as the gentle slope is interpreted to be the stoss-side with running-up MSGLs on it, and the steeper slope is the lee side (Figure 4.17 & Figure 4.18). Seismic transparency are indications of a homogenous unit with little or no change in acoustic impedance.

GZW 1 is interpreted to be the oldest grounding zone wedge as it is the outermost one and the MSGLs overprinting this wedge are themselves overprinted by GZW 2 (Figure 4.17). The size of GZW 1 suggest that this stillstand lasted longer and/or the sediment-access and deposition-rate were greater than when GZW 2 were formed. MSGLs moving far west on the southern side of GZW 2 may perhaps be caused by small readvances during the formation of this grounding zone wedge, perhaps as surges. GZW 2 is observed to erode into and overprint a chaotic glacimarine unit north of it and a slightly transparent lens shaped unit to the south (Figure 4.19). This indicates that GZW 2 is younger than surrounding glacimarine sediments, and therefore represent a relatively young event. The fast flowing ice stream

probably eroded glacimarine sediments, where the second grounding zone wedge later were deposited.

### 4.3.4 Irregular depression & adjacent hills: Glacitectonic landscape

An over-deepening central on Håkjerringdjupet is hard to overlook, so is the adjacent irregular hills. We will start this section by describing the bathymetry, then describe the seismic data before we interpret our observations.

***Description of Bathymetry***

The seafloor in the central parts of Håkjerringdjupet has a morphology dominated by an irregular over-deepened depression (depression 1) bounded by a 50 – 100 m relief escarpment, in the east and north (Figure 4.20). Depression 1 measures approximately an area of 200 $km^2$, with depths ranging from 300 to 400 m below sea level, making it the deepest part of the trough. Within depression 1 the seafloor is relatively smooth, however on a small scale; most of the seabed is occupied by large amounts of circular to sub-circular depressions, interpreted as pockmarks (see section 4.3.1). On a larger scale, a few positive relief features between 50 – c. 80 m high, marked with an *h* in Figure 4.20, disrupt the deep bathymetry centrally in depression 1.

Depression 2 is located west of depression 1 and is surrounded by irregular hills (Figure 4.20). The seafloor within depression 2 is very irregular. It covers a lot smaller area than depression 1 and there is only observed a few pockmarks within the whole depression. Several sets of irregular ridges are observed crossing depression 2 and some continuing onto the adjacent hills (Figure 4.20). Overall the depressions cover an area of about 250 $km^2$.

Irregular hills (h) are prominent just downstream of depression 1. These hills continue in an arcuate shaped chain around depression 2 and cover an area of approximately 200 $Km^2$, reaching elevations between 50 to 100 m higher than its surroundings (Figure 4.20). Their surface is highly irregular, covered by a dense amount of ploughmarks (see section 4.3.5) and larger ridges.

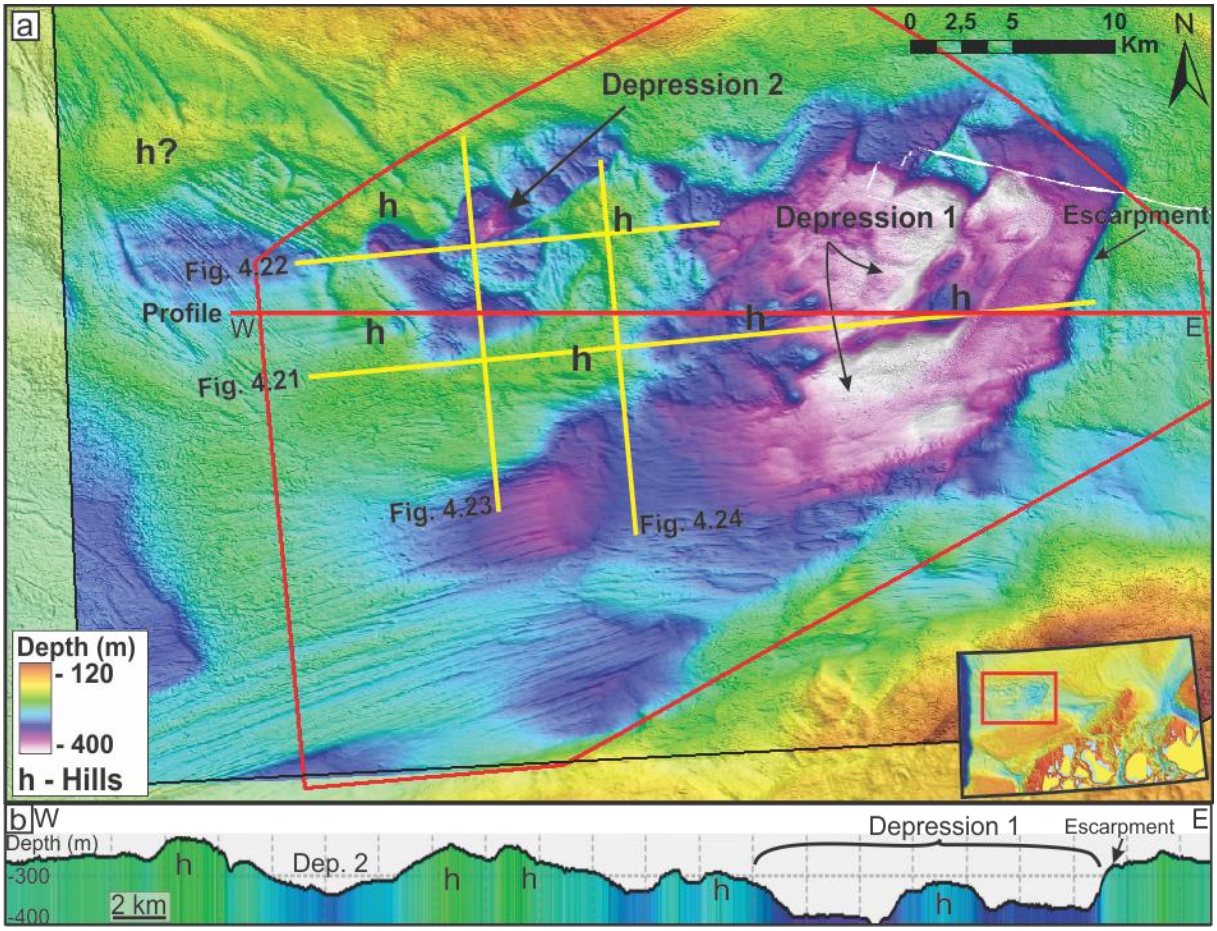


*Figure 4.20:* ***a)*** *Bathymetric map (25 m resolution inside black lines upon 50 m resolution) of depression 1 & 2 and adjacent irregular hills west of it. The colouring of the high resolution map were adapted to better visualize the effect the hill-hole pair have on the bathymetry. Red polygon show the extent of 3D survey FP12_PRCMIG and yellow lines show the location of seismic lines in Fig. 21 – 24. Red line show location of profile in 'b'.* ***b)*** *An E-W oriented bathymetric profile through the irregular hills (h) and the central over-deepening, depression 1 and 2. Location of profile is along the red line in 'a'.*

### *Description of seismic observations*

*Depression*

The subsurface of depression 1 consists of very shallow pre-glacial sedimentary bedrock with sub-parallel reflectors clearly affected by faulting and tilting, seen as discontinuous, vertical displaced and tilted seismic reflectors on seismic sections (Figure 4.21). Clearly the uppermost reflectors of this unit is cut by erosion, marked by URU (Figure 4.21). The sediments above URU are only 20 – 40 ms TWT thick (~15 – 30m), except where the irregular positive relief features described above are present, which are 50 – 100 ms TWT thick (~40 – 75m).

East in depression 2 the glacigenic unit is almost absent much like in depression 1. The glacigenic unit then thickens westward at the paleo-shelf edge where it gradually become

acoustically stratified (Figure 4.22). Patches of acoustically chaotic and discontinuous units are observed on various locations within depression 2 and on the edges onto it (Figure 4.22 & Figure 4.23).

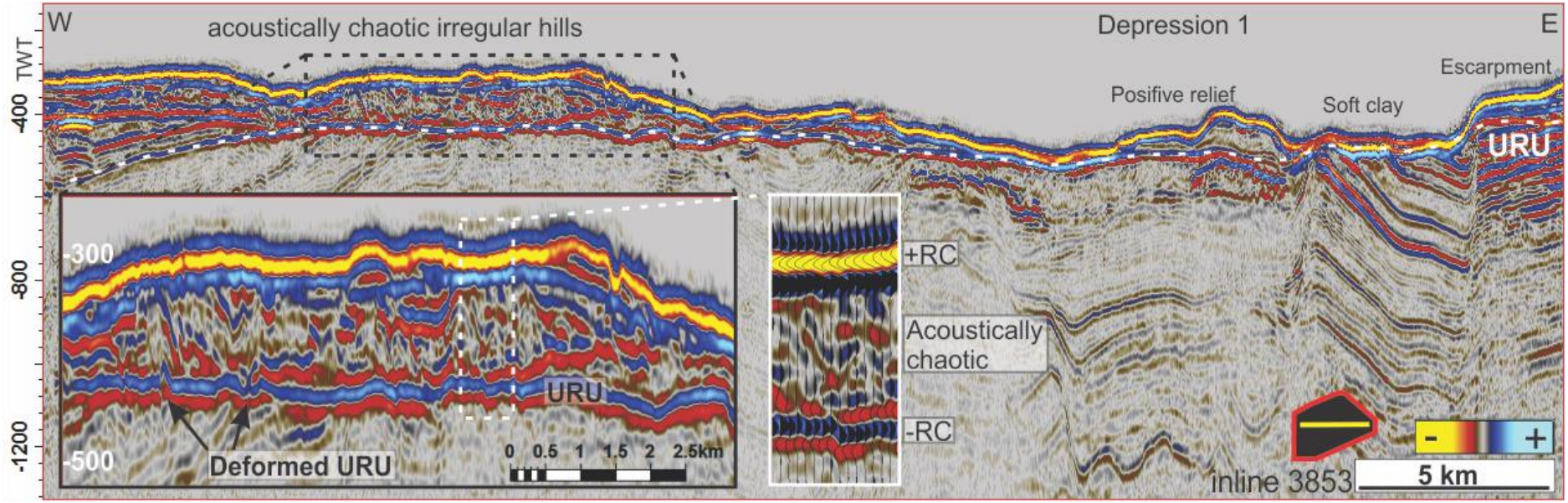


*Figure 4.21: A 3D seismic profile of the irregular hills west of the central over-deepening (depression 1). This show the acoustic chaotic and discontinuous reflection pattern observed within many of these hills, and a reversal in the reflection coefficient at URU compared to the seafloor. In the central over-deepening some irregular positive relief features are disrupting the deep bathymetry. Apart from the positive features the post-glacial sediments are very thin in this area and probably consist of marine/glacimarine soft clay.*

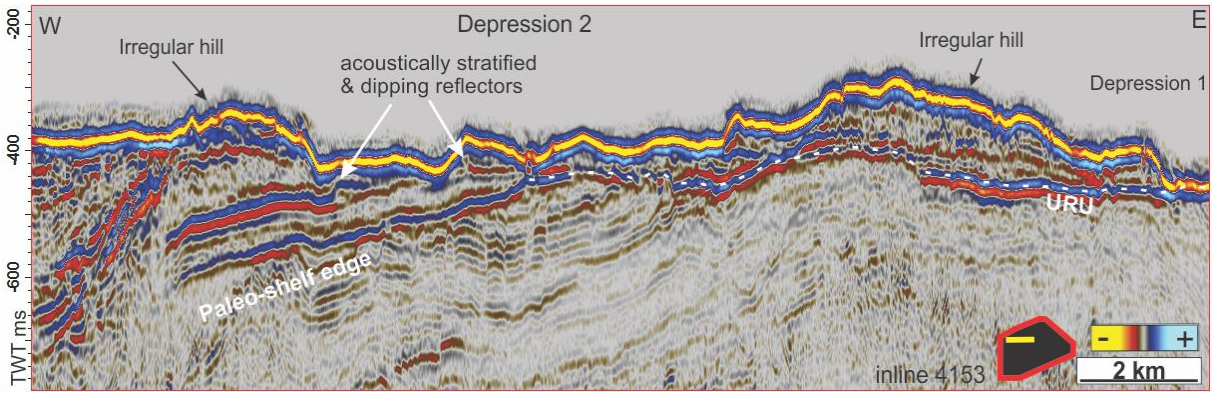


*Figure 4.22: W-E oriented Seismic profile through depression 2 and adjacent irregular hills. This figure show the morphology of the glacigenic deposits which is thickening towards west at the paleo-shelf edge. At this point the deeper reflectors within the unit are observed to become acoustically stratified, while the uppermost and eastern glacigenic deposits are chaotic (irregular hills).*

### *Irregular hills*

3D seismic profiles of the irregular hills in the trough, show a positive reflection coefficient at the seafloor, and a reversed RC compared to the seafloor at URU (Figure 4.21). The reflection within these hill deposits are characterized by chaotic and discontinous reflectors, with rapid change of vertical direction and only traceable for relatively short distances (Figure 4.21 - Figure 4.24). The vertical extent of the hills vary between 50 to 150 ms TWT (equivalent to ~40 – 110 m thick). At some locations beneath these hills, the underlying URU horizon seem to be uneven and deformed, either pushed down or pulled up on seismic sections, and an interpreted surface of URU show a rough bathymetry beneath the irregular hill deposits (Figure 4.21 & Figure 4.23).

On the southern onset of the irregular hills, an abrupt change of the characteristics of the internal seismic reflection occurs. Over an area of c. 500 m the recorded seismic trace change from a chaotic, discontinuous character, to become acoustically stratified (Figure 4.23). Where this occurs, the seismically chaotic unit slightly overprints the acoustically stratified unit. This rapid change in reflection pattern is seen in several seismic lines at the southern and western extent of the irregular hills. As you can see in Figure 4.23 on the seismic and the interpreted URU surface, URU is rough below these chaotic reflectors, while it is smooth and show preserved mega-scale glacial lineations below the acoustically stratified reflectors.

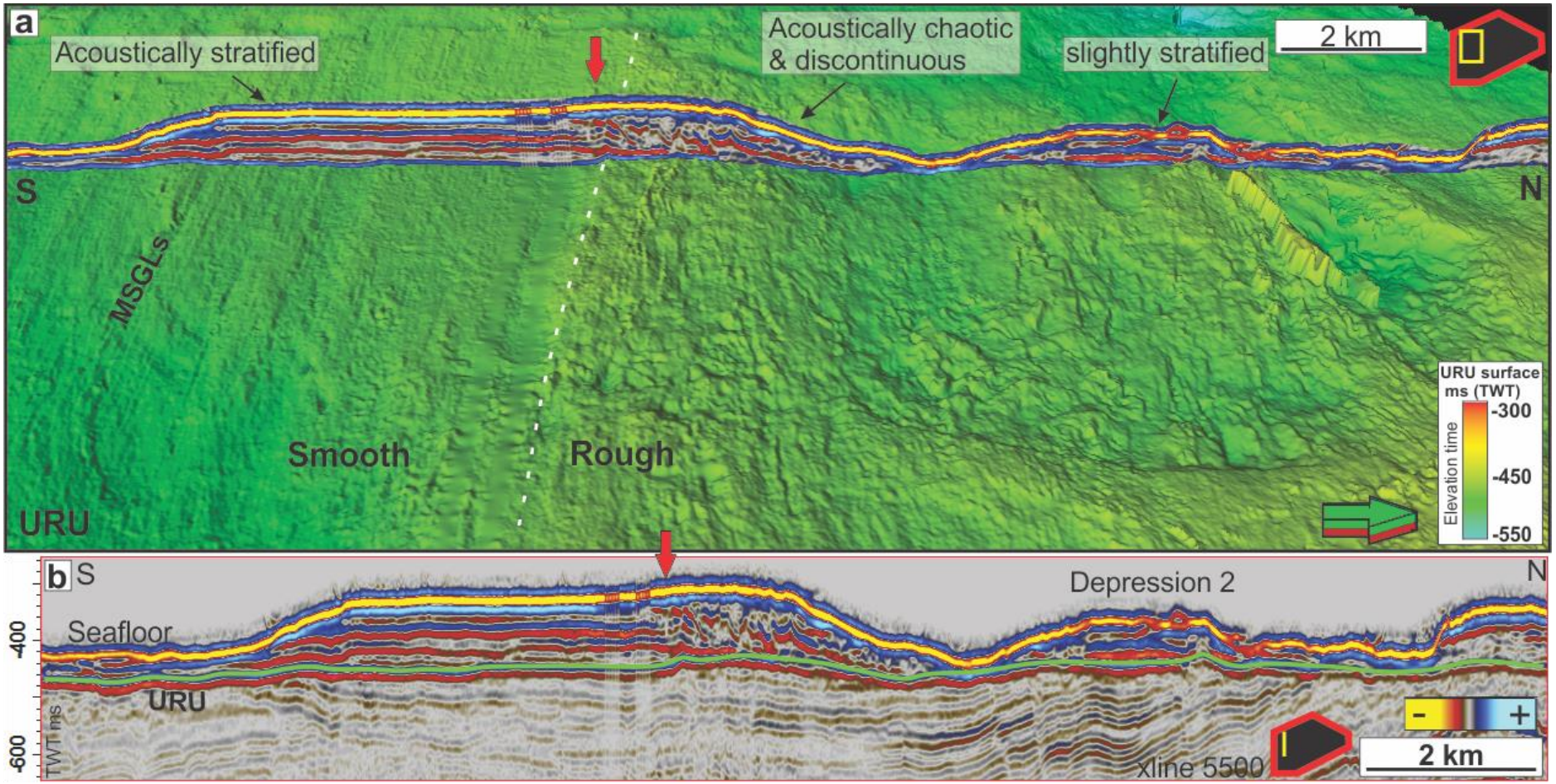


*Figure 4.23:* ***a)*** *A tilted 3D view along the interpreted buried URU surface, looking down at URU towards west. The S-N oriented cross profile show the rapid change and irregularities in the glacigenic deposits above URU. The surface of URU is rougher below acoustically chaotic and discontinuous deposits (right). Below acoustically stratified deposits, Mega-scale glacial lineations (MSGLs) are visible on a smoother surface (left). The transition between the two distinct deposits is marked with a red arrow above the seismic profile and a white dotted line along URU. At this point the acoustically chaotic deposits are slightly overlapping the stratified ones.* ***b)*** *The same S-N oriented seismic cross line as shown in 'a'. Xline 5500 from the 3D survey FP12_PRCMIG show the location and time elevation of the buried URU surface in 'a'.*

North-east on the irregular hills, a seismic unit of chaotic and low acoustic amplitude seem to be placed superimposed on a similar seismic unit of higher acoustic amplitudes (dotted white Figure 4.24). Seen in the same figure, grounding zone wedge 2 seem to be cutting the southern part of the irregular deposits.

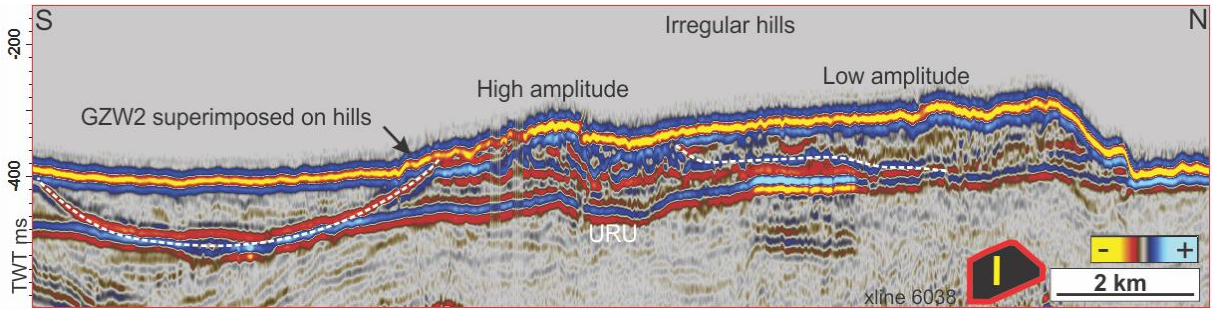


*Figure 4.24: This N-S oriented cross profile show the irregular hills described above and how they change in seismic character. The GZW2 are deposited superimposed on the southern onset of the irregular hills. Chaotic deposits of lower amplitude seem to overlie the high amplitude deposits (white dashed line).*

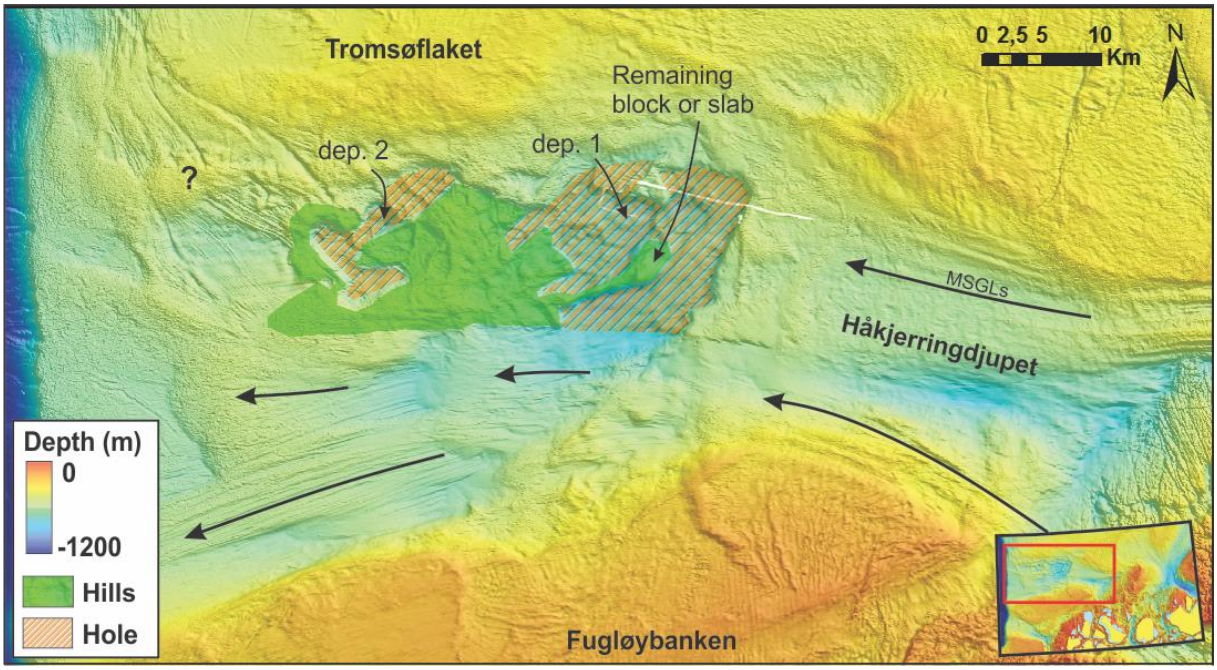


*Figure 4.25: By using 3D seismic data this interpretation of the extent of the glacitectonic hill-hole pair were created. Red coloured area show the extent of the interpreted source depression, areas of erosion (hole), while the green coloured area show the extent of glacitectonic deposits. Arrows indicate the direction of the paleo-ice flow in the area, based on MSGLs and GZW.*

### *Interpretation*

When correlating multibeam bathymetry and 3D seismic data, this area described above of an up to 100 m relief over-deepened area and adjacent hills with an irregular surface bathymetry and clearly deformed reflectors have been interpreted to be a product of glacitectonics that occurred during the last glaciation of Håkjerringdjupet. Based on

classification-methods by Aber *et al.* (1989) (Table 1.1) and observed geomorphology and characteristics of these glacitectonic features, these are furthermore interpreted as a hill-hole pair, where both the *hill* (irregular hills) and *hole* (depression 1 and possibly depression 2) are present (Figure 4.25). The hills are found, as expected, downstream of the interpreted ice flow, and seem to have been transported up to 30 km from the source area. A hill-hole pair is caused when sediments are frozen on to, squeezed and pushed by the enormous force of moving ice, from a source area (e.g. hole), until it is deposited as positive relief features (e.g. hills) downstream.

A correlation between multibeam bathymetry and 3D seismic data were used to map the extent of the irregular hills. Units of chaotic and discontinuous reflection configuration were mapped. By using a correlation with seismic data, deformed glacigenic units could be recognized, and their extent manually plotted in a bathymetrical map using ArcMap (Figure 4.25). Depression 2 may possibly have been eroded or deformed by glacitectonic events, but we cannot be sure if it is a source area, or how important I may have been.

The positive relief hill central within depression 1, does not show the same seismic characteristics as the other irregular hills interpreted as glacitectonically deformed deposits. This hill have an irregular shape but have sub-continuous acoustic reflectors of weak amplitudes, very different from the adjacent glacitectonic hills (Figure 4.21). This hill is therefore interpreted to be a remaining block or slab from a glacitectonic event, moved from its original position and over-run by ice but with its original structure more or less intact, possibly with only smaller deformations (Figure 4.25).

### 4.3.5 Random oriented small furrows: Ploughmarks

*Description*

Vast amounts of random oriented curved to sinuous-shaped furrows are characterizing the small-scale seafloor morphology, both inside the trough and on the banks. They are seen on all the bathymetric data, but best visible at the high 5 m resolution bathymetric map, and seem to occur preferably above 300 m depth, where they cover most parts of the seafloor (). They are found to be up to 20 km long, vary from 20 m to 300 m wide, and vertical reliefs between 1 – 10 m deep (Figure 4.26). Often found to have raised berms (ridges) on one or both sides of a central V- or U- shaped depression. These furrows are also associated with

deeper depressions within them or where they terminate/start. These depressions measure approximately the same width as the furrows, but their relief vary from 4 – 20 m deep.

*Interpretation*

The random oriented curved furrows match the description of what have been interpreted as plough marks, also known as iceberg scours, by earlier work from the Norwegian continental shelf. (Rafaelsen *et al.*, 2002; Dowdeswell *et al.*, 2007; Andreassen *et al.*, 2008). Ploughmarks are formed in glacimarine environments by drifting icebergs driven by ocean currents and wind, scratching the seafloor. They indicate ice loss by calving from marine terminating ice-sheets/glaciers, often associated with ice-streams. The depressions described are interpreted to be iceberg pits, associated with the plough marks. This is where the iceberg have grounded and is unable to move further, leaving a depression in the seafloor (Figure 4.26).

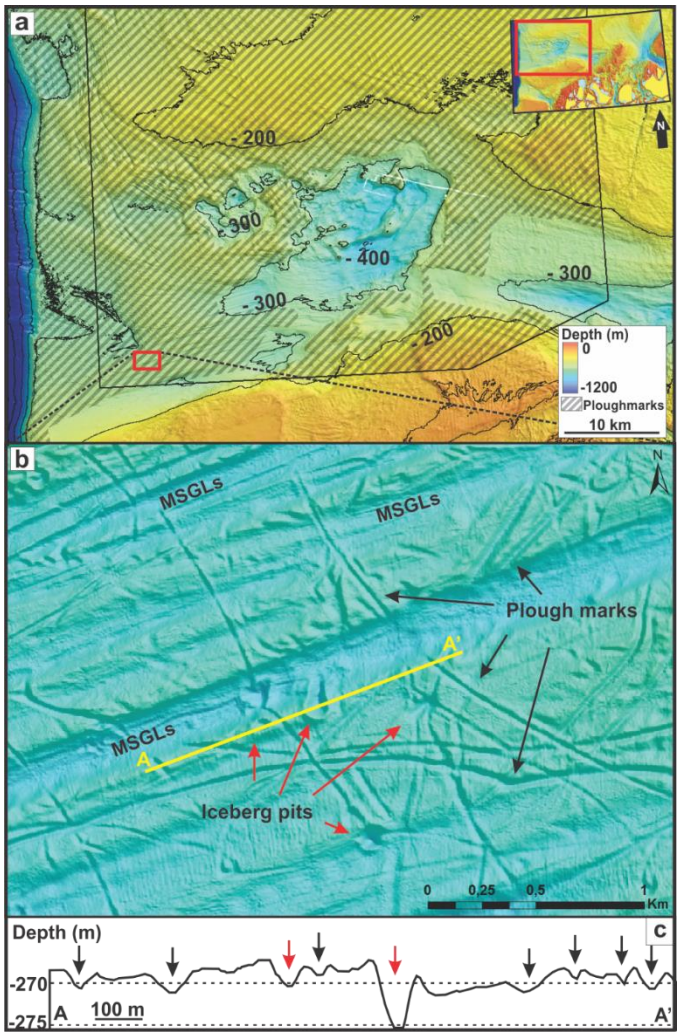


*Figure 4.26: **a)** The grey shading indicate the area within the study area that is covered by ploughmarks. Its abrupt change from present to absent along the black polygon is due to lack of high resolution data outside the polygon, making the mapping hard. The contour lines indicate the depth and is seems like the ploughmarks mostly occur above 300m depth. **b)** The high resolution bathymetric map show how the ploughmarks rapidly change direction and cross other seafloor features as MSGLs and other ploughmarks, and sometimes create iceberg pits. Yellow line A – A' show the profile in c. **c)** A profile along the seafloor that show the negative relief of the ploughmarks (black arrows) and iceberg pits (red arrows).*

# 5 Discussion

We have combined all our observations from our geophysical datasets with the aim to shed a light on connections and interactions between the three processes which have been observed in Håkjerringdjupet: ice streaming, glacitectonics and fluid flow. Ice streaming and glacitectonism are processes associated with very different dynamic and basal conditions, from warm fast flowing to cold slow flowing ice. We discuss how the effects of sub-glacial accumulations of fluids and potential formation of gas hydrates under low temperature – high pressure sub-glacial conditions may be a possible cause for the glacitectonic event observed in Håkjerringdjupet.

## 5.1 Faults & fluid flow

Accumulations and migration of fluids have been inferred to be located proximal to the fault compelx central in the trough. We will discuss this relationship further.

### 5.1.1 Faults

The extensive faulting through the mid-trough area is interpreted to be the southwestern part of the Troms-Finnmark Fault Complex (TFFC) (Figure 5.1). The fault complex is oriented NE-SW, stretching along the continental shelf through Håkjerringdjupet, where it continues into the SW Barents Sea. It is observed affecting deep seated sedimentary bedrock as well as shallower ones. Bright spots, interpreted as gas anomalies caused by shallow gas accumulation and/or migration have been observed and mapped along and adjacent to these faults where they seem to occur most abundant (Figure 5.1). We suggest that this fault complex, located centrally in the trough, have been important for the presence of shallow fluids as the faults seem to have acted as a natural migration pathways for fluids from deeper strata to the shallow subsurface (Figure 5.1) (Cartwright *et al.*, 2007; Vadakkepuliyambatta *et al.*, 2013; Edvardsen, 2015).

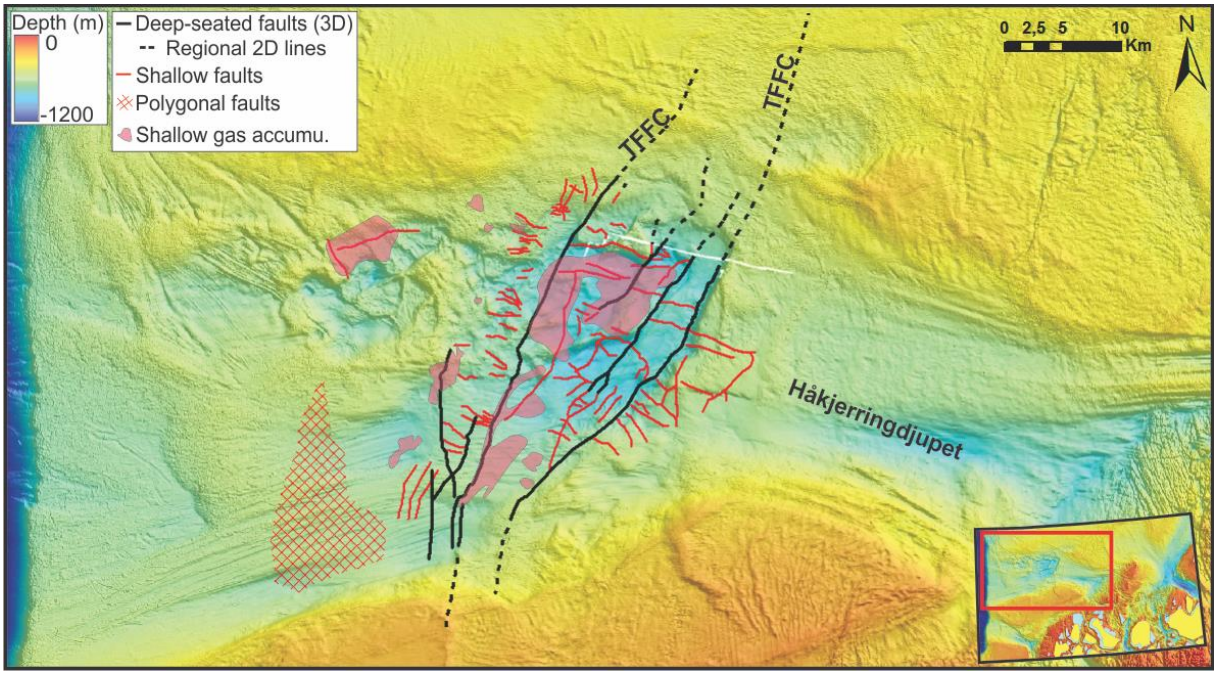


*Figure 5.1: This figure show mapped faults and interpreted shallow gas accumulations. A close relationship is implied between faults, lithological boundaries and gas migration and accumulation. Black dotted lines are interpretations of major faults outside of the 3D cube by the use of regional 2D lines. Red lines show the distribution of shallow faults. By shallow faults we mean faults that are connected to the major faults complex, but they do not extend vertically as deep as the major faults. TFFC = Troms-Finnmark Fault Complex.*

Polygonal faults are often associated with escape of fluids and dewatering to overlying units and pockmarks at the surface (Berndt *et al.*, 2003; Cartwright *et al.*, 2004; Ding *et al.*, 2013). The polygonal faults we observed in the trough may have been caused by gravitational loading by rapid deposition of sediments during glaciations as well as loading caused by the ice sheet itself. These polygonal faults do not show any signs of ongoing fluid escape or shallow gas accumulations, nor do they appear to show any correlation to the formation of the pockmarks observed at the seafloor (Figure 5.1, section 5.1.3). This may be explained by reworking of the sediments at the seafloor, which is highly likely since the area have been heavily glaciated, and that the dewatering process ceased when the glacially induced high-pressure regime became equalized and hydrostatic. There are no signs that the suggested dewatered fluids originated from a deeper source. Another explanation is that the sediments were unconsolidated pre-faulting and contained ground- or saline water within the pores. Thus, we do not associate these polygonal faults with any fluid migration or shallow gas accumulation observed and described in this study.

### 5.1.2 Fluid migration

As mentioned, bright spots, interpreted as low velocity fluids (preferably gaseous) on the 3D seismic data are observed along bedding- and fault planes in pre-glacial sediments. These -planes are believed to act as natural migration pathways for gaseous fluids originating from a deeper source or reservoir. Faulting, erosion and post-glacial uplifting of the area may tilt a reservoir or break traps, causing spilling and upward migration of fluids along these pathways (Solheim *et al.*, 1996; Chand *et al.*, 2008).

The interpreted accumulation of shallow gas seem to be connected to lithological boundaries and along the fault complex that acts as stratigraphic traps within the upper part of the pre-glacial sedimentary unit. Younger glacigenic sediments of probably high density and low permeability overlie this fluid-bearing unit proposed to work as a top seal, preventing or attenuating further fluid escape to the seafloor. One suggestion to such a hardening or consolidation of sub-glacial sediments is due to basal freezing (Christoffersen & Tulaczyk, 2003b). The well report from well 7019/1-1 located on the bank of Tromsøflaket, 20 km north of Håkjerringdjupet, said the uppermost bed were very hard and imbedded with boulders (NPD), supporting our suggestion of a dense and low permeable glacigenic unit, probably sub-glacial till. Furthermore, the same drilling project proved gas bearing intervals of Mesozoic age, supporting a thermogenic origin of the inferred fluids in Håkjerringdjupet. This would explain the negative reflection coefficient seen at URU west in the trough, where high density/velocity glacigenic sediments overlie low velocity gas-filled porous and permeable sedimentary rock.

Where the glacigenic unit thins, evidence of fluids escaping through the seafloor are seen by observations of pockmarks above areas of shallow gas indicators (Figure 5.2). This may imply to be a result of thinning or complete removing of the dense and perhaps low permeable glacigenic sediments, allowing gas-escape through the seafloor (Figure 5.2). However, for pockmarks to be formed, fine grained sediments are the only medium which they may be recorded in. Therefore we cannot rule out the possibility that the glacigenic unit may be permeable, releasing fluids through the seafloor. The glacigenic unit may simply consist of too dense and coarse sediments for pockmarks (of a detectable size) to be formed. The gas seepage forming the pockmarks at today's seafloor are suggested to be of relative young age

(post-glacial) and possibly still active today, as there still are indicators of presence of shallow has in the subsurface (Figure 5.2).

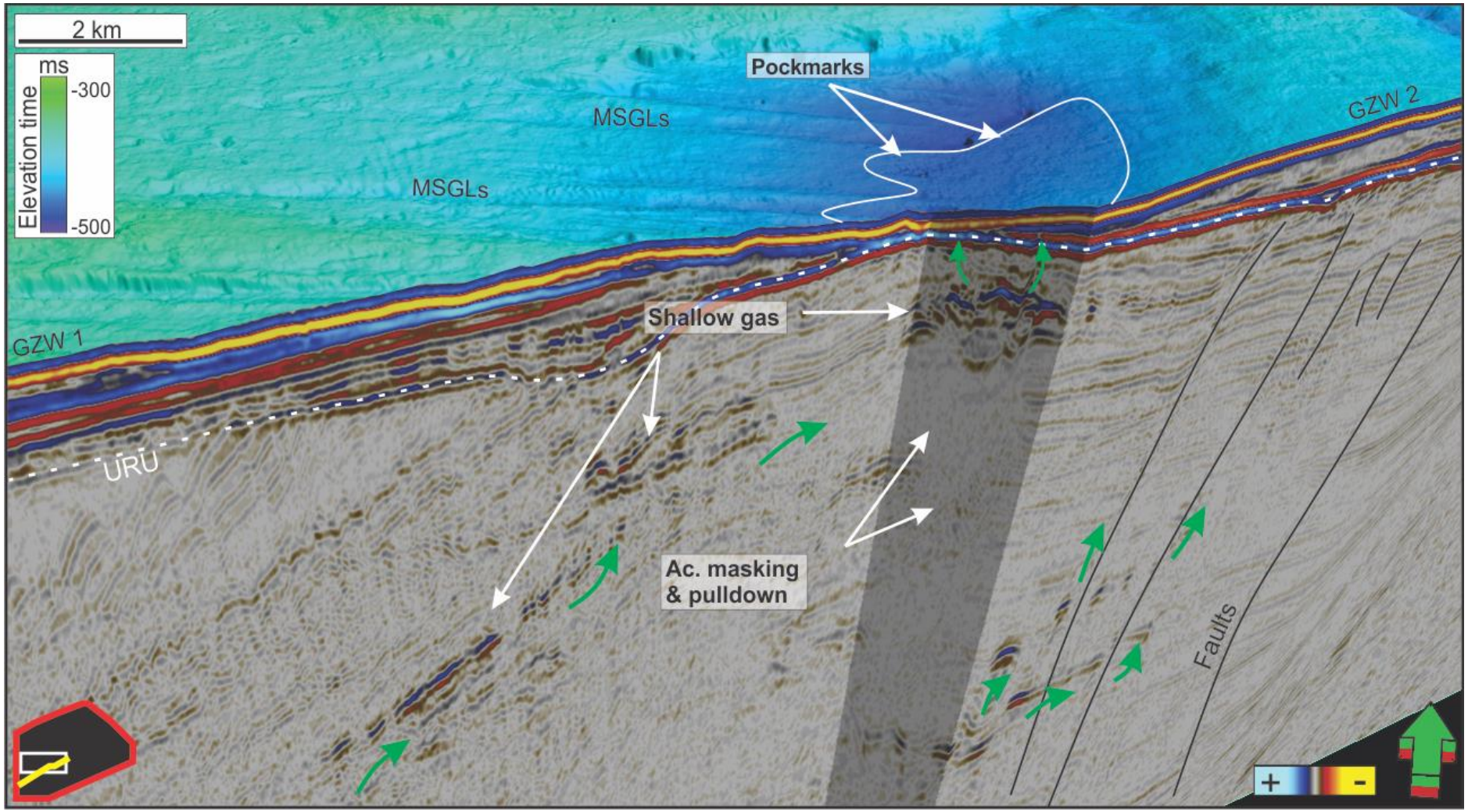


*Figure 5.2: A 3D view of a seismic line showing shallow gas indicators directly below the seafloor where pockmarks (located within the white line) have been observed at the slope of grounding zone wedge 2. This is suggested to provide evidence that the pockmarks are mainly formed by escape of thermogenic fluids migrating along faults and bedding planes from a greater deep within the sedimentary bedrock. The location of this seismic line is also shown in Figure 5.3.*

### 5.1.3 Pockmarks

The distribution of pockmarks is concentrated within depressions where the glacigenic unit is thin and indicators of shallow gas often are present in the shallow sub-surface (Figure 5.2 & Figure 5.3). This indicates a close relationship between pockmarks and shallow gas that have migrated along lithological boundaries and faults. Pockmarks are also observed east of the fault complex, where they occur less dense and not associated with shallow gas accumulations or deep seated faults (see section 4.3.1, Figure 4.13). Backscatter data from Mareano/NGU show low backscatter from the seafloor in the areas covered by pockmarks, indicating that the pockmarks are formed in soft sediments (Figure 4.14). Rise *et al.* (2014) observes an up to 20 m thick layer of stratified soft marine/glacimarine sediments below pockmarks within depression 1, consistent with the observed low backscatter.

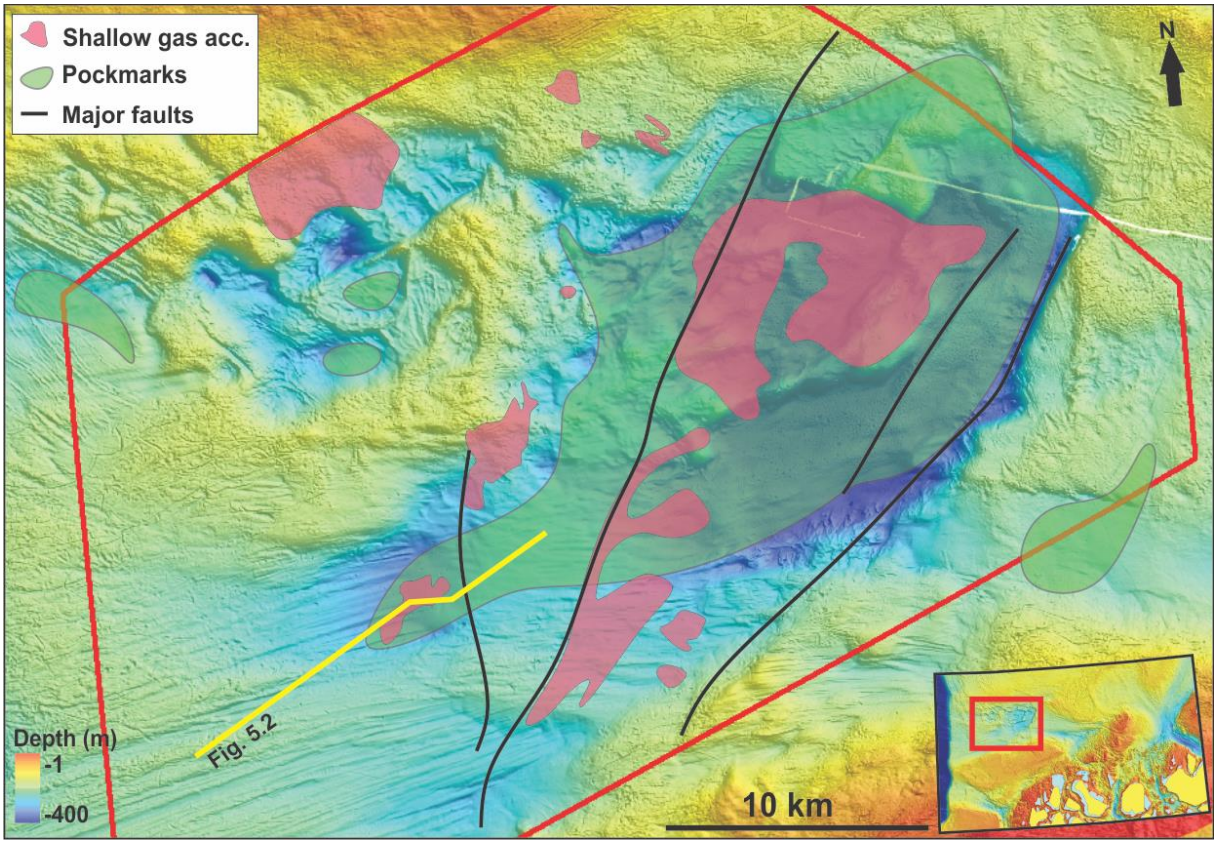


*Figure 5.3: The distribution of pockmarks (green) central in the troughs over-deepening seem to be closely related to accumulation of shallow gas in the sub-surface (red), which again are related to deep seated faults. Yellow line show the location of the seismic line used in Figure 5.2.*

Although the pockmarks are formed in soft sediments, many of them show high backscatter from within their depressions. This may imply that the sediments are normal graded, were coarse sediments are located below the fine grained sediments. The coarse sediments are

exposed when the overlying soft sediments are removed by gas seepage. It may also be due to formation of carbonate crusts (MDAC) or growth of coral reefs. Also positive relief cone-shaped features up to 7 m high of high backscatter were observed emerging from the centre of some pockmarks (Figure 5.4). Three suggestions were made to try explain their origin (see section 4.3.1) and are now discussed further as we suspect they may indicate proof of shallow hydrocarbons:

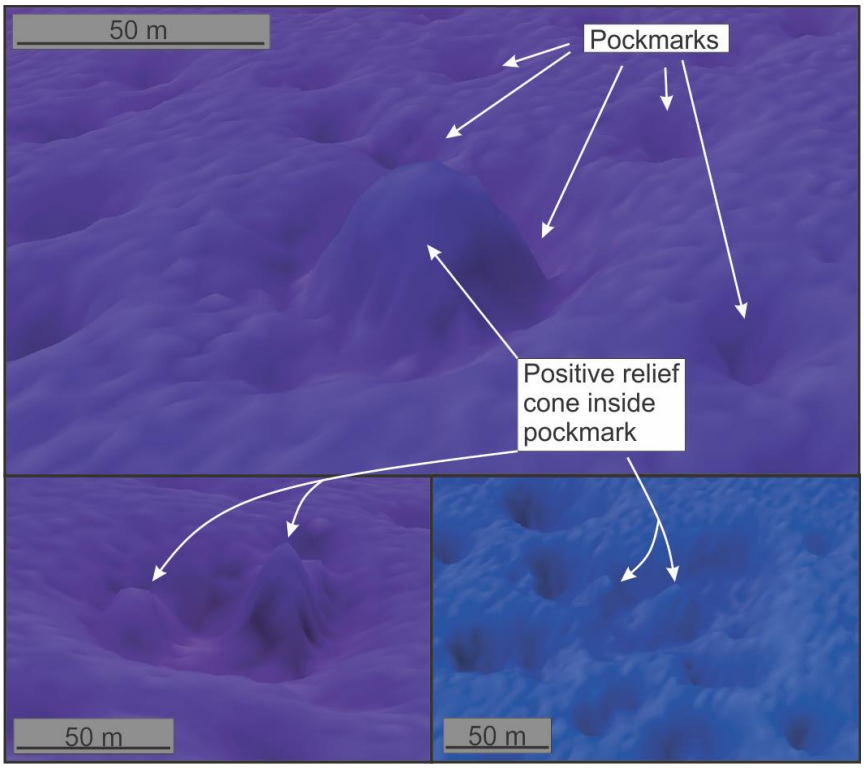


*Figure 5.4: An exaggerated figure of the positive relief cone-shaped structures seen within pockmarks, mainly inside the central over-deepening (>350 m deep). The cones were 3D visualized using Fledermaus.*

1. Large submarine pingoes/gas hydrate mounds due to local build-up of gas hydrates (preferably structure II) (Hovland & Svensen, 2006; Serie *et al.*, 2012). To our knowledge it is not observed submarine hydrate pingoes reaching over 5 m in relief before, but Bondarev *et al.* (2002) described submarine pingo-like structures with elevation of 10-25 m in ice-bound permafrost north of Russia. It is uncertain how likely it is that gas hydrates still are stable within the trough, as the deepest part of the trough is just at the limit of a theoretically structure II gas hydrate stability zone (GHSZ) at 400 m below sea level (Chand *et al.*, 2008).

2. Growth of coral reefs feeding on nutrient fluids escaping from the pockmarks (Hovland & Risk, 2003; Judd & Hovland, 2007; Moumets, 2008; Hovland *et al.*, 2012). This is a very possible suggestion, since the mareano project have identified deep-water coral reefs at

several locations in the trough (www.mareano.no). However, coral reefs would prefer to grow on hard bottom sediments, and its growth would probably rely on a constantly feeding source. Even though we have suggested that these pockmarks are still active, we do not know how constant any seepage is.

3. Formation of methane-derived authigenic carbonate rock (MDAC) also known as carbonate crusts or mounds, due to biochemical processes in the proximity of pockmarks and presence of methane-rich fluids (Aloisi *et al.*, 2002; Hovland *et al.*, 2005; Judd & Hovland, 2007; Chand *et al.*, 2009). Carbonate crusts have been identified and sampled from both the Barents Sea and the Norwegian Sea on the continental shelf, at least one related to pockmarks (Buhl-Mortensen *et al.*, 2012).

We will also open the possibilities that it may be a combination of crust precipitation of MDACs which provide a hard surface supporting growth of coral reefs. This could explain the height that these features reach.

### 5.1.4 Gas Hydrates

Submarine pingoes, MDACs and coral reefs, all support the suggestion of migrating hydrocarbon-rich fluids to the shallow subsurface and to the seafloor (Aloisi *et al.*, 2002; Hovland & Svensen, 2006; Judd & Hovland, 2007). A thermogenic origin of the fluids have been implied as well, and thus they may contain heavier hydrocarbons (e.g. butane, propane etc.), as supported by signs that these fluids have migrated from a deeper source and discoveries in well 7019/1-1.

Gas hydrates are formed under low temperature – high pressure conditions, where gas molecules are trapped within a cage of frozen water molecules. Under present temperature – pressure conditions, Håkjerringdjupet is just at the boundary for gas hydrates to be stable (Figure 5.5a). However, when the trough was glaciated the temperature – pressure conditions were different. Modelling of the gas hydrate stability zone (GHSZ) in the Barents Sea by Chand *et al.* (2008) show that reduced bottom temperature and increased pressure induced by ice loading on the shelf would cause a distinct thickening of the GHSZ during glaciations. Figure 5.5 show a theoretical stability diagram for the GHSZ at present day conditions (a) and under ice cover (b). An approximately 400 m thick GHSZ for methane hydrates (structure I) are inferred by the diagram during glaciations. If the gas present

contains heavier hydrocarbons (e.g. butane or propane), the GHSZ would be even thicker (Chand *et al.*, 2008).

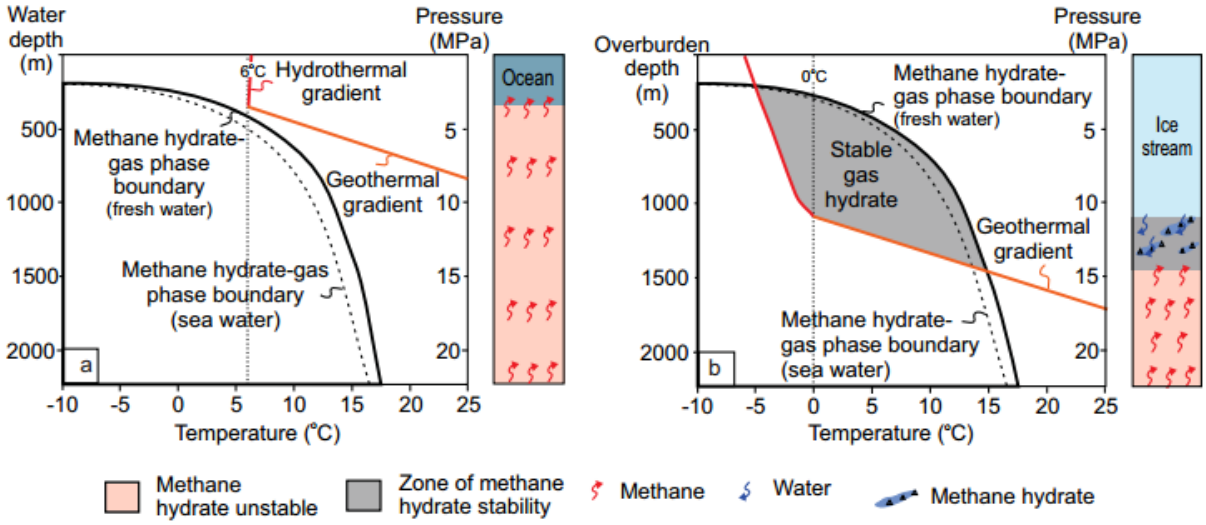


*Figure 5.5: A theoretical stability diagram for methane hydrates in a marine and subglacial environment.* ***a)*** *Today, Håkjerringdjupet is purely in a marine environment, outside of the methane hydrate stability zone.* ***b)*** *Under past glacial ice cover, high pressure – low temperature conditions created a 400 m thick gas hydrate stability zone beneath Håkjerringdjupet Ice Stream. Figure from Winsborrow et al. (2016).*

Based on the observations of present shallow gas indicators, pockmarks and the methane hydrate stability diagram (Figure 5.5), we will suggest that it is very likely that gas hydrates could and did form during low temperature – high pressure conditions in a sub-glacial environment. The only limitations would have been sufficient supply of water and gas. Today, stable conditions for gas hydrates within Håkjerringdjupet are unlikely (Figure 5.5), but plausible in the over-deepened area if higher order of hydrocarbons are present and with a geothermal gradient below 31°C/km (Chand *et al.*, 2008). It is therefore legitimate to suggest that dissociation of gas hydrates during and after deglaciation would have contributed to release of large amounts of free gas into the overlying layers and through the seafloor, forming pockmarks, as suggested by Rise *et al.* (2014) (Solheim & Elverhoi, 1993; Fichler *et al.*, 2005; Chand *et al.*, 2008).

Perhaps more interesting, gas hydrate formation have been shown to harden the sediments (Figure 5.6). As hydrate formation depend on water, it could potentially drain the surrounding sediments, reducing the pore water pressure and forming hard ice. This have shown to drastically increased the consolidation and shear strength of sediments containing gas hydrates (Figure 5.6) (Ben Clennell *et al.*, 1999; Durham *et al.*, 2003; Winters *et al.*, 2004; Hyodo *et al.*, 2013).

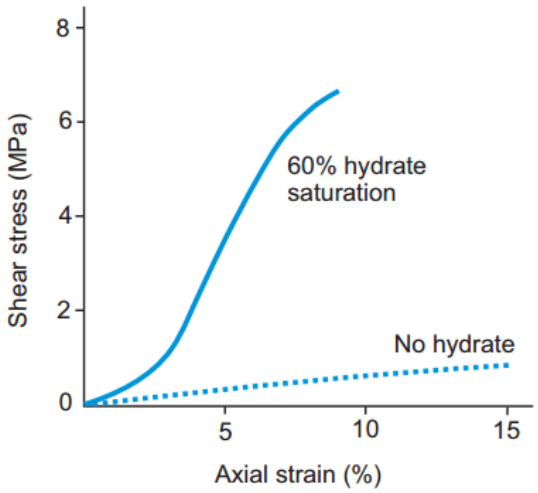


*Figure 5.6: A graph where shear stress (applied force) is plotted against axial strain (amount of deformation) for sediments with 60% hydrate saturation and complete hydrate free sediments. Sediments saturated with gas hydrates have a much higher shear strength than non-hydrate sediments. Figure from Winsborrow et al. (2016), based on Winters et al. (2004).*

## 5.2 Ice streaming & glacitectonics

Extensive evidence of a Late Weichselian grounded ice stream within Håkjerringdjupet have been observed and described along the E-W oriented trough, where ice were drained from the northern Fennoscandian Ice Sheet out to the shelf edge (section 4.3.2 & 4.3.3 and Figure 5.7). The trough have been a pathway for active grounded fast flowing ice streams reaching the shelf edge for perhaps several generations of glaciation, supported by observations of mega-scale glacial lineations at today's seafloor and at the buried paleo-seafloor URU, both terminating at the (paleo-) shelf edge (Figure 5.7). Fast ice flow rely on soft deformable sub-glacial till and basal meltwater that lubricated the bed of the ice (E. C. King *et al.*, 2009).

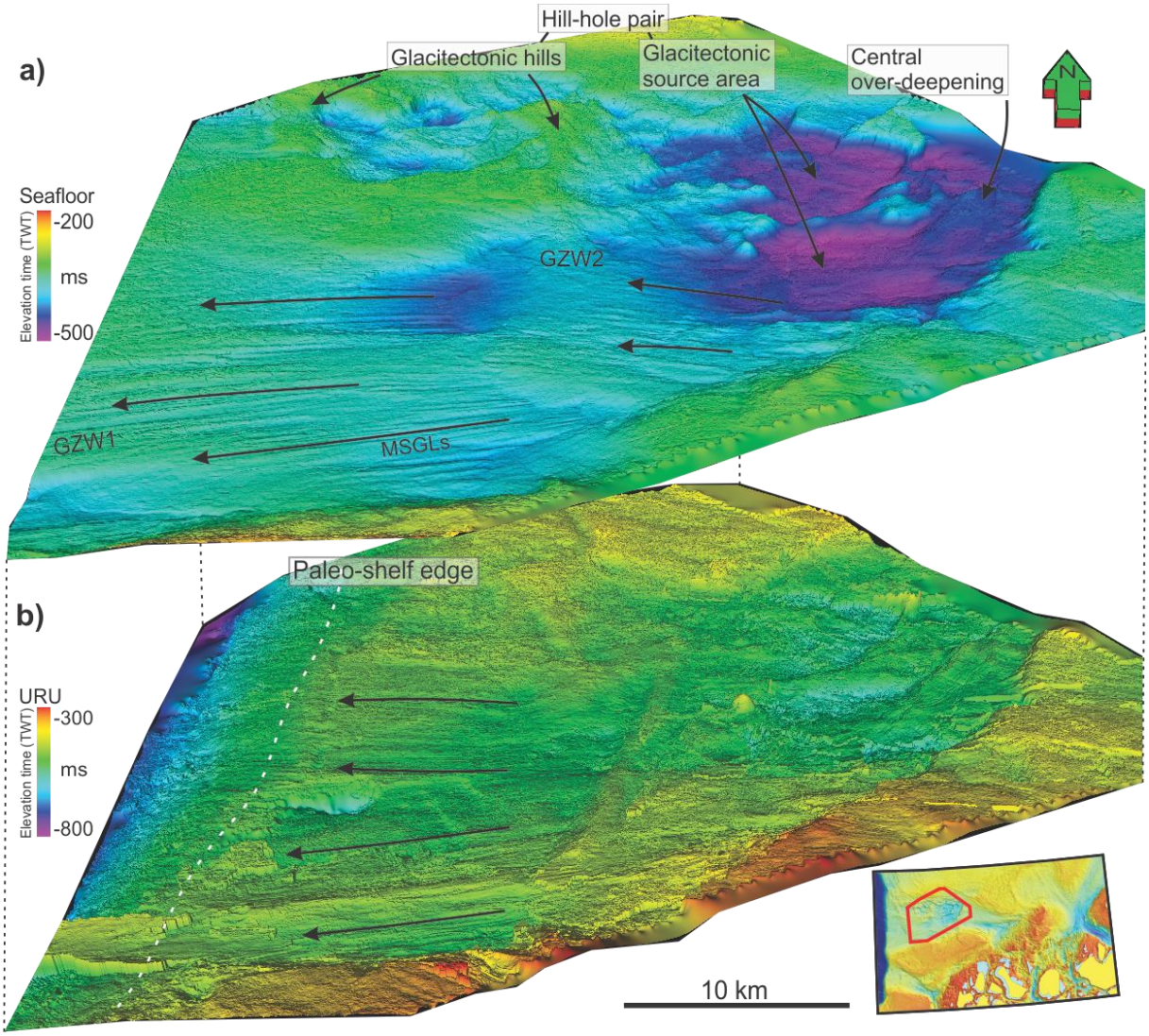


*Figure 5.7: The 3D seismic survey FP12_PRCMIG were used to 3D visualize the interpreted seafloor and URU surfaces, aiming to show evidence of fast and slow flowing ice with in Håkjerringdjupet. The distance between the seafloor and URU is exaggerated.* ***a)*** *The present-day seafloor. Its southern part is dominated by landforms as MSGLs and grounding zone wedges (GZW1 & GZW2), while its northern half is dominated by an irregular glacitectonic hill-hole pair.* ***b)*** *The acoustically interpreted URU surface show how past glaciations have formed MSGLs, terminating at the paleo-shelf edge (white dotted line).*

Perhaps more surprisingly, a hill-hole pair, indications of slow flowing ice and high basal traction, occupies the northern half of the trough with its source depression located in the troughs central over-deepening, directly above the fault complex – an area associated with shallow gas accumulations (Figure 5.7, see section 4.2 & 5.1, Figure 5.1 & Figure 5.3). These are indicating an interesting connection between ice stream dynamics and shallow fluid accumulations. Figure 5.8 indicates where the glacitectonic erosion occurred, located just above interpreted shallow gas accumulations in an area where pockmarks are abundant at the seafloor (Figure 5.1 & Figure 5.3).

As indicated in Figure 5.7 & Figure 5.8, the main focus of the active Late Weichselian ice streaming is believed to have been located at the trough's southern part, the only area where MSGLs are observed through the whole trough, all the way to the shelf edge. Grounding zone wedges located here indicate an episodic deglaciation with at least two stillstands/readvances of the ice margin and continuously fast flowing ice, inferred by superimposed MSGLs. Indicators of shallow gas accumulations are sparser in the south and the faults less extensive developed. Gas accumulations are only seen in the mid-trough part around the area where grounding zone wedge 2 is located, and very few pockmarks occur at the seafloor compared to the northern half of the trough (Figure 5.3).

North in the trough the glacitectonic hill-hole pair is dominating the seafloor bathymetry. Its southern margin is trough parallel and the E–W oriented extent of the deposits are interpreted to imply that the sediments were transported mainly sub-glacially rather than pro-glacial (Figure 5.7 & Figure 5.8). The only mega-scale glacial lineations observed in the northern half were recognized east of the fault complex and the mid-trough escarpment (Figure 5.8). This is believed to indicate that the ice in the northern half of the trough only were partly fast flowing during the last deglaciation. Implied by the absence of MSGLs, fast flowing ice did not override any of the glacitectonic landforms NW in the trough. Hence, any overriding ice is implied to must have been slow moving and perhaps cold based (Figure 5.7 - Figure 5.12).

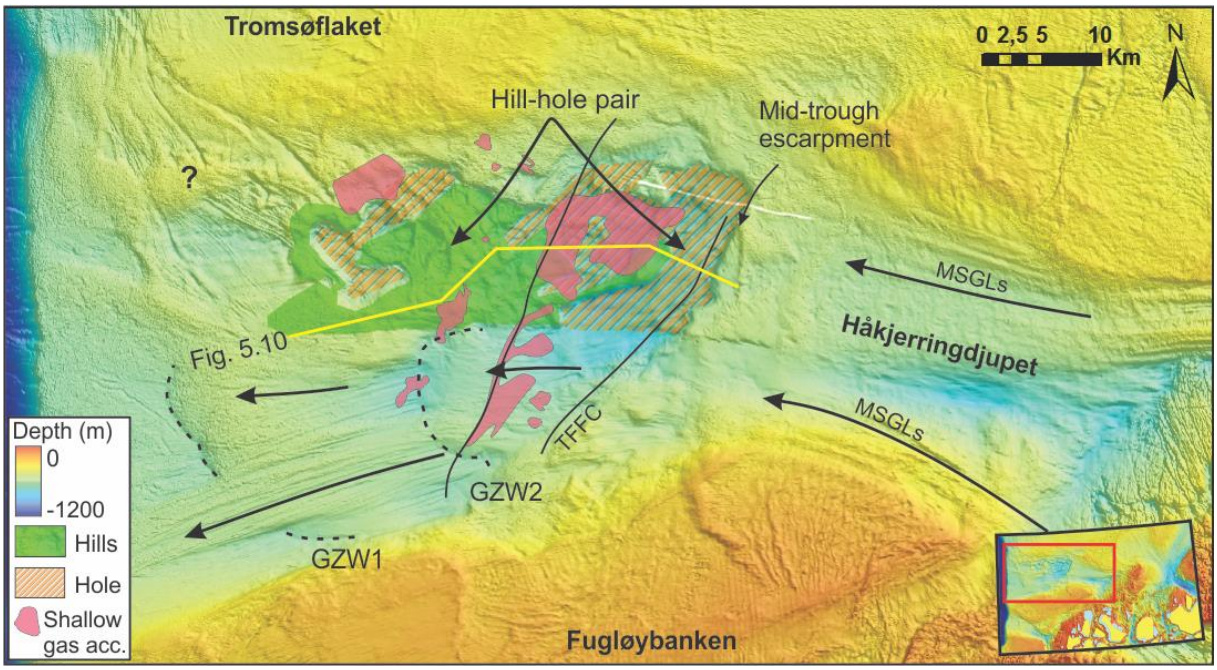


*Figure 5.8: A distinct change in ice dynamics is implied from the northern half to the southern half of the trough. MSGLs, evidence of fast flowing ice is most prominent south, while a glacitectonic hill-hole pair is dominating the seafloor in the northern half. A linkage between fluid flow features and glacitectonics are inferred by the rapid change of the ice stream dynamics from north to south, and east to west of the mid-trough escarpment. Fluid flow features, such as shallow gas accumulations are associated with the TFFC, and are more prominent in the northern half together with an abundance of pockmarks (Figure 5.3). A clear transition from warm based fast ice to cold based slow ice is seen at grounding zone wedge 2 (GZW2), where its northern end is sub-parallel to the glacitectonic deposits. Yellow line indicate the location of seismic line in Figure 5.10. '?' shows an area which could not be fully interpreted but may possibly be of glacitectonic origin.*

### 5.2.1 Ice stream stagnation and basal freeze-on

Interestingly, the northern half of the central over-deepening (glacitectonic source area) is the area that is most extensive faulted by the TFFC and have earlier been described to show the strongest indicators of past and perhaps present fluid flow and shallow gas accumulation (see section 4.2.2, 4.3.1, 5.1 and Figure 5.8). No evidence of fast flowing ice inside or west of the central over-deepening, and glacitectonic rafted hills directly downstream, are here interpreted to imply that a change in ice stream dynamics occurred at this location.

Assuming the northern part of the trough once were fast flowing as a part of an active ice stream, as the shape of the trough and the eastern MSGLs imply (Figure 5.8), we need to explain what could cause a decrease or stoppage in the ice velocity, and hence the onset for the glacitectonic event. Sub-glacial conditions are by many regarded as a key issue trying to understand the dynamics of ice streams and their behaviour, and so called sticky spots, areas of local high basal friction, have been implied to cause switching, freezing and complete stagnation of contemporary and paleo-ice streams (Alley, 1993; Stokes *et al.*, 2007; Winsborrow *et al.*, 2016). Basal freeze-on of sub-glacial sediments onto the ice-bed is

here suggested to be the most relevant issue, as we imply that the sediments were sub-glacially, and not pro-glacially transported during any glacitectonic event.

Numerical models on the effects of basal freeze-on beneath fast flowing ice streams have been conducted in several studies (Tulaczyk *et al.*, 2000; Bougamont *et al.*, 2003; Christoffersen & Tulaczyk, 2003a, 2003b). Freezing of the ice bed occur when the basal conductive heat loss exceeds the frictional shear heat generated at the bed ice interface (Tulaczyk *et al.*, 2000). These models describe how sub-glacial freeze-on potentially could extract pore water during ice growth, dewatering the till and decreasing porosity and pore-water pressure (Figure 5.9). This would result in consolidation (in undrained sediments) and increased shear strength of sub-glacial till (Figure 5.9). This will continue until the shear strength reaches the driving stress of the ice, causing stoppage of the overlying ice flow (Bougamont *et al.*, 2003; Christoffersen & Tulaczyk, 2003a; Stokes *et al.*, 2007). According to Christoffersen and Tulaczyk (2003a), such a stoppage could take less than a century from the basal freezing were initiated.

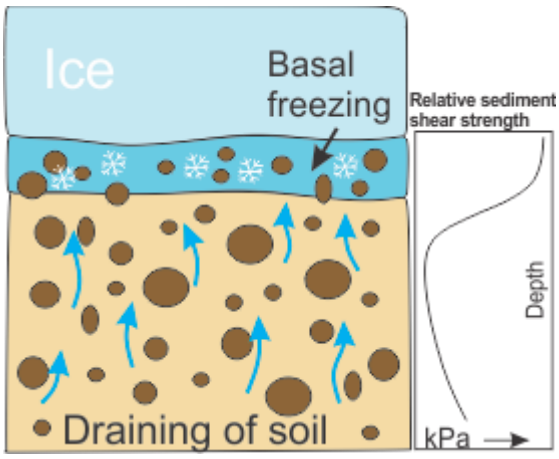


*Figure 5.9: A concept sketch which show how basal freezing potentially could drain water from the sediments. This results in highly increased shear strength in the frozen sediments and therefore increased basal drag. Figure based on Christoffersen and Tulaczyk (2003a).*

Several mechanisms have been proposed to trigger basal freeze-on and stagnation of contemporary and paleo-ice streams: (1) Change or reorganization of meltwater drainage, and therefore its availability, so called “water piracy” (Anandakrishnan & Alley, 1997). (2) Basal freeze-on due to dynamical changes within the ice stream, such as reduced ice discharge or ice thickness (Payne & Dongelmans, 1997; Tulaczyk *et al.*, 2000; Bougamont *et al.*, 2003; Christoffersen & Tulaczyk, 2003a). At last we introduce a new mechanism, (3) basal freezing and ice stream stagnation due to sub-glacial gas hydrate formation. A similar theory have only recently been presented by Winsborrow *et al.* (2016).

Payne and Dongelmans (1997) described how reduced ice stream discharge may cause the bed of an ice stream to freeze by reduced shear heat and meltwater production at the bed (Tulaczyk *et al.*, 2000; Stokes *et al.*, 2007). Another factor such as thinning of the ice

thickness of any glacier or ice stream is known to make it more vulnerable to temperature changes (faster heat exchange), and may often cause the ice to become cold based (Payne & Dongelmans, 1997; Tulaczyk *et al.*, 2000; Bougamont *et al.*, 2003; Stokes *et al.*, 2007). Such a thinning and reduced ice discharge is natural to assume during a phase of deglaciation, also in Håkjerringdjupet, and would increase the chances of basal freeze-on and possibly shut-down of the ice stream.

Fluid accumulations in shallow subglacial sediments are here suggested to have triggered or enhanced the sub-glacial freezing process in Håkjerringdjupet by formation of gas hydrates under low temperature - high pressure conditions. Such conditions have existed during glaciations, and perhaps most favourable in the northern half, where an abundance of fluid flow features (e.g. shallow gas and pockmarks) have been identified, concentrated around the deep seated fault complex (Figure 5.8 & Figure 5.10). The only restrictions on hydrate formations would then rely on sufficient water and gas supply in the sediments. The gas supply could be restricted by a low gas flux through the faults or by formation of a deeper gas hydrate layer in the substrata, which could act as a cap, preventing further upward migration of gas, as gas hydrates are known to have low permeability (Hovland, 2005). Water are restricted in undrained and cold conditions, where liquid water is not available as it already has turned to ice, or where sufficient water inflow do not exist. Modelling of physical properties of natural and laboratory-formed methane gas hydrates (structure I) have proved that formation of hydrates increase the shear strength of sediments up to 20 times more effective than freezing of purely water-saturated sediments (Figure 5.9) (Durham *et al.*, 2003; Winters *et al.*, 2004; Hyodo *et al.*, 2013).

Based on the theories presented above we would suggest that conditions suitable for the formation of gas hydrates existed as long as the trough were ice-covered, and furthermore that gas hydrates would severely increase the shear strength of sub-glacial sediments, therefore also increase basal drag beneath the ice stream. On this basis we would propose that sticky spots, induced by gas hydrate formation, could have existed below Håkjerringdjupet Ice Stream and therefore be the cause of ice stream stagnation, basal freeze-on and following glacitectonic erosion.

As we will discuss later, the deglaciation phase is also thought to have influenced the coming glacitectonic event during episodes of readvancing (see section 5.2.2). During deglaciation

the ice margin retreated rapidly but episodic, as evidenced by preserved MSGL and GZWs, and the ice thickness were likely to be thinning. We suggest that quiescent phases of ice flow combined with gas hydrate induced sticky spots caused increased basal drag and enhanced the basal freezing, if not initiated it, at the northern half of the ice stream. We acknowledge that sub-glacial gas hydrates potentially could have formed during the whole glaciation, and therefore the glacitectonic hill-hole pair could be a result of several smaller events occurring over a long period of time. However, we would like to make an additional suggestion: continuous ice streaming through last glacial maximum and parts of the deglaciation phase were possible even if gas hydrates existed. The thought is that the thick fast flowing ice produced enough heat and meltwater at the ice bed interface, which helped keep the bed lubricated and the till soft, hence too unstable conditions for gas hydrates to form and freeze directly onto the ice bed (Parizek *et al.*, 2002; Stokes *et al.*, 2007; Wadham *et al.*, 2012). Even if freeze-on occurred before the deglaciation were initiated, we will still suggest that the deglaciation phase could enhance any basal freeze-on and therefore potentially trigger larger glacitectonic events.

The southern half of the ice stream show indications to have been continuously fast flowing, and no glacitectonic deposits are observed here. A decrease in ice stream width below a threshold value would allow continuous active ice streaming as a result of a concentrated ice flow that generates sufficient heat and meltwater for lubrication of the bed (Bougamont *et al.*, 2003; Stokes *et al.*, 2007). If the ice stream is affected by one part of it shutting down or ice flow prevented, as a response to this, a reorganization of the ice stream could potentially occur, which is what we might see in the southern part of the trough where evidence of continuous ice streaming are observed. Similar reorganizations of ice streams have earlier been referred to as flow switching, and can occur on relative short time scales (Conway *et al.*, 2002; Hulbe & Fahnestock, 2007; Winsborrow *et al.*, 2012). If the ice flow continued up-stream of the stagnant ice in the north, the ice thickness may increase, or bulge, this could increase the meltwater production, potentially drain meltwater to the southern part of the ice stream (Anandakrishnan & Alley, 1997; Vogel *et al.*, 2005). Our suggestion is that the southern half of the ice stream were not prevented by the stagnation or reduced velocities in the north. Instead, as a response to the basal freezing and perhaps stoppage of the ice stream in the north, we suggest the active ice stream were reorganized and concentrated

south in the trough and therefore experienced ongoing rapid ice flow which allowed basal meltwater generation and lubrication of the bed to continue. Thus prevented a complete shutdown of the Håkjerringdjupet Ice Stream.

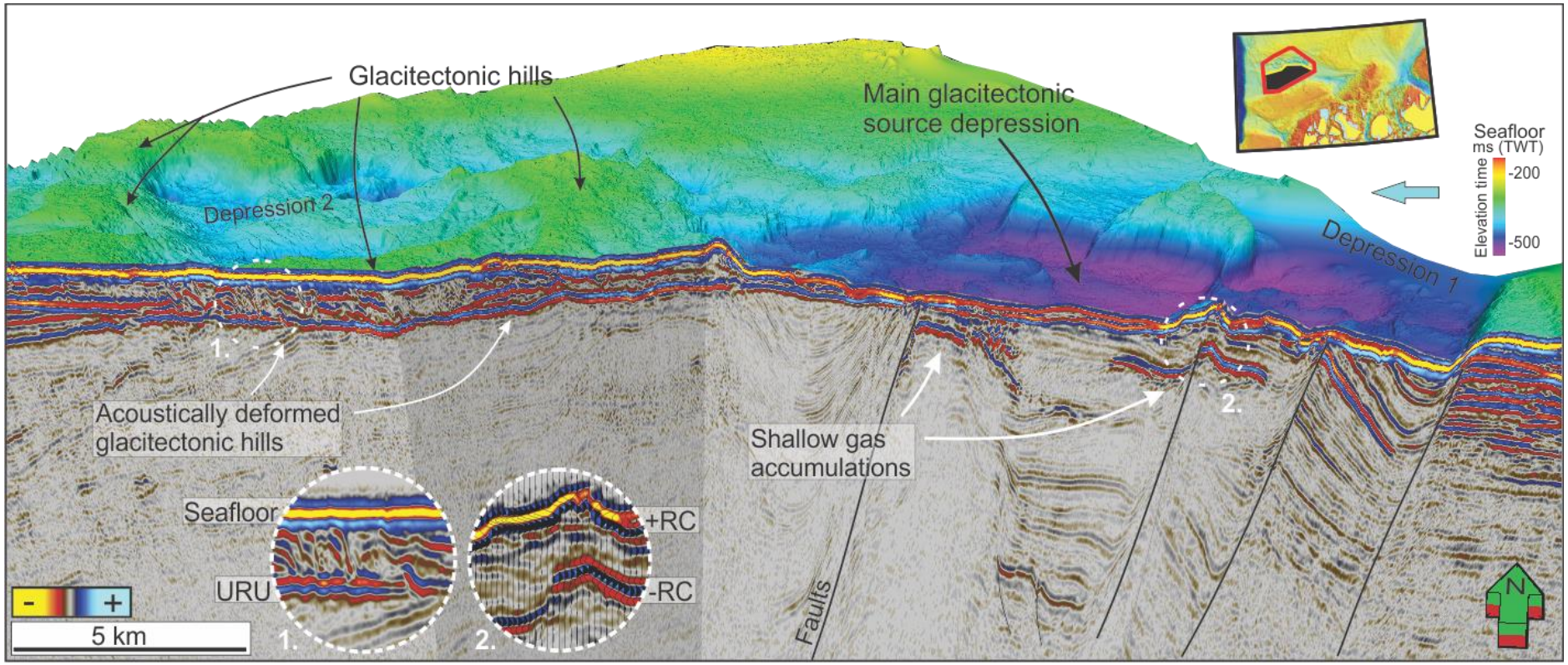


*Figure 5.10: A 3D view of the glacitectonic hill-hole pair located central in Håkjerringdjupet. This figure aim towards showing the correlation between faults and gas accumulation at the source depression and the downstream glacitectonic hills. This hill—hole pair is suggested to be a result of gas hydrate induced basal drag in the depressions and subsequent erosion and deposition of the sediments downstream as the ice stream advanced. Enhanced circle 1 show the deformed and thrusted glacitectonic deposits with possibly embedded blocks or slabs, as well as a deformed URU. Circle 2 show how shallow gas accumulations are associated with faults and indicated by a reversal in polarity and a negative reflection coefficient compared to the seafloor, which is also seen at URU below the glacitectonic hills. Blue arrow indicate the inferred direction of the ice flow. The location of the seismic line is also indicated in Figure 5.8.*

### 5.2.2 Glacitectonic event

The glacitectonic event occurred exclusively on the northern half of the trough, where the source of the glacitectonic deposits are suggested to be located in the over-deepened depression 1, an area which is acoustically dominated by deep seated faults and shallow gas accumulations below an abundance of pockmarks at the seafloor (Figure 5.10). We suggest that depression 1 is an area which show promising characteristics that could have been able to sustain stable gas hydrates under glacially induced suitable temp/pressure conditions. Gas hydrates would increase the shear strength in sub-glacial sediments, creating localized patches of high basal friction, sticky spots, increasing the basal drag at the ice bed interface and probably cause freeze-on of sediments to the ice bed (Christoffersen & Tulaczyk, 2003a; Durham *et al.*, 2003; Winters *et al.*, 2004; Stokes *et al.*, 2007; Hyodo *et al.*, 2013).

A quiescent ice flow during deglaciation and thinning of the ice is suggested to have made the ice stream vulnerable to basal temperature changes and potential enhanced basal freeze-on to local gas hydrate-induced sticky spots. Subsequent readvance of the ice margin during the episodic deglaciation is therefore suggested to be a possible trigger for the glacitectonic event, perhaps contributed by continuous ice flow up-stream of the sticky spot, creating a bulge of ice and increased meltwater generation (Vogel *et al.*, 2005). Increased ice velocities and thus driving stress must have exceeded the shear strength in the substrata below the frozen sediments at the sticky spots. A weak zone is therefore suggested to have been located in the sub-surface, buried at a depth equal to the heights of the glacitectonic hills of 50 – 100 m. This would potentially mark a transition between consolidated/frozen above and under-consolidated/non-frozen sediments below. We assume this layer of frozen sediments have contained gas hydrates, and we have previous established that the gas hydrate stability zone were 400 m deep (Figure 5.5). This means that the glacitectonic erosion of sediments only occurred at the upper fraction of the GHSZ. The URU show to be over-deepened in the source area, perhaps because of faulting or as a part of the glacitectonic erosion. Gas hydrates may have formed through the whole GHSZ, but the transition of pre-glacial and glacigenic sediments may have acted as a natural weak zone for detachment to occur. The glacigenic unit of unsorted and coarse sediments may have favoured a denser formation of gas hydrates, resulting in a stronger shear strength in the upper glacigenic unit than the pre-glacial below. The negative reflection coefficient often

observed at URU may indeed suggest that the pre-glacial unit is un-consolidated, or *less* consolidated than the glacigenic unit above, supporting this suggestion (see section 5.1.2 & Figure 5.10).

The glacitectonic deposits have been transported up to 30 km downstream from the source area to their current position as glacitectonic hills. Yet, the full extent of the glacitectonic deposits may be larger as lack of good seismic data outside of the 3D survey FP12_PRCMIG prevents interpretation of some irregular features down-stream closer to the shelf edge (Figure 5.8). It is interesting that the interpreted glacitectonic hills have such a trough-parallel margin at its southern side. The glacitectonic hills abruptly end where mega-scale glacial lineations and acoustically stratified deposits are observed just south. We believe this indicate exactly how important basal conditions are for ice stream dynamics and how abruptly it can change within an ice stream (Figure 5.8 & Figure 5.11). As discussed in section 5.2.1, this may have been because of reorganization of the ice stream, where the ice flow and meltwater drainage were concentrated at the trough's southern half. It could also be explained by absence of sub-glacial gas hydrates. Shallow gas accumulations is admittedly observed below the southern part of the trough as well, however, signs of these fluids migrating to and through the seafloor are sparse. In fact, very few pockmarks are observed south in the trough. It could be that the fluids located south, were too deep to affect the basal conditions of the ice stream. It may also be thought that, since this area is less extensive faulted, that the gas flux to the ice bed were too low for gas hydrates to form.

Irregularities are seen at the surface of URU, which seem to be deformed underneath the glacitectonic deposits (Figure 5.11 & Figure 5.12). However, it is important to remember that the URU surface is a product of interpreted seismic data, which show a time-image, and not a depth image. It is therefore possible that acoustic irregularities within the glacigenic deposits may cause the URU surface to *appear* deformed, or appear *more* deformed than it really is, as a result of acoustic velocity contrasts within the deposits (Rafaelsen *et al.*, 2007). The consistent deformation of URU below glacitectonic hills are here suggested to be real, and further imply that where the glacitectonic event occurred and along its transportation pathway, glacimarine sediments and probably upper part of the pre-glacial unit were affected, either by further erosion or deformation (Figure 5.7b, Figure 5.10 - Figure 5.12).

Acoustically the glacitectonic deposits show signs of clear deformation with possibly embedded slightly less deformed blocks or slabs (Figure 5.10 - Figure 5.12). The glacitectonic deposits were observed cutting into and/or deforming acoustically stratified glacimarine deposits west in the trough (Figure 5.11). We think this indicate that the glacitectonic deposits are younger than the adjacent acoustically stratified unit. South-east, grounding zone wedge 2 seem to have eroded into the glacitectonic hills (Figure 5.12), implying that the glacitectonic hills are older than GZW 2.

Glacitectonic deposits overlapping each other were described from the north-eastern glacitectonic hills, with a distinct change in acoustic amplitude (Figure 5.12). Two origins to this overlapping is suggested: (1) the glacitectonic hills were deposited during one single event. It is possible that this part of the hills were moved as one piece, where their pre-glacitectonic stratigraphic location was kept more or less intact. Mainly with an inner deformation of the sediments. Or, (2) at least two glacitectonic events must have occurred at different times, causing younger glacitectonic sediments to override older ones. The distinct change in acoustic amplitude may imply that the origin or type of sediments eroded and transported may have changed from one glacitectonic event to another. The location and orientation of this overriding unit fits quite well with GZW2, which also erode into the rafted hills (Figure 5.12). Sættem (1994) suggested that the glacitectonic hill-hole pair were overrun by a subsequent advance of the ice, depositing a glacigenic unit called Nordvestnaget Drift (see section 2.4.1). This unit have not been recognized in this study, but may be consistent with several glacitectonic events. This may also explain the detached irregular hills seen down-stream, not fully interpreted, which may origin from a not yet described glacitectonic event (Figure 5.8).

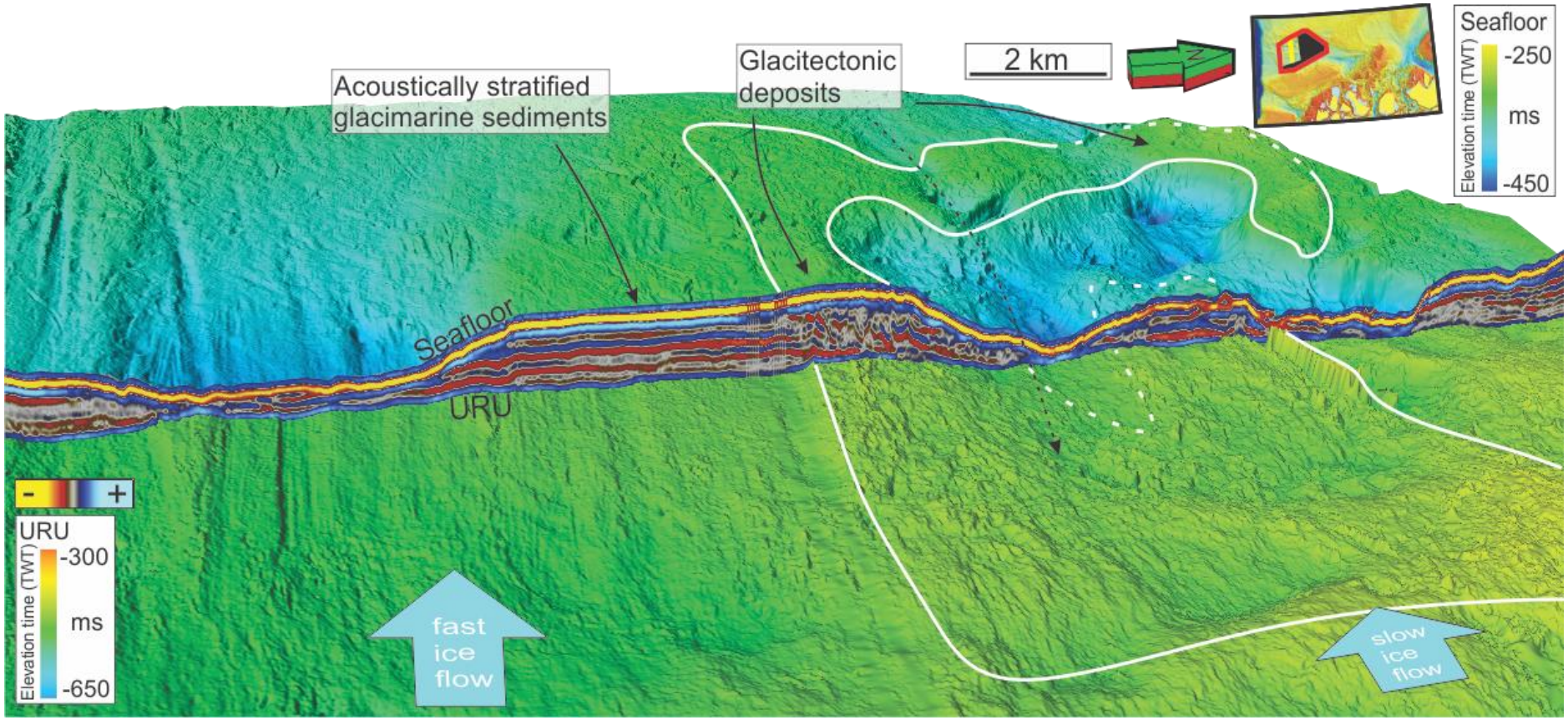


*Figure 5.11: Clear morphological differences are seen at the transition between the hill-hole pair to the right in this figure and MSGLs located to the left. MSGLs are signs of fast flowing warm-based ice, which is completely different from the slow and frozen ice associated with glacitectonism.*

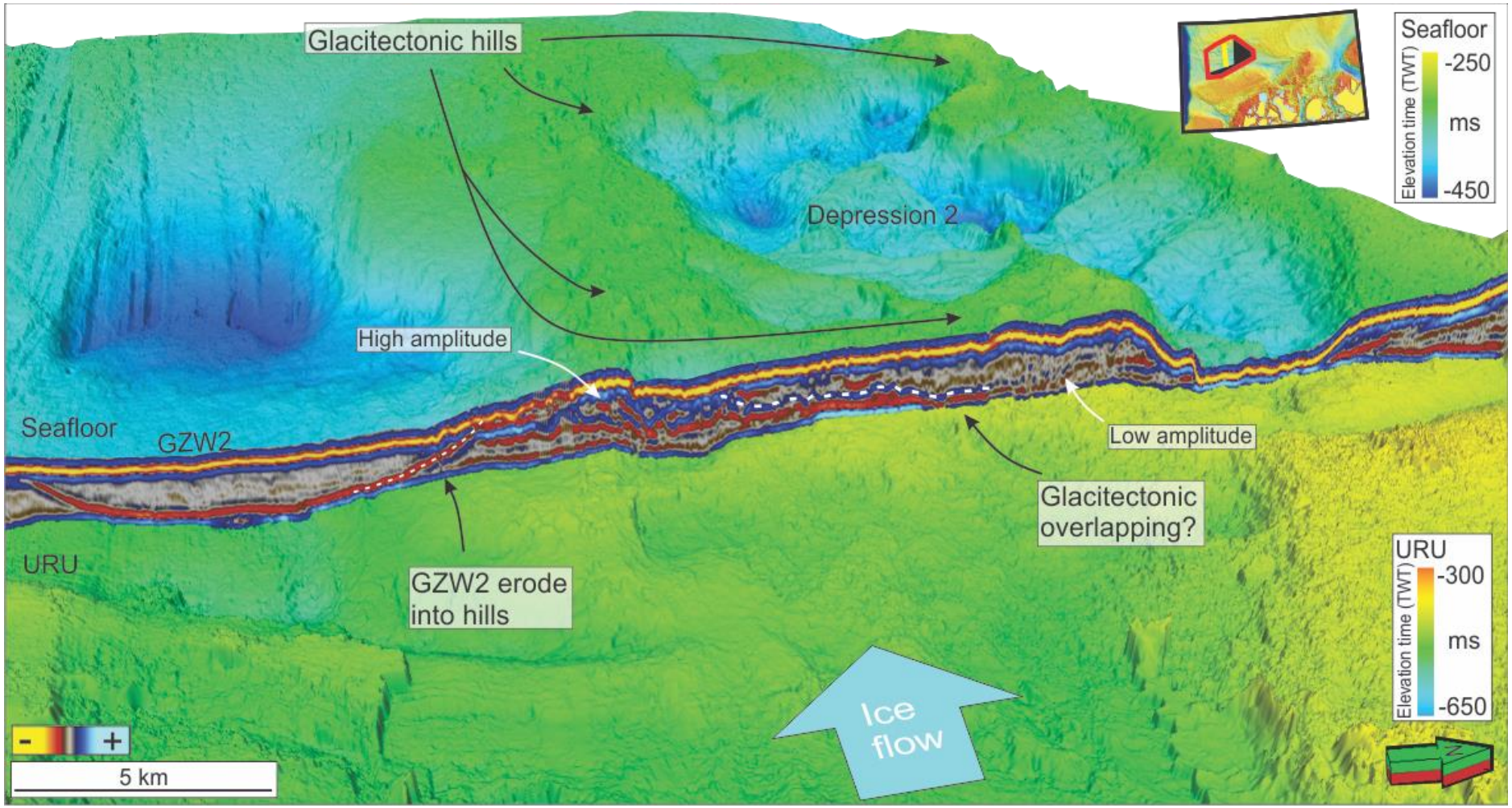


*Figure 5.12: The north-eastern glacitectonic hills show change in acoustic characteristics and possible a sign of glacitectonic overlapping (white dotted line), which may imply that several glacitectonic events occurred. This figure show a 3-D 'step' visualization of the glacitectonic hills, where the upper part of the figure show the seafloor, cut by a N-S oriented seismic cross profile, and the bottom part show the eastward extension of the irregular URU surface. Grounding zone wedge 2 (GZW2) is seen here to partly erode into the southern onset of the glacitectonic hills of high amplitude.*

In the case of this study we favour a theory of several glacitectonic events occurring in Håkjerringdjupet, originating from the same area of gas hydrate formation. We believe the glacitectonic overlapping implied in Figure 4.12 is a strong indication that readvancing of the ice margin during deglaciation indeed were important for glacitectonic events to occur. However, we do not rule out that glacitectonic rafting also could have occurred while the trough were fully glaciated.

Figure 5.13 is a sketch which show the concept of gas hydrate formation under an ice stream, based on a seismic line from Håkjerringdjupet. The sketch illustrate how gas hydrate formation occur spatially above the fault complex, which are pathways for upward fluid migration. The gas hydrates freeze onto the ice-bed and prevents fast ice flow. Detachment occur when the driving stress exceeds the shear strength during advances, causing glacitectonic rafting and deformation. Patches of subglacial gas hydrates could occur as long as gas migrated through the faults.

Sequel to our interpretations – potential methane reservoirs have been hypothesized in sedimentary basins beneath the Antarctic Ice Sheet (Wadham *et al.*, 2012). As methane is a common component in marine sediments and bedrock and potentially occur beneath Antarctica, our interpretation of gas hydrate induced sticky spots could therefore potentially apply to worldwide contemporary glaciers and ice streams as well (Kvenvolden & Lorenson, 2001; Wallmann *et al.*, 2012; Winsborrow *et al.*, 2016). The worldwide distribution of gas hydrates beneath paleo- and contemporary glaciers and ice streams and their general impact on sub-glacial conditions could therefore provide interesting topics for future studies on glacier dynamics and modelling.

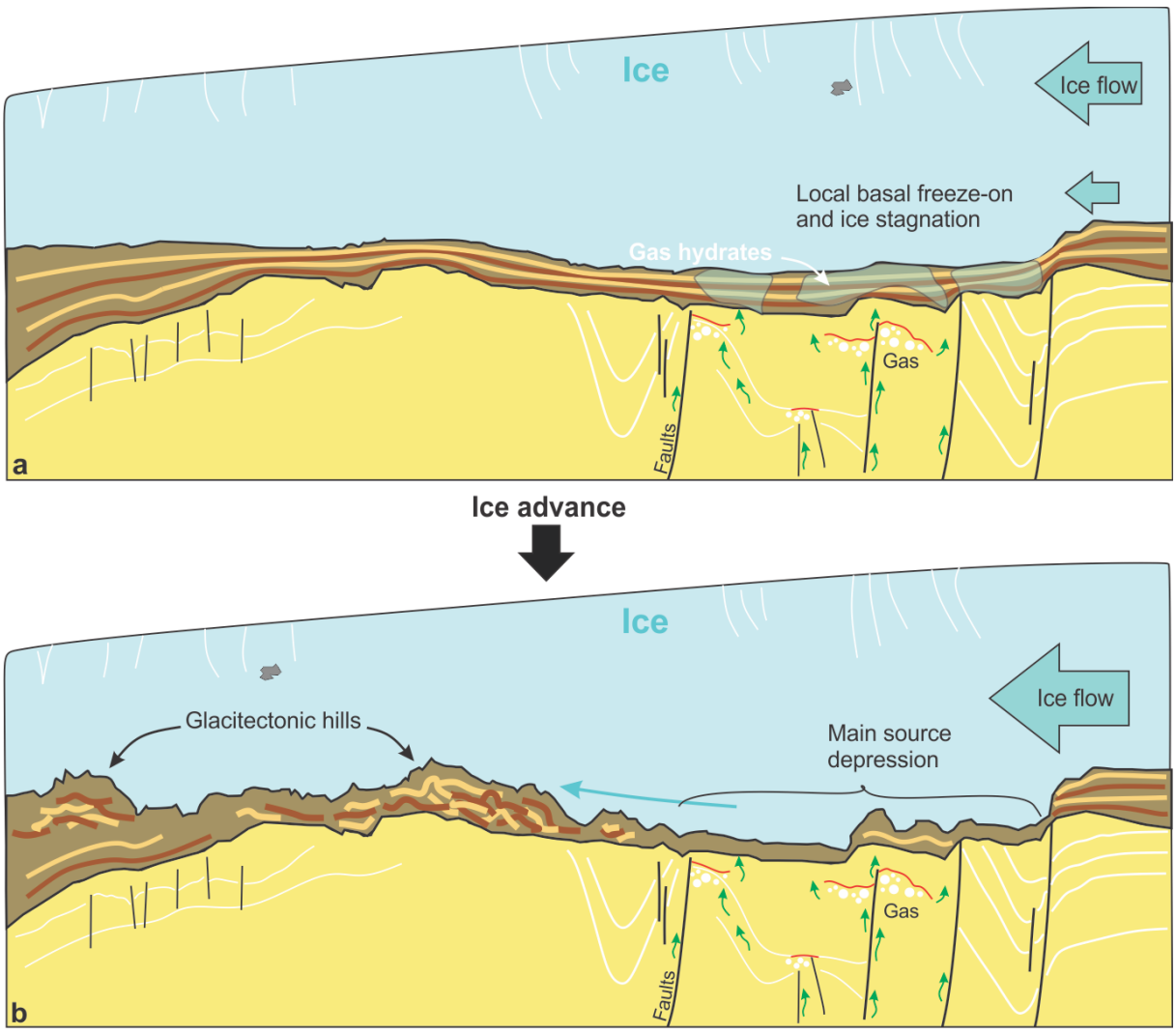


*Figure 5.13: This sketch visualize a possible onset for a glacitectonic event. The lower, lighter colours indicate the pre-glacial unit. Green arrows indicate possible fluid migration, which are trapped and accumulated (white circles) at lithological boundaries (red lines) connected to the faults. The glacigenic unit is coloured with darker colours.* ***a)*** *Upwards gas migration to shallower strata form patches of gas hydrates beneath the ice, causing freezing of the sediments on to the ice-bed and prevent fast ice flow and possibly stagnation (indicated by smaller arrow). Note that the sediments have not yet been deformed.* ***b)*** *Major advancing of the ice is believed to cause detachment of the frozen sediments close to the transition between the lower pre-glacial and the upper glacigenic unit. The frozen sediments are sub-glacially transported downstream and deposited as deformed glacitectonic hills. A stone embedded in the ice make it easier to trace the ice movement.*

## 5.3 A 6-stage reconstruction of Håkjerringdjupet Ice Stream

Based on our interpretation of the geophysical and bathymetric datasets we have summarized our previously discussed interactions between ice streaming, glacitectonic and fluid flow. In the following we will therefore propose a 6 stage reconstruction of Håkjerringdjupet Ice Stream, in the aim to shed a light on the possibilities for the occurrence of several glacitectonic events, during a phase of episodic ice margin retreat and readvances. Gas hydrate formation on the northern half have probably played a major role by producing patches of localized sub-glacial sticky spots and basal freeze-on. The term 'cold based ice' is here used for cold based ice on the banks, and where the ice stream is hindered within the trough by increased basal shear strength over areas of where gas hydrates formed sticky spots.

1. *LGM*: During Last Glacial Maximum, Håkjerringdjupet Ice Stream extended out to the shelf edge, draining ice from the Fennoscanndian Ice Sheet (FIS). Fast ice streaming ensured meltwater generation and lubrication of the bed, perhaps even if gas hydrates formed sub-glacially in the north. Occasionally glacitectonic rafting could occur. Glacimarine sediments were rapidly transported from the continental shelf and deposited on the slope over the shelf edge.
2. *1st retreat*: As deglaciation was initiated, the ice retreated over 20 km from the shelf edge. As a combination of reduced ice drainage and thickness and high basal shear strength induced by gas hydrates, the northern half of the ice stream were slowing down and freeze-on occurred. This may have caused a complete shut-down of the northern part of the ice stream. In response to the sub-glacial freeze-on and stoppage of the ice stream in the north, a reorganization of the ice stream occurred and fast flowing ice were concentrated south in the trough, supported by preserved MSGLs.
3. *1st readvance*: The 1st readvance moved the ice margin closer to the shelf edge forming grounding zone wedge 1 (GZW1). The readvance of the ice margin also affected the ice north in the trough and is suggested to be a possible onset of the a glacitectonic event. The stagnant ice in the north are suggested to have been pushed by increased ice drainage and driving stress from the ice sheet in the east, eroding subglacial frozen sediments/rocks mainly from the central over-deepening and

possibly depression 2 (Figure 5.14). The ice transported these sediments sub-glacially 10 – 30 km west where they were deposited as glacitectonically deformed hills, a process which caused deformation of adjacent pre-glacial and stratified glacimarine sediments as well. We believe that the lateral E-W oriented extent of the glacitectonic deposits are proof that the sediments were transported sub-glacially and not pro-glacially. The ice stream-parallel southern onset of the glacitectonic hills show how important basal conditions are, indicating the transition between warm (south) and cold (north) based ice (Figure 5.14).

4. *2nd retreat*: A second phase of rapid retreat, shown by well-preserved MSGLs, brought the ice margin over 20 km further east from GZW 1. The major part of the ice loss were probably due to calving of the ice front, supported by an abundance of plough marks and ice-berg pits dominating the seafloor above 300 m depth. We suggest that this retreat again caused a hiatus in the northern ice flow, hindered by sticky spots, allowing additional basal freeze-on in areas where gas hydrate formation favourably occurred.
5. *2nd readvance*: As the ice reached this mid-trough position a new readvance occurred forming grounding zone wedge 2, which partly erode into the previous deposited glacitectonic hills (Figure 5.12). We suggest that this second readvance of the ice margin again caused increased driving stress and the cold based ice to erode sub-glacially frozen sediments from the central over-deepening. This event is suggested to may have deposited the north-eastern-most glacitectonic hills that seem to overprint the older glacitectonic deposits (Figure 5.12). The location of these deposits correlate well with the location and orientation of GZW 2, which support that they occurred at the same readvance.
6. *Slow retreat*: Further deglaciation and rapid ice margin retreat continued east of the fault complex. Here the ice margin is thought to stabilize forming an end moraine/small grounding zone wedge just east of the escarpment. This part of the trough show MSGLs at its northern and southern part, indicating that all the ice within the trough were warm based and fast flowing, thus not hindered by high basal drag east of the fault complex. From this point the retreat of the ice margin proceeded in a much slower rate suggested by recessional moraines located in the eastern end of the trough (Winsborrow *et al.*, 2012).

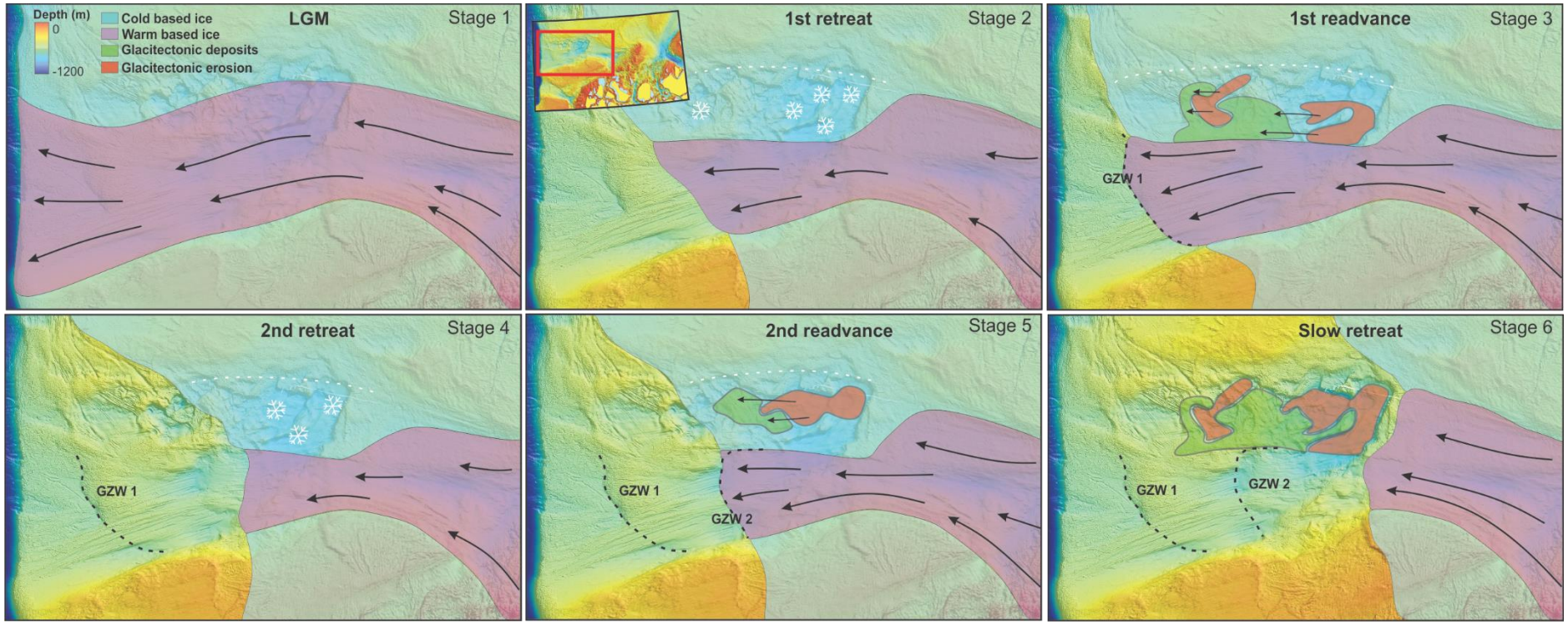


*Figure 5.14: The proposed 6 stage reconstruction of the Late Weichselian Håkjerringdjupet Ice Stream from LGM at Stage 1 to almost a complete ice-free trough at the end of Stage 6. During retreat of the ice margin (stage 2 & 4), reduced ice discharge and flow attenuation at sticky spots of high basal drag causes freeze-on of basal sediments onto the bed of the ice. Glacitectonic events are believed to occur during readvances (Stage 3 & 5) of the ice margin, where increased ice discharge and driving stress from the ice in the east force erosion of sub-glacially frozen sediments. White snowflakes indicate areas where gas hydrate have caused local sticky spots and basal freezing is suggested to have occurred.*

# 6 Summary and conclusions

This study have used high resolution multibeam swath bathymetry as well as 2D and 3D seismic datasets to investigate the interaction between ice streaming, glacitectonics and fluid flow in Håkjerringdjupet, SW Barents Sea. Several flow-sets of mega-scale glacial lineations and associated grounding zone wedges on the seafloor indicate that Håkjerringdjupet have been extensively glaciated by a grounded Late Weichselian ice stream. Yet, a glacitectonic hill-hole pair, located in the trough's northern part, show evidence of sub-glacially rafted sediments, implying high basal friction and slow ice movement. The source area for the hill-hole pair is located directly above the Troms – Finnmark Fault Complex, a deep-seated fault complex with associated fluid migration and shallow gas accumulations.

- High amplitude anomalies, interpreted to be shallow gas accumulations are seen along and proximal to the NE-SW oriented Troms-Finnmark Fault Complex. The deep-seated fault complex intersects at the central part of Håkjerringdjupet which is over-deepened, and is implied to be an important pathway for fluid migration from a deeper source to the shallow subsurface.
- Our suggestion is that an extended gas hydrate stability zone during glaciations would cause local formations of sub-glacial gas hydrates where sufficient gas and water have been available. This would have enhanced the shear strength of basal sediments severely, thus increased the friction at the ice-bed interface, preventing fast ice flow. Thereby, we introduce the possibilities a new type of mechanism or 'sticky spot' which could cause freeze-on and prevent fast flowing ice and perhaps stagnation of contemporary and paleo-ice streams – areas of increased basal friction and freeze-on due to subglacial gas hydrate formation.
- Based on our interpretation of our data we favour sub-glacial gas hydrate formation to have occurred locally north in the trough, closely related to the deep-seated fault complex and fluid migration. However, gas hydrates could also have formed elsewhere, but probably did not form directly at the bed of the ice, thus not preventing fast ice flow (e.g. south in the trough).
- We suggest that the glacitectonic hill-hole pair most likely is a result of several glacitectonic events, which occurred through the last glaciation, with the main source

area located in the central over-deepening, and perhaps depression 2. Further, we favour a theory where the deglaciation phase made the ice stream vulnerable to temperature changes, thus enhanced basal cooling and freeze-on provided by sub-glacial gas hydrate formation. Subsequent readvance caused sub-glacial erosion and transportation of on-frozen sediments. Based on our results and in our best effort, we suggested a 6-stage reconstruction of Håkjerringdjupet Ice Stream in the attempt to explain the relative glacitectonic events we have observed (Figure 5.14).

- The depth of the glacitectonic detachment were probably at a transition between a strong, frozen unit and a lower weak unit. A possible shear depth for the glacitectonic rafting is proposed to have been located at or close to the Upper Regional Unconformity (URU), the transition between buried weak or un-consolidated pre-glacial sediments and overlying stiff and frozen glacigenic sediments.
- As a response to sub-glacial gas hydrates and prevented ice flow in the northern part of the ice stream, we suggest a reorganization, or switching, of the ice flow occurred. The ice flow were concentrated at the southern part of the trough, where meltwater generation and fast ice flow were maintained, and continuous through the whole glaciation, supported by observed mega-scale glacial lineations. Thus, preventing a complete shutdown of Håkjerringdjupet Ice Stream.
- Gas hydrate induced sticky spots are not thought to be outstanding for Håkjerringdjupet. Similar sub-glacial conditions could apply for paleo- and contemporary glaciers worldwide where conditions for gas hydrate formation exists. This could provide interesting studies on exactly how common these events are and their importance to ice stream dynamics in general.

# 7 References:


Aber, J. S., & Ber, A. (2007). *Glaciotectonism* (1st ed.). Amsterdam ; Boston: Elsevier.

Aber, J. S., Croot, D. G., & Fenton, M. M. (1989). *Glaciotectonic landforms and structures*. Dordrecht Holland ; Boston: Kluwer Academic Publishers.

Alley, R. B. (1993). In Search of Ice-Stream Sticky Spots. *Journal of Glaciology, 39*(133), 447-454.

Aloisi, G., Bouloubassi, I., Heijs, S. K., Pancost, R. D., Pierre, C., Damste, J. S. S., Gottschal, J. C., Forney, L. J., & Rouchy, J. M. (2002). CH4-consuming microorganisms and the formation of carbonate crusts at cold seeps. *Earth and Planetary Science Letters, 203*(1), 195-203.

Amundsen, L., & Landrø, M. (2012). Gas Hydrates Part I: Burning Ice. *GEOExPro, 9*(3), 4.

Anandakrishnan, S., & Alley, R. B. (1997). Stagnation of ice stream C, West Antarctica by water piracy. *Geophysical Research Letters, 24*(3), 265-268.

Andreassen, K., Hart, P. E., & MacKay, M. (1997). Amplitude versus offset modeling of the bottom simulating reflection associated with submarine gas hydrates. *Marine Geology, 137*(1-2), 25-40.

Andreassen, K., Laberg, J. S., & Vorren, T. O. (2008). Seafloor geomorphology of the SW Barents Sea and its glaci-dynamic implications. *Geomorphology, 97*(1-2), 157-177.

Andreassen, K., Nilssen, E. G., & Odegaard, C. M. (2007a). Analysis of shallow gas and fluid migration within the Plio-Pleistocene sedimentary succession of the SW Barents Sea continental margin using 3D seismic data. *Geo-Marine Letters, 27*(2-4), 155-171.

Andreassen, K., Nilssen, L. C., Rafaelsen, L., & Kuilman, L. (2004). Three-dimensional seismic data from the Barents Sea margin reveal evidence of past ice streams and their dynamics. *Geology, 32*(8), 729-732.

Andreassen, K., Odegaard, C. M., & Rafaelsen, B. (2007b). Imprints of former ice streams, imaged and interpreted using industry three-dimensional seismic data from the south-western Barents Sea. *Seismic Geomorphology: Applications to Hydrocarbon Exploration and Production, 277*, 151-169.

Andreassen, K., & Winsborrow, M. (2009). Signature of ice streaming in Bjornoyrenna, Polar North Atlantic, through the Pleistocene and implications for ice-stream dynamics. *Annals of Glaciology, 50*(52), 17-26.

Andreassen, K., Winsborrow, M. C. M., Bjamadottir, L. R., & Ruther, D. C. (2014). Ice stream retreat dynamics inferred from an assemblage of landforms in the northern Barents Sea. *Quaternary Science Reviews, 92*, 246-257.

Anstey, N. A. (1977). *Seismic interpretation : the physical aspects : being a record of the short course, The new seismic interpreter*. Boston: International Human Resources Development Corp.

Batchelor, C. L., & Dowdeswell, J. A. (2015). Ice-sheet grounding-zone wedges (GZWs) on high-latitude continental margins. *Marine Geology, 363*, 65-92.

Ben Clennell, M., Hovland, M., Booth, J. S., Henry, P., & Winters, W. J. (1999). Formation of natural gas hydrates in marine sediments 1. Conceptual model of gas hydrate growth conditioned by host sediment properties. *Journal of Geophysical Research-Solid Earth, 104*(B10), 22985-23003.

Benn, D. I., & Evans, D. J. A. (2010). *Glaciers & glaciation* (2. ed.). New York: Hodder Education.

Berndt, C. (2005). Focused fluid flow in passive continental margins. *Philosophical Transactions of the Royal Society a-Mathematical Physical and Engineering Sciences, 363*(1837), 2855-2871.

Berndt, C., Bunz, S., & Mienert, J. (2003). Polygonal fault systems on the mid-Norwegian margin: a long-term source for fluid flow. *Subsurface Sediment Mobilization, 216*, 283-290.

Bluemle, J. P., & Clayton, L. (1984). Large-Scale Glacial Thrusting and Related Processes in North-Dakota. *Boreas, 13*(3), 279-299.

Bondarev, V. N., Rokos, S. I., Kostin, D. A., Dlugach, A. G., & Polyakova, N. A. (2002). Underpermafrost accumulations of gas in the upper part of the sedimentary cover of the Pechora Sea. *Geologiya I Geofizika, 43*(7), 587-598.

Bougamont, M., Tulaczyk, S., & Joughin, I. (2003). Response of subglacial sediments to basal freeze-on - 2. Application in numerical modeling of the recent stoppage of Ice Stream C, West Antarctica. *Journal of Geophysical Research-Solid Earth, 108*(B4).

Boulton, G. S., Dongelmans, P., Punkari, M., & Broadgate, M. (2001). Palaeoglaciology of an ice sheet through a glacial cycle: the European ice sheet through the Weichselian. *Quaternary Science Reviews, 20*(4), 591-625.

Brown, A. R. (1999). *Interpretation of three-dimensional seismic data* (5th ed.). Tulsa, Okla.: American Association of Petroleum Geologists and the Society of Exploration Geophysicists.

Buhl-Mortensen, L., Bøe, R., Dolan, M. F. J., Buhl-Mortensen, P., Thorsnes, T., Elvenes, S., & Hodnesdal, H. (2012). 51 Banks, Troughs, and Canyons in the Continental Margin off Lofoten, Vesterålen, and Troms, Norway *Seafloor Geomorphology as Benthic Habitat* (pp. 703-715): Elsevier.

Cartwright, J., Huuse, M., & Aplin, A. (2007). Seal bypass systems. *Aapg Bulletin, 91*(8), 1141-1166.

Cartwright, J., Wattrus, N., Rausch, D., & Bolton, A. (2004). Recognition of an early Holocene polygonal fault system in Lake Superior: Implications for the compaction of fine-grained sediments. *Geology, 32*(3), 253-256.

Chand, S., Mienert, J., Andreassen, K., Knies, J., Plassen, L., & Fotland, B. (2008). Gas hydrate stability zone modelling in areas of salt tectonics and pockmarks of the Barents Sea suggests an active hydrocarbon venting system. *Marine and Petroleum Geology, 25*(7), 625-636.

Chand, S., Rise, L., Ottesen, D., Dolan, M. F. J., Bellec, V., & Boe, R. (2009). Pockmark-like depressions near the Goliat hydrocarbon field, Barents Sea: Morphology and genesis. *Marine and Petroleum Geology, 26*(7), 1035-1042.

Chand, S., Thorsnes, T., Rise, L., Brunstad, H., Stoddart, D., Boe, R., Lagstad, P., & Svolsbru, T. (2012). Multiple episodes of fluid flow in the SW Barents Sea (Loppa High) evidenced by gas flares, pockmarks and gas hydrate accumulation. *Earth and Planetary Science Letters, 331*, 305-314.

Chaouch, A., & Mari, J. L. (2006). 3-D land seismic surveys: Definition of geophysical parameters. *Oil & Gas Science and Technology-Revue D Ifp Energies Nouvelles, 61*(5), 611-630.

Christoffersen, P., & Tulaczyk, S. (2003a). Response of subglacial sediments to basal freeze-on - 1. Theory and comparison to observations from beneath the West Antarctic Ice Sheet. *Journal of Geophysical Research-Solid Earth, 108*(B4).

Christoffersen, P., & Tulaczyk, S. (2003b). Signature of palaeo-ice-stream stagnation: till consolidation induced by basal freeze-on. *Boreas, 32*(1), 114-129.

Clark, C. D., Evans, D. J. A., & Piotrowski, J. A. (2003a). Palaeo-ice streams: an introduction. *Boreas, 32*(1), 1-3.

Clark, C. D., Tulaczyk, S. M., Stokes, C. R., & Canals, M. (2003b). A groove-ploughing theory for the production of mega-scale glacial lineations, and implications for ice-stream mechanics. *Journal of Glaciology, 49*(165), 240-256.

Clark, P. U., Dyke, A. S., Shakun, J. D., Carlson, A. E., Clark, J., Wohlfarth, B., Mitrovica, J. X., Hostetler, S. W., & McCabe, A. M. (2009). The Last Glacial Maximum. *Science, 325*(5941), 710-714.

Conway, H., Catania, G., Raymond, C. F., Gades, A. M., Scambos, T. A., & Engelhardt, H. (2002). Switch of flow direction in an Antarctic ice stream. *Nature, 419*(6906), 465-467.

Ding, X. J., Liu, G. D., Sun, M. L., & Wang, P. G. (2013). Origin of polygonal fault systems: A case from the Sanzhao sag in the Songliao Basin, East China. *Petroleum Exploration and Development, 40*(3), 333-343.

Dore, A. G. (1995). Barents Sea Geology, Petroleum Resources and Commercial Potential. *Arctic, 48*(3), 207-221.

Dore, A. G., & Jensen, L. N. (1996). The impact of late Cenozoic uplift and erosion on hydrocarbon exploration: Offshore Norway and some other uplifted basins. *Global and Planetary Change, 12*(1-4), 415-436.

Dowdeswell, J. A., Ottesen, D., Rise, L., & Craig, J. (2007). Identification and preservation of landforms diagnostic of past ice-sheet activity on continental shelves from three-dimensional seismic evidence. *Geology, 35*(4), 359-362.

Durham, W. B., Kirby, S. H., Stern, L. A., & Zhang, W. (2003). The strength and rheology of methane clathrate hydrate. *Journal of Geophysical Research-Solid Earth, 108*(B4).

Edvardsen, A. (2015). *Faulting and the relationship to fluid migration and shallow gas accumulation in the Hammerfest Basin, SW Barents Sea.* (MSc), University of Tromsø.

Faleide, J. I., Gudlaugsson, S. T., & Jacquart, G. (1984). Evolution of the Western Barents Sea. *Marine and Petroleum Geology, 1*(2), 123-150.

Faleide, J. I., Solheim, A., Fiedler, A., Hjelstuen, B. O., Andersen, E. S., & Vanneste, K. (1996). Late Cenozoic evolution of the western Barents Sea-Svalbard continental margin. *Global and Planetary Change, 12*(1-4), 53-74.

Faleide, J. I., Tsikalas, F., Breivik, A. J., Mjelde, R., Ritzmann, O., Engen, O., Wilson, J., & Eldholm, O. (2008). Structure and evolution of the continental margin off Norway and Barents Sea. *Episodes, 31*(1), 82-91.

Faleide, J. I., Vagnes, E., & Gudlaugsson, S. T. (1993). Late Mesozoic-Cenozoic Evolution of the South-Western Barents Sea in a Regional Rift Shear Tectonic Setting. *Marine and Petroleum Geology, 10*(3), 186-214.

Fichler, C., Henriksen, S., Rueslaatten, H., & Hovland, M. (2005). North Sea Quaternary morphology from seismic and magnetic data: indications for gas hydrates during glaciation? *Petroleum Geoscience, 11*(4), 331-337.

Gabrielsen, R. H. (1984). Long-Lived Fault Zones and Their Influence on the Tectonic Development of the Southwestern Barents Sea. *Journal of the Geological Society, 141*(Jul), 651-662.

Gabrielsen, R. H., Færseth, R. B., Jensen, L. N., & Riis, F. (1990). *Structural elements of the Norwegian continental shelf Part I: The Barents Sea Region.* (Vol. 6): Oljedirektoratet.

Gudlaugsson, S. T., Faleide, J. I., Johansen, S. E., & Breivik, A. J. (1998). Late Palaeozoic structural development of the South-western Barents Sea. *Marine and Petroleum Geology, 15*(1), 73-102.

Hogan, K. A., Dowdeswell, J. A., Noormets, R., Evans, J., & Cofaigh, C. O. (2010). Evidence for full-glacial flow and retreat of the Late Weichselian Ice Sheet from the waters around Kong Karls Land, eastern Svalbard. *Quaternary Science Reviews, 29*(25-26), 3563-3582.

Hovland, M. (2005). Gas Hydrates. *Elsevier, Petroleum Geology*.

Hovland, M., Gardner, J. V., & Judd, A. G. (2002). The significance of pockmarks to understanding fluid flow processes and geohazards. *Geofluids, 2*(2), 127-136.

Hovland, M., Jensen, S., & Indreiten, T. (2012). Unit pockmarks associated with Lophelia coral reefs off mid-Norway: more evidence of control by 'fertilizing' bottom currents. *Geo-Marine Letters, 32*(5-6), 545-554.

Hovland, M., & Risk, M. (2003). Do Norwegian deep-water coral reefs rely on seeping fluids? *Marine Geology, 198*(1-2), 83-96.

Hovland, M., & Svensen, H. (2006). Submarine pingoes: Indicators of shallow gas hydrates in a pockmark at Nyegga, Norwegian Sea. *Marine Geology, 228*(1-4), 15-23.

Hovland, M., Svensen, H., Forsberg, C. F., Johansen, H., Fichler, C., Fossa, J. H., Jonsson, R., & Rueslatten, H. (2005). Complex pockmarks with carbonate-ridges off mid-Norway: Products of sediment degassing. *Marine Geology, 218*(1-4), 191-206.

Hughes, A. L. C., Gyllencreutz, R., Lohne, Ø. S., Mangerud, J., & Svendsen, J. I. (2015). The last Eurasian ice sheets - a chronological database and time-slice reconstruction, DATED-1. *Boreas*.

Hulbe, C., & Fahnestock, M. (2007). Century-scale discharge stagnation and reactivation of the Ross ice streams, West Antarctica. *Journal of Geophysical Research-Earth Surface, 112*(F3).

Hyodo, M., Li, Y. H., Yoneda, J., Nakata, Y., Yoshimoto, N., Nishimura, A., & Song, Y. C. (2013). Mechanical behavior of gas-saturated methane hydrate-bearing sediments. *Journal of Geophysical Research-Solid Earth, 118*(10), 5185-5194.

Indrevær, K., Bergh, S. G., Koehl, J. B., Hansen, J. A., Schermer, E. R., & Ingebrigtsen, A. (2013). Post-Caledonian brittle fault zones on the hyperextended SW Barents Sea margin: New insights

into onshore and offshore margin architecture. *Norwegian Journal of Geology, 93*(3-4), 167-188.

Jakobsson, M., Mayer, L., Coakley, B., Dowdeswell, J. A., Forbes, S., Fridman, B., Hodnesdal, H., Noormets, R., Pedersen, R., Rebesco, M., Schenke, H. W., Zarayskaya, Y., Accettella, D., Armstrong, A., Anderson, R. M., Bienhoff, P., Camerlenghi, A., Church, I., Edwards, M., Gardner, J. V., Hall, J. K., Hell, B., Hestvik, O., Kristoffersen, Y., Marcussen, C., Mohammad, R., Mosher, D., Nghiem, S. V., Pedrosa, M. T., Travaglini, P. G., & Weatherall, P. (2012). The International Bathymetric Chart of the Arctic Ocean (IBCAO) Version 3.0. *Geophysical Research Letters, 39*.

Judd, A. G., & Hovland, M. (2007). *Seabed fluid flow : the impact of geology, biology and the marine environment*. Cambridge ; New York: Cambridge University Press.

King, E. C., Hindmarsh, R. C. A., & Stokes, C. R. (2009). Formation of mega-scale glacial lineations observed beneath a West Antarctic ice stream. *Nature Geoscience, 2*(8), 585-588.

King, L. H., & Maclean, B. (1970). Pockmarks on Scotian Shelf. *Geological Society of America Bulletin, 81*(10), 3141-&.

Knies, J., Matthiessen, J., Vogt, C., Laberg, J. S., Hjelstuen, B. O., Smelror, M., Larsen, E., Andreassen, K., Eidvin, T., & Vorren, T. O. (2009). The Plio-Pleistocene glaciation of the Barents Sea-Svalbard region: a new model based on revised chronostratigraphy. *Quaternary Science Reviews, 28*(9-10), 812-829.

Kvenvolden, K. A., & Lorenson, T. D. (2001). Global occurrences of gas hydrate. *Proceedings of the Eleventh (2001) International Offshore and Polar Engineering Conference, Vol I*, 462-467.

Laberg, J. S., Andreassen, K., Knies, J., Vorren, T. O., & Winsborrow, M. (2010). Late Pliocene-Pleistocene development of the Barents Sea Ice Sheet. *Geology, 38*(2), 107-110.

Laberg, J. S., & Vorren, T. O. (1996). The Middle and Late Pleistocene evolution of the Bear Island Trough Mouth Fan. *Global and Planetary Change, 12*(1-4), 309-330.

Lee, J. R., & Phillips, E. (2013). Glacitectonics - a key approach to examining ice dynamics, substrate rheology and ice-bed coupling. *Proceedings of the Geologists' Association, 124*, 731-737.

Mareano/NGU.

Maslin, M., Owen, M., Betts, R., Day, S., Dunkley Jones, T., & Ridgwell, A. (2010). Gas hydrates: past and future geohazard? *Philosophical Transactions of the Royal Society a-Mathematical Physical and Engineering Sciences, 368*(1919), 2369-2393.

Moran, S. R., Clayton, L., Hooke, R. L., Fenton, M. M., & Andriashek, L. D. (1980). Glacier-Bed Landforms of the Prairie Region of North-America. *Journal of Glaciology, 25*(93), 457-476.

Moumets, H. (2008). *The Fugløy cold-water coral reefs on the south-western Barents Sea shelf: their morphology, distribution and environmental setting.* (MSc), University of Tromsø, Munin.

Nesje, A. (2012). *Brelære: Bre, Landskap, Klimaendringer og Datering* (2nd ed.): Høyskoleforlaget AS - Norwegian Academic Press.

NPD. Norwegian Petroleum Directorate. Retrieved 04.26.2016, from NPD www.npd.no

Nøttvedt, A., Johannessen, E. P., & Surlyk, F. (2008). The mesozoic of western Scandinavia and East Greenland. *Episodes, 31*(1), 59-65.

Ó Cofaigh, C., Dowdeswell, J. A., Allen, C. S., Hiemstra, J. F., Pudsey, C. J., Evans, J., & Evans, D. J. A. (2005). Flow dynamics and till genesis associated with a marine-based Antarctic palaeo-ice stream. *Quaternary Science Reviews, 24*(5-6), 709-740.

Ó Cofaigh, C., Taylor, J., Dowdeswell, J. A., & Pudsey, C. J. (2003). Palaeo-ice streams, trough mouth fans and high-latitude continental slope sedimentation. *Boreas, 32*(1), 37-55.

Ostanin, I., Anka, Z., di Primio, R., & Bernal, A. (2012). Identification of a large Upper Cretaceous polygonal fault network in the Hammerfest basin: Implications on the reactivation of regional faulting and gas leakage dynamics, SW Barents Sea. *Marine Geology, 332*, 109-125.

Ostanin, I., Anka, Z., di Primio, R., & Bernal, A. (2013). Hydrocarbon plumbing systems above the Snohvit gas field: Structural control and implications for thermogenic methane leakage in the Hammerfest Basin, SW Barents Sea. *Marine and Petroleum Geology, 43*, 127-146.

Ottesen, D., Dowdeswell, J. A., & Rise, L. (2005). Submarine landforms and the reconstruction of fast-flowing ice streams within a large Quaternary ice sheet: The 2500-km-long Norwegian-Svalbard margin (57 degrees-80 degrees N). *Geological Society of America Bulletin, 117*(7-8), 1033-1050.

Ottesen, D., Stokes, C. R., Rise, L., & Olsen, L. (2008). Ice-sheet dynamics and ice streaming along the coastal parts of northern Norway. *Quaternary Science Reviews, 27*(9-10), 922-940.

Parizek, B. R., Alley, R. B., Anandakrishnan, S., & Conway, H. (2002). Sub-catchment melt and long-term stability of ice stream D, West Antarctica. *Geophysical Research Letters, 29*(8).

Patton, H., Andreassen, K., Bjarnadottir, L. R., Dowdeswell, J. A., Winsborrow, M. C. M., Noormets, R., Polyak, L., Auriac, A., & Hubbard, A. (2015). Geophysical constraints on the dynamics and retreat of the Barents Sea ice sheet as a paleobenchmark for models of marine ice sheet deglaciation. *Reviews of Geophysics, 53*(4), 1051-1098.

Payne, A. J., & Dongelmans, P. W. (1997). Self-organization in the thermomechanical flow of ice sheets. *Journal of Geophysical Research-Solid Earth, 102*(B6), 12219-12233.

Rafaelsen, B. (Unpublished). *Seismic resolution (and frequency filtering)*. University of Tromsø.

Rafaelsen, B., Andreassen, K., Hogstad, K., & Kuilman, L. W. (2007). Large-scale glaciotectonic-imbricated thrust sheets on three-dimensional seismic data: facts or artefacts? *Basin Research, 19*(1), 87-103.

Rafaelsen, B., Andreassen, K., Kuilman, L. W., Lebesbye, E., Hogstad, K., & Midtbo, M. (2002). Geomorphology of buried glacigenic horizons in the Barents Sea from three-dimensional seismic data. *Glacier-Influenced Sedimentation on High-Latitude Continental Margins, 203*, 259-276.

Ramberg, I. B., Bryhni, I., Nøttvedt, A., & Norsk geologisk forening. (2007). *Landet blir til : Norges geologi* (2. oppl. med rettelser. ed.). Trondheim: Norsk geologisk forening.

Reemst, P., Cloetingh, S., & Fanavoll, S. (1994). Tectonostratigraphic Modeling of Cenozoic Uplift and Erosion in the South-Western Barents Sea. *Marine and Petroleum Geology, 11*(4), 478-490.

Rise, L., Bellec, V. K., Chand, S., & Boe, R. (2014). Pockmarks in the southwestern Barents Sea and Finn mark fjords. *Norwegian Journal of Geology, 94*(4), 263-282.

Rokoengen, K., Bugge, T., & Lofaldli, M. (1979). Quaternary Geology and Deglaciation of the Continental-Shelf Off Troms, North Norway. *Boreas, 8*(2), 217-227.

Rydningen, T. A., Vorren, T. O., Laberg, J. S., & Kolstad, V. (2013). The marine-based NW Fennoscandian ice sheet: glacial and deglacial dynamics as reconstructed from submarine landforms. *Quaternary Science Reviews, 68*, 126-141.

Selley, R. C. (1998). *Elements of petroleum geology* (2nd ed.). San Diego: Academic Press.

Serie, C., Huuse, M., & Schodt, N. H. (2012). Gas hydrate pingoes: Deep seafloor evidence of focused fluid flow on continental margins. *Geology, 40*(3), 207-210.

Sheriff, R. E. (1985). Aspects of seismic resolution. *Seismic Stratigraphy II: American Association of Petroleum Geologists*, 10.

Sheriff, R. E. (2006). *Encyclopedic dictionary of exploration geophysics* (4th ed.): Society of Exploration Geophysicists, Tulsa.

Simm, R., & Bacon, M. (2014). *Seismic amplitude : an interpreter's handbook*. Cambridge ; New York: Cambridge University Press.

Slater, G. (1927). Structure of the Mud Buttes and Tit Hills in Alberta. *Bulletin of the Geological Society of America, 38*(1/4), 721-730.

Solheim, A., & Elverhoi, A. (1993). Gas-Related Sea-Floor Craters in the Barents Sea. *Geo-Marine Letters, 13*(4), 235-243.

Solheim, A., Riis, F., Elverhoi, A., Faleide, J. I., Jensen, L. N., & Cloetingh, S. (1996). Impact of glaciations on basin evolution: Data and models from the Norwegian margin and adjacent areas - Introduction and summary. *Global and Planetary Change, 12*(1-4), 1-9.

Stokes, C. R., & Clark, C. D. (1999). Geomorphological criteria for identifying Pleistocene ice streams. *Annals of Glaciology, 28*, 67-74.

Stokes, C. R., Clark, C. D., Lian, O. B., & Tulaczyk, S. (2006). Geomorphological Map of Ribbed Moraines on the Dubawnt Lake Palaeo-Ice Stream Bed: A Signature of Ice Stream Shut-down? *Journal of Maps*, 1-9.

Stokes, C. R., Clark, C. D., Lian, O. B., & Tulaczyk, S. (2007). Ice stream sticky spots: A review of their identification and influence beneath contemporary and palaeo-ice streams. *Earth-Science Reviews, 81*(3-4), 217-249.

Svendsen, J. I., Alexanderson, H., Astakhov, V. I., Demidov, I., Dowdeswell, J. A., Funder, S., Gataullin, V., Henriksen, M., Hjort, C., Houmark-Nielsen, M., Hubberten, H. W., Ingolfsson, O., Jakobsson, M., Kjaer, K. H., Larsen, E., Lokrantz, H., Lunkka, J. P., Lysa, A., Mangerud, J., Matiouchkov, A., Murray, A., Moller, P., Niessen, F., Nikolskaya, O., Polyak, L., Saarnisto, M., Siegert, C., Siegert, M. J., Spielhagen, R. F., & Stein, R. (2004). Late quaternary ice sheet history of northern Eurasia. *Quaternary Science Reviews, 23*(11-13), 1229-1271.

Sættem, J. (1990). Glaciotectonic Forms and Structures on the Norwegian Continental-Shelf - Observations, Processes and Implications. *Norsk Geologisk Tidsskrift, 70*(2), 81-94.

Sættem, J. (1994). Glaciotectonic Structures Along the Southern Barents Shelf Margin. *Formation and Deformation of Glacial Deposits*, 95-113.

Sættem, J., Poole, D. A. R., Ellingsen, L., & Sejrup, H. P. (1992a). Glacial Geology of Outer Bjornoyrenna, Southwestern Barents Sea. *Marine Geology, 103*(1-3), 15-51.

Sættem, J., Rise, L., & Westgaard, D. A. (1992b). Composition and Properties of Glacigenic Sediments in the Southwestern Barents Sea. *Marine Geotechnology, 10*, 229-255.

Tulaczyk, S., Kamb, W. B., & Engelhardt, H. F. (2000). Basal mechanics of Ice Stream B, West Antarctica 2. Undrained plastic bed model. *Journal of Geophysical Research-Solid Earth, 105*(B1), 483-494.

Vadakkepuliyambatta, S., Bunz, S., Mienert, J., & Chand, S. (2013). Distribution of subsurface fluid-flow systems in the SW Barents Sea. *Marine and Petroleum Geology, 43*, 208-221.

Veeken, P. C. H. (2007). *Seismic stratigraphy, basin analysis and reservoir characterisation Handbook of geophysical exploration Seismic exploration,* (pp. 1 online resource (xi, 509 pages)). Amsterdam ; Boston, Elsevier,.

Veeken, P. C. H., & Moerkerken, B. v. (2013). *Seismic stratigraphy and depositional facies models* (pp. 1 online resource.). Houten, EAGE Publications,.

Vogel, S. W., Tulaczyk, S., Kamb, B., Engelhardt, H., Carsey, F. D., Behar, A. E., Lane, A. L., & Joughin, I. (2005). Subglacial conditions during and after stoppage of an Antarctic Ice Stream: Is reactivation imminent? *Geophysical Research Letters, 32*(14).

Vorren, T. O., Richardsen, G., Knutsen, S. M., & Henriksen, E. (1991). Cenozoic Erosion and Sedimentation in the Western Barents Sea. *Marine and Petroleum Geology, 8*(3), 317-340.

Vorren, T. O., Rokoengen, K., Bugge, T., & Larsen, O., A. (Cartographer). (1992). Kontinentalsokkelen, tykkelsen på kvartære sedimenter: Nasjonaltas for Norge, map number 2.3.9: Statens Kartverk, scale 1:3,000,000.

Wadham, J. L., Arndt, S., Tulaczyk, S., Stibal, M., Tranter, M., Telling, J., Lis, G. P., Lawson, E., Ridgwell, A., Dubnick, A., Sharp, M. J., Anesio, A. M., & Butler, C. E. H. (2012). Potential methane reservoirs beneath Antarctica. *Nature, 488*(7413), 633-637.

Wallmann, K., Pinero, E., Burwicz, E., Haeckel, M., Hensen, C., Dale, A., & Ruepke, L. (2012). The Global Inventory of Methane Hydrate in Marine Sediments: A Theoretical Approach. *Energies, 5*(7), 2449-2498.

Winsborrow, M. C. M., Andreassen, K., Corner, G. D., & Laberg, J. S. (2010a). Deglaciation of a marine-based ice sheet: Late Weichselian palaeo-ice dynamics and retreat in the southern Barents Sea reconstructed from onshore and offshore glacial geomorphology. *Quaternary Science Reviews, 29*(3-4), 424-442.

Winsborrow, M. C. M., Andreassen, K., Hubbard, A., Plaza-Faverola, A., Gudlaugsson, E., & Patton, H. (2016). Regulation of ice stream flow through subglacial formation of gas hydrates. *Nature Geosci, advance online publication*.

Winsborrow, M. C. M., Clark, C. D., & Stokes, C. R. (2010b). What controls the location of ice streams? *Earth-Science Reviews, 103*(1-2), 45-59.

Winsborrow, M. C. M., Stokes, C. R., & Andreassen, K. (2012). Ice-stream flow switching during deglaciation of the southwestern Barents Sea. *Geological Society of America Bulletin, 124*(3-4), 275-290.

Winters, W. J., Pecher, I. A., Waite, W. F., & Mason, D. H. (2004). Physical properties and rock physics models of sediment containing natural and laboratory-formed methane gas hydrate. *American Mineralogist, 89*(8-9), 1221-1227.